

The Pomeron and Gauge/String Duality

Richard C. Brower^{*}, Joseph Polchinski[†], Matthew J. Strassler[‡] and Chung-I Tan[§]

ABSTRACT: The traditional description of high-energy small-angle scattering in QCD has two components — a soft Pomeron Regge pole for the tensor glueball, and a hard BFKL Pomeron in leading order at weak coupling. On the basis of gauge/string duality, we present a coherent treatment of the Pomeron. In large- N QCD-like theories, we use curved-space string-theory to describe simultaneously both the BFKL regime and the classic Regge regime. The problem reduces to finding the spectrum of a single j -plane Schrödinger operator. For ultraviolet-conformal theories, the spectrum exhibits a set of Regge trajectories at positive t , and a leading j -plane cut for negative t , the cross-over point being model-dependent. For theories with logarithmically-running couplings, one instead finds a discrete spectrum of poles at all t , where the Regge trajectories at positive t continuously become a set of slowly-varying and closely-spaced poles at negative t . Our results agree with expectations for the BFKL Pomeron at negative t , and with the expected glueball spectrum at positive t , but provide a framework in which they are unified. Effects beyond the single Pomeron exchange are briefly discussed.

^{*}Physics Department, Boston University, Boston MA 02215

[†]Kavli Institute for Theoretical Physics, University of California, Santa Barbara, CA 93106-4030

[‡]Department of Physics, University of Washington, Seattle, WA 98195

[§]Physics Department, Brown University, Providence, RI 02912

Contents

| | |
|--|-----------|
| 1. Introduction | 2 |
| 2. A heuristic derivation | 8 |
| 3. A systematic derivation | 19 |
| 3.1 Regge behavior in flat spacetime | 19 |
| 3.1.1 Example: Bosonic string tachyons | 20 |
| 3.1.2 Generalizations | 21 |
| 3.2 Regge behavior in warped spacetime | 24 |
| 3.3 BFKL and anomalous dimensions | 26 |
| 3.4 Extension to general λ | 28 |
| 4. Derivation in light-cone gauge | 31 |
| 4.1 Open string scattering in flat spacetime | 32 |
| 4.1.1 Brief discussion for light-cone gauge at high energies | 33 |
| 4.1.2 Regge behavior | 35 |
| 4.1.3 Diffusion in transverse space | 38 |
| 4.2 Regge behavior in warped spacetime | 40 |
| 5. Regge Trajectories in UV-conformal Theories | 42 |
| 5.1 The hard-wall model | 43 |
| 5.1.1 Scattering of hadrons for $t < 0$. | 44 |
| 5.1.2 Regge trajectories at $t > 0$ | 45 |
| 5.2 The analytic structure at all t (constant coupling) | 49 |
| 6. Effect of Running Coupling | 50 |
| 6.1 Effect in UV | 51 |
| 6.2 The analytic structure at all t (running coupling) | 54 |
| 7. Outlook | 56 |

1. Introduction

As a phenomenological model for hadrons in QCD, string theory in flat space has not been widely successful. In what we may call the “classic Regge regime” (s much greater than Λ_{QCD}^2 , with $|t|$ of order or smaller than Λ_{QCD}^2) [1, 2], hadronic scattering data suggests that QCD amplitudes exhibit “Regge behavior” similar to that of flat-space classical string theory. By Regge behavior is meant that, *e.g.* for $2 \rightarrow 2$ scattering amplitudes, $\mathcal{A}(s, t) \sim s^{\alpha(t)}$, where the functions $\alpha(t)$ are called “Regge trajectories”. For most kinematics, however, strings in flat space disagree qualitatively with QCD. In elastic scattering at large angles ($s \sim -t \gg \Lambda_{QCD}^2$), QCD amplitudes are suppressed by powers of s , while amplitudes in string theory are exponentially suppressed. For scattering with $s \gg -t \gg \Lambda_{QCD}^2$ (small fixed angles and ultra-high energies), string amplitudes continue to show Regge behavior with a linear trajectory, but QCD amplitudes behave differently. The asymptotic Regge regime is physically important, as it dominates total cross-sections and differential cross-sections $d\sigma/dt$ at small angle. Unfortunately neither direct perturbative computation nor lattice gauge theory methods can be used to compute QCD amplitudes in this kinematic region. Many attempts have been made to clarify the physics of this regime, as well as the related physics of small- x structure functions in deep inelastic scattering, but the situation remains murky.

QCD is an especially difficult theory in which to investigate this issue, and were it not for the data we would have no good intuition for the physics. An important simplification is expected to occur when the number of colors N is taken very large. In the limit $N \rightarrow \infty$ followed by $s \rightarrow \infty$, scattering amplitudes in the Regge regime are dominated by what is known as single-Pomeron exchange. The Pomeron is a coherent color-singlet object, built from gluons, whose properties are universal; it is the object which is exchanged by any pair of hadrons that scatter at high energy and large impact parameter.¹ In string theory, this is the object which is exchanged in tree-level scattering in the Regge regime; it is not the graviton but the graviton’s Regge trajectory. In real QCD at fixed N , and in string theory at finite string coupling, multi-Pomeron exchange eventually comes to dominate as $s \rightarrow \infty$. We will not address this regime in the present paper (aside from a few comments in the conclusions), focusing instead on clarifying the properties of single Pomeron

¹The Pomeron is a Regge singularity initially proposed by Chew and Frautschi [1] and independently by Gribov [2], in honor of I. Ia. Pomeranchuk, who first addressed the general question of the possible equality of total cross-sections for particle-particle and particle-antiparticle interactions at high energies. Even before the theory of QCD was introduced, it was recognized that the Pomeron propagator should be endowed with the topology of a cylinder in a $1/N$ expansion, *i.e.*, it represents the exchange of a closed-string-like structure. See [3, 4]. This topological feature was explored extensively in the 1980’s, through the optical theorem, to understand patterns of particle production [5]. Interest in the phenomenological importance of the Pomeron was rekindled in the 1990’s; see [6].

exchange.

Even the single Pomeron is very subtle in QCD. At positive t , the notion of a “soft” Pomeron — a Regge trajectory on which lies the lightest 2^{++} glueball state — is generally accepted.² It generalizes the observed “soft” charge-carrying Reggeons, such as the rho trajectory for the ρ meson and its higher spin recurrences [15]. All glueball states are expected to become stable as $N \rightarrow \infty$. At negative t , the notion of a “hard” Pomeron has emerged from perturbative resummation of Feynman diagrams, as pioneered by Balitsky, Fadin, Lipatov, and Kuraev [16, 17, 18], referred to as “BFKL”; for a modern introduction and a more complete list of references, see [19]. The original calculation is at leading order in α and resums all terms of order $[\alpha \ln(s/t)]^n$, $n \geq 0$. The BFKL approach has been controversial, especially following the understanding that in QCD the next-order correction to BFKL is large and of opposite sign to the leading-order answer [20, 21]. Meanwhile, no existing calculational method, or experimental data, can simultaneously address the physics at both positive and negative t . All in all, the relation between the two Pomerons, the theoretical status of the BFKL method, and the physics of the $|t| < \Lambda_{QCD}^2$ region have never been made entirely clear.

Importantly, the large size of the correction to the leading-order BFKL result is in part due to the large size of the beta function in QCD. For this reason, a second significant simplification for an analysis of the Regge regime involves specializing to large- N gauge theories whose beta function is either zero or small, in particular of order $1/N$. If the beta function vanishes, the theory is strictly conformally invariant, and the BFKL computation can be carried out without confusing the effects arising from the running coupling with those from other sources. Indeed, it has been shown that the next-order corrections to the BFKL result in $\mathcal{N} = 4$ Yang-Mills are a third as large as those in QCD, making the analysis much more reasonable and interpretable. We will also see that our analysis is especially simple in this case. Theories with a small beta function can then be understood as a small perturbation on the conformally invariant case.

Although the resummation calculation of BFKL applies at $s \gg |t|$, it is only valid in regimes where confinement effects can be completely neglected. At best, these include (1) computations in the regime $s \gg -t \gg \Lambda_{QCD}^2$, where the large momentum transfer implies that the scattering takes place on scales small compared to the confinement scale, and (2) computations, for any $t \leq 0$, but with s not exponentially large, concerning hadrons whose size ρ is sufficiently small compared to Λ_{QCD}^{-1} , as would be the case for quarkonium states with quarks of mass $M \gg \Lambda_{QCD}$.

²Due to mixing with ordinary mesons, experimental identification of glueball states has been challenging. The best evidence for their existence has been through lattice gauge theory [7]. For inferring the property of the Pomeron trajectory from lattice data, see [8]. The relevant tensor glueball state was first studied in [9, 10, 11] from an AdS/CFT duality perspective. For first attempts at calculating glueball masses using AdS/CFT, following work of [12], see [13, 14].

For this reason, the cleanest application of BFKL is to quarkonium-quarkonium scattering [22], or to deep-inelastic scattering off a quarkonium state, or to off-shell photon-photon scattering [18]. But it cannot be used to study the classic Regge regime, for which the physics of confinement is dominant.

In this paper, we aim to show, in certain large- N QCD-like theories with beta functions that are vanishing or small in the ultraviolet, how the BFKL regime (which disagrees with flat-space string theory) and the classic Regge regime (which roughly agrees with it) can both simultaneously be described using curved-space string theory. We will extend this to all values of $s \gg \Lambda_{QCD}^2$ and t , obtaining thereby the full analytic structure of the single-Pomeron exchange kernel, including both the soft Pomeron at positive t and the hard Pomeron at negative t . This is technically impossible in QCD, where computations in lattice gauge theory and perturbative gauge theory calculations are separated by a kinematic range where the physics is both strongly coupled and Lorentzian in character.

As an illustration of the form of our results, we briefly summarize our investigation of the simplest case: the scattering of two objects by conformally-invariant dynamics. In conformally-invariant theories there are, of course, no hadrons, but we may either consider four-point functions of operators that are functions of nonzero momentum p_i , with $s = -(p_1 + p_3)^2 \gg -t = (p_1 + p_2)^2$, or we may add massive quarks as a probe of the theory, at the cost of only a $1/N$ violation of conformal invariance, and consider the scattering of quarkonium bound states. For $t = 0$, the single-Pomeron-exchange amplitude for scattering of two such objects A and B , with center-of-mass energy \sqrt{s} , is of the form

$$\int \frac{dp_\perp}{p_\perp} \int \frac{dp'_\perp}{p'_\perp} \Phi_A(p_\perp) \mathcal{K}(p_\perp, p'_\perp, s) \Phi_B(p'_\perp) \quad (1.1)$$

where p_\perp (p'_\perp) is the magnitude of the transverse momentum with which the first (second) object is probed by the Pomeron. The two functions Φ_i , called “impact factors”, describe the transverse structure of the objects undergoing the scattering. These impact factors are convolved together with the BFKL kernel \mathcal{K} .

When the 't Hooft coupling $g^2 N$ is very small and N is very large, the computation can be done using the methods of BFKL, according to which, at leading nontrivial order in α , the kernel can be written exactly as an inverse Mellin transform in the spin j

$$\mathcal{K}(p_\perp, p'_\perp, s) = \int_{C-i\infty}^{C+i\infty} \frac{dj}{2i\pi} s^j \int_{-\infty}^{\infty} d\nu e^{i\nu \ln(p_\perp/p'_\perp)} \frac{1}{j - \hat{j}(\nu)} \quad (1.2)$$

with the j -plane contour to the right of all j -plane singularities, and

$$\hat{j}(\nu) = 1 + \frac{\alpha N}{\pi} \left[-2\gamma_E - \Psi \left(\frac{1}{2} + i \frac{\nu}{2} \right) - \Psi \left(\frac{1}{2} - i \frac{\nu}{2} \right) \right] + O(\alpha^2) \quad (1.3)$$

where γ_E is Euler's constant and $\Psi(z)$ is the Digamma function.³ (Here we limit ourselves to the term with conformal spin equal to zero.) A good approximation to this kernel can be found by expanding the function \hat{j} to second order in ν

$$\hat{j}(\nu) = j_0 - \mathcal{D}\nu^2 + \text{order}(\nu^4), \quad (1.4)$$

where

$$j_0 = 1 + \frac{4 \ln 2}{\pi} \alpha N, \quad \mathcal{D} = \frac{7\zeta(3)}{2\pi} \alpha N. \quad (1.5)$$

From this one obtains

$$\mathcal{K}(p_\perp, p'_\perp, s) \approx \frac{s^{j_0}}{\sqrt{4\pi\mathcal{D} \ln s}} e^{-(\ln p'_\perp - \ln p_\perp)^2 / 4\mathcal{D} \ln s} \quad (1.6)$$

Strictly speaking, s must be replaced with s/s_0 , where $\sqrt{s_0}$ is a characteristic energy scale which we will discuss later. We may recognize \mathcal{K} , in this approximation, as a power of s times a diffusion kernel, with the diffusion occurring in the variable $\ln p_\perp$ over a diffusion time $\tau \sim \ln s$.

This is a very curious result. Ordinary Regge behavior $\mathcal{A} \sim s^{\alpha(t)}$, in flat-space string theory or in the classic Regge regime, is related to diffusion in *transverse position* space. Around the ‘‘intercept’’ at $t = 0$, the Regge trajectories are initially linear, with $\alpha(t) = \alpha_0 + \alpha't + \dots$; the higher order corrections are zero in ordinary flat-space string theory and are apparently small in QCD. The Regge amplitudes, Fourier transformed into position space, take a diffusive form. Suppose the scattering particles are traveling initially along the x^1 axis, with the momentum transfer k^μ completely transverse to the x^0, x^1 coordinates, so that $t = -\mathbf{k}_\perp^2$; then

$$\int d^{d-2} k_\perp e^{i\mathbf{k}_\perp \cdot \mathbf{x}_\perp} s^{\alpha(t)} \approx s^{\alpha_0} \int d^{d-2} k_\perp e^{i\mathbf{k}_\perp \cdot \mathbf{x}_\perp} e^{-\alpha' k_\perp^2 \ln s} = \frac{s^{\alpha_0} e^{-x_\perp^2 / 4\alpha' \ln s}}{(4\pi\alpha' \ln s)^{(d-2)/2}}. \quad (1.7)$$

From the point of view of one string (or hadron), the other string (or hadron) grows, with $\langle x_\perp^2 \rangle \sim \alpha' \ln s$, via diffusion, with a diffusion time $\propto \ln s$. This can also be viewed as due to a time-resolution effect; for a modern discussion, see Ref. [23]. The time-dilation of the boosted string, as viewed by the ‘‘target’’, resolves more and more of its quantum fluctuations. This tends to make the string appear longer, and consequently larger, by an amount that grows like a random walk in the dimensions transverse to the motion of the string. This is explicit in our later discussion of Regge physics in the light-cone frame, in Sec. 4.

The similarity between these two types of diffusion, in two different variables ($\ln p_\perp$ versus x_\perp) and in two different regimes (far from confinement for BFKL, deep within confinement for the classic Regge regime), is not accidental. This can be seen

³Note that in many papers a different normalization of ν is used; in particular our variable ν is twice as large as that used in [19].

by considering the same scattering problem at large g^2N , where BFKL methods cannot be applied but where string theoretic methods, which resum the expansion in g^2N to all orders, can be used. The scattering of two states in a conformal field theory translates into the scattering of strings on a curved background of the form $AdS_5 \times W$. The coordinates on the AdS_5 space are x^μ , the usual Minkowski coordinates, and r , the fifth coordinate that runs from $r = 0$ at the horizon of the Poincaré patch of AdS_5 to $r = \infty$ at its boundary. The coordinate r is related to the energy scale μ in the quantum field theory; $r \rightarrow 0$ corresponds to the infrared and $r \rightarrow \infty$ to the ultraviolet. We will show the resulting kernel at $t = 0$ for the scattering of two strings on an AdS_5 space via single-Pomeron exchange is

$$\mathcal{K}(r, r', s) = \frac{s^{j_0}}{\sqrt{4\pi\mathcal{D}\ln s}} e^{-(\ln r - \ln r')^2/4\mathcal{D}\ln s} \quad (1.8)$$

where

$$j_0 = 2 - \frac{2}{\sqrt{\lambda}} + O(1/\lambda), \quad \mathcal{D} = \frac{1}{2\sqrt{\lambda}} + O(1/\lambda) . \quad (1.9)$$

Here $\lambda \equiv R^4/\alpha'^2$, where R is the curvature radius of the AdS_5 space and $2\pi\alpha'$ is the inverse of the string tension. Note that $\lambda = g_{YM}^2 N = 4\pi\alpha N$ in $\mathcal{N} = 4$ supersymmetric Yang-Mills theory — the numerical coefficient can differ in other theories but the proportionality always holds — so large λ is large 't Hooft coupling. Comparing this with Eq. (1.6), one sees that the fifth coordinate r of the string theory should be identified in this context with k_\perp of the gauge theory. The identification of r and k_\perp has its source in the UV/IR correspondence [24] and has been suggested in numerous contexts (see for example [25, 26, 27] for related applications.) Note that the effective diffusion time τ is of order $\ln s$ for both the BFKL and the Regge diffusion, at both large and small λ .

This success is consistent with others that have emerged in recent years. The duality of gauge theory and string theory has led us to expect that many of the failures of string theory as a good model of the physics of QCD are due not to having the wrong string theory, but to putting the right string theory on the wrong space-time background, namely flat Minkowski space. It is now known that much better phenomenological string models for QCD are given by string theory on certain curved spaces. The result just described implies that at large N , vanishing beta function, and $t = 0$, *the form of the BFKL result may be interpreted as the Regge physics of a string theory compactified to AdS_5 , in the form of diffusion along the curved fifth dimension.* The only substantial difference between the small 't Hooft coupling result (1.6) and the large 't Hooft coupling result (1.8) lies in the coefficients; compare Eqs. (1.5) and (1.9). This is strongly suggestive that the kernel is always of the form (1.6), with the overall power j_0 and the diffusion constant \mathcal{D} being continuously varying functions of αN . Indeed, such a result follows from the constraints of conformal invariance.

The extension of the single-Pomeron kernel to nonzero $t < 0$ (physical scattering at small angles) is quite involved in the BFKL regime [28, 29]. By contrast, using string-theory methods, the kernel in the strong-coupling approximation is easily derived. We will argue that aspects of our result are necessarily true in an asymptotically conformally-invariant theory. As before, the result depends on coefficients that are functions of the 't Hooft coupling. The weak- and strong-coupling results at finite t have the same formal structure, and qualitative similarities. They differ in that at weak coupling the Pomeron can couple to individual partons, while at strong coupling it couples only to the entire hadron, in analogy with the physics of deep inelastic scattering in the two regimes [30].

In sections 2, 3 and 4, we will derive the result (1.8), and its extension to $t < 0$, in three ways. The first uses a low-brow approach which returns to the results of earlier work [30]. The second carefully obtains the result from string theory in conformal gauge, introduces Pomeron vertex operators as computational tools in string theory, and discusses a number of underlying theoretical aspects of the calculation. The final derivation uses light-cone gauge.

Next we will generalize our results to include effects of confinement, first considering theories whose ultraviolet physics is conformally invariant (Sec. 5), and then considering theories with a logarithmically running coupling (Sec. 6). We use string theory to study the full analytic structure of the single-Pomeron exchange amplitude, for all values of t . For $t \ll -\Lambda^2$, with Λ of order the confinement scale, the kernel is nearly independent of confinement, and our results from the conformal case require no modification if the beta function vanishes in the ultraviolet, and a more substantial but model-independent modification if the coupling runs. For $t \gg +\Lambda^2$ the Regge trajectories on which the hadronic resonances sit can be identified and studied. It is straightforward to compute the hadron spectrum using differential equations which match directly to the equations governing the diffusion at $t < 0$. This makes it possible to answer long-standing questions concerning the behavior, as t is taken from positive to negative, of the Regge trajectories $\alpha(t)$. Details of the Regge-trajectories are model-dependent, but their presence and their general t -dependence are not. The region $|t| \sim \Lambda^2$, which dominates total cross-sections and near-forward scattering, is the most model-dependent. In addition to computing the kernel's asymptotic form at large s , we also note various transient effects which are present for s not asymptotically large, some of which are also model-independent.

Our all- t results for the analytic behavior of the single-Pomeron exchange amplitude are consistent with what is known from a combination of data at positive t and analytic work in field theory at negative t . The structure of our formalism makes concrete the intuitive approach suggested in [31], which suggested a unified treatment of the Pomeron and developed an intuitive picture of diffusion in both

hard and soft regimes.⁴ We believe our result is the first, however, to connect the positive and negative t behavior in a reliable and consistent theoretical framework.⁵

2. A heuristic derivation

In ref. [25], it was argued that scattering amplitudes in gauge theories with good string dual descriptions can be expressed in a simple general form, in which the underlying ten-dimensional amplitude is essentially local and the four-dimensional amplitude is given by a coherent sum over scattering anywhere in the six transverse dimensions. In this section we will apply this to scattering in the Regge limit. We will see that at a certain point the approximation breaks down, and we will need to make an educated guess as to the correct amplitude. In the next section we will make a more systematic world-sheet analysis, seeing why the local approximation breaks down and how to correct it.

For conformally invariant gauge theories, the metric of the dual string theory is a product⁶ $AdS_5 \times W$,

$$ds^2 = \frac{r^2}{R^2} \eta_{\mu\nu} dx^\mu dx^\nu + \frac{R^2}{r^2} dr^2 + ds_W^2, \quad (2.1)$$

where $0 < r < \infty$. We use x^M for the ten-dimensional coordinates, or (x^μ, r, θ) with θ being the five coordinates on W , or (x^μ, y^m) when we discuss all six transverse coordinates y together. Our convention is that the metric signature is spacelike-positive. For the dual to $\mathcal{N} = 4$ supersymmetric Yang-Mills theory [24] the AdS radius R is

$$R^2 \equiv \sqrt{\lambda} \alpha' = (4\pi g_{\text{string}} N)^{1/2} \alpha' = (g_{\text{YM}}^2 N)^{1/2} \alpha', \quad (2.2)$$

and W is a 5-sphere of this same radius. By a “good string dual description” we mean that $\lambda \gg 1$, so that the spacetime curvature is small on the string scale, and $g_{\text{string}} \ll 1$ so that we can use string perturbation theory.

We are interested in gauge theories that are conformally invariant at high energy but with the invariance broken at low energy, resulting in a mass gap and confinement. Roughly speaking, this means that the dual string metric is of the AdS form but with a lower cutoff on the coordinate r , so that $r_0 < r < \infty$. More precisely, the

⁴See also [19], Section 5.6.

⁵Our results contradict the earliest attempts [32] to connect positive and negative t , where it was proposed that Regge trajectories at positive t flatten out and extend to negative integer values of j as $t \rightarrow -\infty$. Our approach and conclusions differ as well from refs. [33, 34]; in particular [34] finds a Pomeron intercept that is independent of λ . The conjectures of [35] also differ from our results, though by not as great a degree; we will see below there is a certain commonality of viewpoint at the point of departure, though in the end our approach and conclusions are distinct from theirs.

⁶More generally it could be a warped product, where the AdS metric is multiplied by a function of the coordinates on W .

product structure breaks down in the infrared, and we must use a general warped product

$$ds^2 = G_{MN}dx^M dx^N = e^{2A(y)}\eta_{\mu\nu}dx^\mu dx^\nu + G_{\perp mn}dy^m dy^n . \quad (2.3)$$

To simplify the discussion we define the radial coordinate by $r^2/R^2 = e^{2A}$, so that $r_0^2/R^2 = \min(e^{2A})$. (In models where e^{2A} has more than one local minimum, r is not a good coordinate, and one should everywhere replace r/R with e^A .) The precise metric depends on the details of the conformal symmetry breaking. Most of the physics that we will study takes place in the conformal region where the metric is the approximate *AdS* product (2.1). Even here we might generalize to geometries that evolve slowly with r , as in cascading gauge theories and in the running coupling example to be studied in Sec. 6.

Glueballs arise as discrete modes in the six-dimensional transverse ‘cavity.’ For example, a scalar glueball created by the operator $F_{\mu\nu}F^{\mu\nu}$ would have a dilaton wavefunction

$$\Phi(x, y) = e^{ip \cdot x} \psi(y) . \quad (2.4)$$

Local operators in the gauge theory also translate into bulk excitations, the difference being their boundary conditions (non-normalizable rather than normalizable) as $r \rightarrow \infty$ [36, 37, 38]. The Pomeron is a closed string state, and at leading large- N order its properties do not depend on the open string spectrum. Thus we can study its physics without introducing branes and open strings, though it will later be useful to do so in order to model quarkonium scattering and to discuss open string trajectories. The open string wavefunctions are of the same form (2.4) but with support restricted to whatever branes have been embedded in the transverse space.

In the string picture, scattering amplitudes are given as usual by path integrals over string world-sheets embedded in the deformed $AdS_5 \times W$, with appropriate vertex operators for the external states. Aside from a few remarks at the end, we will consider only the leading $1/N$ approximation, corresponding to spherical world-sheets. In general this would still be a forbidding calculation, but a great simplification occurs at $\lambda \gg 1$. The string world-sheet action contains factors of R^2 from the spacetime metric and $1/\alpha'$ from the string tension, which combine into $R^2/\alpha' = \sqrt{\lambda}$. Thus the string world-sheet coupling $1/\sqrt{\lambda}$ is small, and the world-sheet path integral is almost Gaussian. It is not exactly Gaussian because the constant mode on the world-sheet has no quadratic term. We must therefore separate the fields on the string world-sheet into their zero modes and the remaining nonzero-mode parts,

$$X^M(\sigma^1, \sigma^2) = x^M + X'^M(\sigma^1, \sigma^2) . \quad (2.5)$$

At fixed x^M , the Gaussian integral over the nonzero modes is exactly as one would do in flat spacetime,⁷ thus producing the ten-dimensional flat spacetime S-matrix

⁷The RR backgrounds have scaled away with the curvature, so we are spared dealing with them.

that would be seen by a local observer (except that the momentum delta function from the zero modes is missing.) We denote this amplitude $i\mathcal{A}_{\text{local}}(x, y)$. Integrating over the zero mode then gives the S-matrix

$$\mathcal{S} = i \int d^4x d^6y \sqrt{-G} \mathcal{A}_{\text{local}}(x, y) . \quad (2.6)$$

We define $\mathcal{A}_{\text{local}}$ to be a scalar; the $\sqrt{-G}$ then arises from the path integral measure, which respects coordinate invariance.

The dependence on the external states is implicit, but for high energy scattering it can be put in a more explicit form. In the wavefunction (2.4), the gradients in the transverse directions are generally of order $1/R$, much less than string scale. In the noncompact directions we will be considering momenta at least of order the string scale, and in fact much larger. It follows that the local inertial observer sees momenta directed essentially in the noncompact directions. In terms of inertial coordinates parallel to the μ axes, the momenta are

$$\tilde{p}^\mu = \frac{R}{r} p^\mu . \quad (2.7)$$

The p^μ , which appear in the wavefunction (2.4), are the conserved Noether momenta and so are identified with the gauge theory momenta, while the \tilde{p}^μ are the momenta seen by a local inertial observer. Thus,

$$\mathcal{A}_{\text{local}}(x, y) \rightarrow \mathcal{T}_{10}(\tilde{p}) \prod_{\substack{\text{ext.} \\ \text{states}}} e^{ip_i \cdot x} \psi_i(y) , \quad (2.8)$$

the flat-spacetime scattering amplitude with momenta \tilde{p} times the product of the wavefunctions at (x, y) . The integral over x produces the four-dimensional momentum delta function. Then, for scattering of scalars, the general local superposition (2.6) becomes

$$\mathcal{T}_4 = \int d^6y \sqrt{-G} \mathcal{T}_{10}(\tilde{p}) \prod_{\substack{\text{ext.} \\ \text{states}}} \psi_i(y) , \quad (2.9)$$

where $\mathcal{S} = i(2\pi)^4 \delta^4(\Sigma p) \mathcal{T}_4$. Note that G is the determinant of the full ten-dimensional metric. For external states with spin, \mathcal{T}_{10} is naturally written with tangent space indices, and so would be contracted with the external wavefunctions in tangent space form.

The final results (2.6), (2.9) are simple and intuitive, just a coherent superposition over all possible scattering locations. The scattering is effectively local because the scale of fluctuations of the string world-sheet is set by α' , which is small compared to the variations of the geometry. The Gaussian approximation that leads to this local expression is rather robust. It will break down later in this section, but only because we introduce a competing large parameter. In the next section we will analyze this breakdown at the world-sheet level, and see how to correct it.

Now let us apply this to Regge scattering, focusing for simplicity on $2 \rightarrow 2$ scattering of scalars. Thus $s = -(p_1 + p_3)^2$ is taken large, with $t = -(p_1 + p_2)^2$ fixed. The local inertial quantities are

$$\tilde{s} = \frac{R^2}{r^2}s, \quad \tilde{t} = \frac{R^2}{r^2}t, \quad (2.10)$$

and so for scattering at a given value of r the ten-dimensional process is also in the Regge regime. Thus at fixed r we have

$$\mathcal{T}_{10}(\tilde{s}, \tilde{t}) \rightarrow f(\alpha'\tilde{t})(\alpha'\tilde{s})^{2+\alpha'\tilde{t}/2}, \quad (2.11)$$

with f a process-dependent function. In fact the relevant value of r in the superposition (2.9) evolves with s but does so only slowly, so we remain well within the regime where the form (2.11) is valid. Thus we have

$$\mathcal{T}_4(s, t) = \int d^6y \sqrt{-G} f(\alpha'R^2t/r^2)(\alpha'R^2s/r^2)^{2+\alpha'R^2t/2r^2} \prod_{i=1}^4 \psi_i(y). \quad (2.12)$$

Examining the exponent of s , we see that the intercept, the exponent at $t = 0$, is 2 just as in flat spacetime. We also see that the slope, the coefficient of t , depends on r as

$$\frac{\alpha'_{\text{eff}}(r)}{2} = \frac{R^2\alpha'}{2r^2}. \quad (2.13)$$

The 2's appears in the denominator because this is a closed string trajectory. It is as though, in this ‘‘ultralocal’’ approximation, the five-dimensional Pomeron gives rise to a continuum of four-dimensional Pomerons, one for each value of r and each with a different slope.⁸ This is illustrated schematically in Fig. 1.

At large s , the highest trajectory will dominate. For positive t , this would be the one at the minimum value r_0 :

$$\alpha'_{\text{eff}}(t > 0) = \frac{R^2\alpha'}{r_0^2} \equiv \alpha'_0. \quad (2.14)$$

For negative t , it would be the trajectories at large r . The wavefunctions in the superposition (2.12) make the integral converge at large r , so at any given s the dominant r is finite, but as s increases the dominant r moves slowly toward infinity and so we have

$$\alpha'_{\text{eff}}(t < 0) = 0. \quad (2.15)$$

We see that, in this approximation, the dominant trajectory has a kink at $t = 0$, similar to (though more abrupt than) the behavior in QCD. Moreover, as also

⁸The notion of a tension depending on a fifth dimension dates to [39]. The idea of superposing many four-dimensional Pomerons is conceptually anticipated in the work of [26], and more technically in that of [35], where an idea similar to that of the next paragraph is considered.

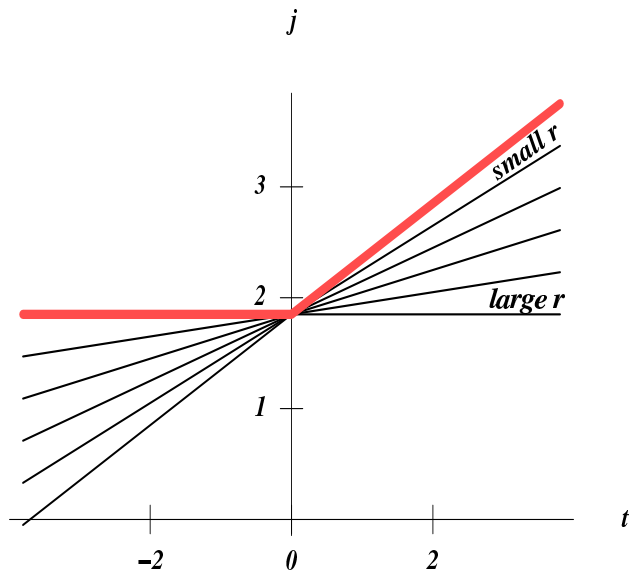


Figure 1: In the ultralocal approximation, the slope of the leading trajectory redshifts from order one at small r down to zero as $r \rightarrow \infty$; trajectories at several different r values, with their different slopes, are shown. The leading singularity (the singularity with largest j at fixed t) is the usual linear Regge trajectory for $t > 0$ but is a constant near 2 for $t < 0$. The full story is more elaborate, as will be shown.

happens in QCD, the nature of the Pomeron changes. For positive t it sits at small r and so its properties are determined by the confining dynamics: it is a glueball. At negative t it sits at large r and so is effectively a very small object, analogous to the tiny (and therefore perturbative) two-gluon Pomeron of BFKL [26].

However, we can go well beyond the ultralocal approximation. Note that we have two large quantities, λ and s . In the discussion thus far, we have taken λ large first, making the Gaussian approximation, and then considered large s within this approximation. But in order to expose a wider range of QCD-like physics, we would like to keep values of s which are large compared to λ . More precisely, the interesting physics arises in the limit

$$\lambda, s \rightarrow \infty, \quad \frac{\ln s}{\sqrt{\lambda}} \text{ fixed} . \quad (2.16)$$

Thus s is exponentially large in $\sqrt{\lambda}$. This is an enormous scale from the point of view of AdS/CFT physics, but to reach real QCD we must continue to small λ and so the physics that we find in this regime can become important.

In the regime (2.16) it is necessary to retain terms of order $1/\sqrt{\lambda}$ in the exponent $2 + \alpha' t/2$ of s . Thus in the ten-dimensional momentum transfer \tilde{t} we must keep a term previously dropped, coming from the momentum transfer in the six transverse directions:

$$\alpha' \tilde{t} \rightarrow \alpha' \nabla_P^2 \equiv \frac{\alpha' R^2 t}{r^2} + \alpha' \nabla_{\perp P}^2 . \quad (2.17)$$

The transverse Laplacian is proportional to R^{-2} , so that the added term is indeed of order $\alpha'/R^2 = 1/\sqrt{\lambda}$. The Laplacian acts in the t -channel, on the product of the wavefunctions of states 1 and 2 (or 3 and 4). The subscript P indicates that we must use the appropriate curved spacetime Laplacian for the Pomeron being exchanged in the t -channel; we will determine this shortly.

The inclusion of the transverse momentum transfer leads to several new effects. First, we will now be able to determine the first strong coupling correction, $O(1/\sqrt{\lambda})$, to the intercept 2. Second, we will see that $s^{\alpha' \bar{t}/2}$ is now a diffusion operator in all eight transverse dimensions, not just the Minkowski directions, and that this leads to BFKL-like physics. Third, to obtain the Regge exponents we will now have to diagonalize the differential operator (2.17), so that instead of the ‘ultralocal’ Pomerons (2.13) that arose in the earlier regime, we will have a more normal spectral problem.⁹

Now let us determine the form of $\nabla_{\perp P}^2$. We first make some definitions. The scalar Laplacian is

$$\begin{aligned} \nabla_0^2 \phi &= (-G)^{-1/2} \partial_M [(-G)^{1/2} G^{MN} \partial_N \phi] \\ &= (r/R)^{-4} G_{\perp}^{-1/2} \partial_M [(r/R)^4 G_{\perp}^{1/2} G^{MN} \partial_N \phi] . \end{aligned} \quad (2.18)$$

To study the contribution of the exchange of a transverse traceless field of spin j at high energies, it is useful to define the Laplacian in light-cone coordinates,

$$x^{\pm} = \frac{1}{\sqrt{2}}(x^0 \pm x^1) . \quad (2.19)$$

Specifically, consider the tensor component ϕ_{+j} , with j indices $+$, in a frame where the Pomeron momentum components $(p_1 + p_2)^{\pm}$ vanish. The covariant Laplacian reduces to

$$\nabla_j^2 \phi_{+j} = (r/R)^j \nabla_0^2 [(r/R)^{-j} \phi_{+j}] + \frac{j}{4} \mathcal{R}_{+}^{+} \phi_{+j} , \quad (2.20)$$

where \mathcal{R} is the Ricci tensor. It is convenient to define also

$$\begin{aligned} \Delta_j &= \nabla_j^2 - \frac{j}{4} \mathcal{R}_{+}^{+} \\ \Delta_j \phi_{+j} &= (r/R)^j \nabla_0^2 [(r/R)^{-j} \phi_{+j}] . \end{aligned} \quad (2.21)$$

As we will see these expressions make sense even for noninteger j ; they define an on-shell Regge exchange process.

The difference between Δ_j and ∇_j^2 is a curvature term and so covariance alone does not determine the Laplacian to this order. We must resolve this ambiguity

⁹Ref. [35] proposes a different modification of the ultralocal Pomeron spectrum, an Ansatz based on straight trajectories with a discrete set of slopes. The structure that we find in AdS/CFT, where the trajectories are given by the eigenvalues of an effective Hamiltonian, is more closely parallel to that found by BFKL in perturbation theory.

in order to find the shift in the Regge intercept, and so we must look at the dynamics. For transverse traceless fluctuations of the metric, h_{++} , one finds from the supergravity field equations that the wave equation in a warped background is

$$\Delta_2 h_{++} = 0 . \quad (2.22)$$

A simple way to check this is to note that in the long-wavelength limit the transverse traceless perturbation becomes $h_{++} = (r/R)^2$; this is a linear reparameterization of the background metric $(r/R)^2 \eta_{\mu\nu}$ and so must satisfy the correct wave equation. From the explicit form (2.21) it follows that this is the case for the equation (2.22), and would not be true with an added curvature term. Now, we have noted that the Regge intercept differs from 2 by an amount of order $1/\sqrt{\lambda}$. If it were exactly 2 we would be sitting on the graviton pole, so we conclude that $\Delta_P = \Delta_2$ up to a correction of order $1/\sqrt{\lambda}$. The Laplacian term is already of order $1/\sqrt{\lambda}$, so the shift is second order and can be neglected:

$$\nabla_P^2 \rightarrow \Delta_2 + O(j-2) . \quad (2.23)$$

Thus

$$\mathcal{I}_4(s, t) = \int d^6 y \sqrt{-G} \psi_3(y) \psi_4(y) f(\alpha' R^2 t/r^2) (\alpha' R^2 s/r^2)^{2+\alpha' \Delta_2/2} \psi_1(y) \psi_2(y) . \quad (2.24)$$

This somewhat heuristic argument will be supported by the more formal treatment in the next section ¹⁰.

Now let us work out the explicit form of the amplitude for processes that take place in the high-energy *AdS* product region (or in an exactly conformal theory, such as discussed above Eq. (1.1) in the introduction.) In terms of the coordinate $u = \ln(r/r_0)$, which is $\gg 1$ in the high energy region, the metric is

$$ds^2 = \frac{r_0^2}{R^2} e^{2u} \eta_{\mu\nu} dx^\mu dx^\nu + R^2 du^2 + ds_W^2 . \quad (2.25)$$

The Laplacian is

$$\begin{aligned} \alpha' \Delta_2 &= \frac{1}{\sqrt{\lambda}} (\partial_u^2 - 4) + \alpha'_0 t e^{-2u} + \alpha' \nabla_W^2 \\ &= \frac{1}{\sqrt{\lambda}} [\partial_u^2 - 4 + z_0^2 t e^{-2u}] + \alpha' \nabla_W^2 , \end{aligned} \quad (2.26)$$

where $\alpha'_0 = \alpha'_{\text{eff}}(r_0) = R^2 \alpha'/r_0^2$ is the infrared slope (2.14), and $1/z_0 = r_0/R^2$ is the mass scale of the lightest glueballs (Kaluza-Klein excitations). Note that $1/\sqrt{\alpha'_0} = \lambda^{1/4}/z_0$.

¹⁰In flat space, the function f has a pole at zero, from massless t -channel exchange. In a more precise treatment, we need to replace the argument of f with the curved-spacetime propagator $\alpha' \Delta_2$. See Sec. 3.2. In most cases we are interested in the imaginary part of \mathcal{T} , and $\text{Im } f(0)$ is finite.

For simplicity we assume that the wavefunctions are independent of W , and consider first the case $t = 0$. Then Eq. (2.24) becomes

$$\mathcal{I}m \mathcal{T}_4 = \text{const} \times s^2 \int du \psi_3(u)\psi_4(u)/\sqrt{\lambda} [\alpha'_{\text{eff}}(r)s]^{(\partial_u^2-4)/2\sqrt{\lambda}} \psi_1(u)\psi_2(u). \quad (2.27)$$

We have canceled a factor of r^4 from $\sqrt{-G}$ against a factor of r^{-4} from the Regge amplitude. In doing this we have assumed that the latter factor acts to the left of the diffusion operator, rather than being symmetrized with it (the difference is of the same order as the effects that we are retaining). This follows automatically from the more systematic analysis of the next section, but in fact one can already deduce it from the symmetry of the diffusion kernel, which would not hold with any other ordering.

The amplitude (2.27) will indeed be dominated by large u provided that one or more wavefunctions are strongly peaked at large u (as is the case for quarkonium states or external operators of large momentum), and also provided that s is not too large (else the diffusion will reach the confinement scale). The latter effect will be considered in more detail in Sec. 5.

The s -dependence now takes the form

$$s^{2+(\partial_u^2-4)/2\sqrt{\lambda}}. \quad (2.28)$$

This gives diffusion in u over a time

$$\tau = \frac{1}{2\sqrt{\lambda}} \ln\left([\alpha'_{\text{eff}}(\bar{r})] s\right). \quad (2.29)$$

where \bar{r} is an averaged value of r appropriate to the particular physical process.¹¹

Recall that a diffusion operator resembles a Schrödinger operator in imaginary time, and can be similarly treated. We need to solve

$$H\Psi_E(u) = [-\partial_u^2 + V(u)]\Psi_E(u) = E\Psi_E(u) \quad (2.30)$$

¹¹While the precise choice of \bar{r} is a subleading effect, confusion might arise were it not addressed here. In particular, \bar{r} is not, in general, r_0 . In this and the earlier equations we have retained $\alpha'_{\text{eff}}(r)$ to a small power. This is necessary for good form with units, but there is also some physics in it. We could imagine that at the values of r relevant to the physics, $\ln(\bar{r}/r_0)$ may be large enough that we would wish to retain effects of order $\ln(\bar{r}/r_0)/\sqrt{\lambda}$; keeping $\alpha'_{\text{eff}}(\bar{r})$ does this. If $\psi_1\psi_2$ and $\psi_3\psi_4$ are peaked at a common scale \bar{r} , we can replace $\alpha'_{\text{eff}}(r)$ with $\alpha'_{\text{eff}}(\bar{r})$; any correction is higher order in $1/\sqrt{\lambda}$. If they are peaked at two different scales r_1 and r_3 then we can replace it with the geometric mean of $\alpha'_{\text{eff}}(r_1)$ and $\alpha'_{\text{eff}}(r_3)$. Thus the diffusion time appearing in $e^{\tau\partial_u^2}$ is, more generally, to be taken as

$$\tau = \frac{1}{2\sqrt{\lambda}} \ln\left(s\sqrt{\alpha'_{\text{eff}}(r_1)\alpha'_{\text{eff}}(r_3)}\right).$$

with $V(u) = 4$. This has the same eigenstates as a free particle; its delta-function normalizable eigenstates are $e^{i\nu u}$ for $-\infty < \nu < \infty$, with eigenvalues $E = 4 + \nu^2$. That is, this operator has a continuum of states with a continuum of energies — a cut in the E plane starting at 4. The operator $2 + (\partial_u^2 - 4)/2\sqrt{\lambda}$ therefore has eigenvalues

$$j = j_0 - \mathcal{D}\nu^2 \quad (2.31)$$

with

$$j_0 = 2 - \frac{2}{\sqrt{\lambda}}, \quad \mathcal{D} = \frac{1}{2\sqrt{\lambda}}. \quad (2.32)$$

Thus there is a cut in the j plane ending at j_0 . This is the same behavior as found by BFKL in perturbative contexts, and we can identify j_0 as the strong coupling limit of the BFKL exponent. This exponent has also been derived recently in ref. [40]; we will discuss this work more fully in Sec. 3.3.

The high- s behavior of amplitudes is roughly of the form s^{j_0} , but this would be strictly true only if the leading eigenvalue of Δ_2 were discrete, so that the leading singularity in the j plane would be a pole rather than a cut. The precise form is

$$\text{Im } \mathcal{A}(s, t = 0) \propto \int du du' \psi_3(u) \psi_4(u) \mathcal{K}(u, u', \tau) \psi_1(u') \psi_2(u') \quad (2.33)$$

where

$$\mathcal{K}(u, u', \tau) = s^{j_0} \mathcal{K}_0(u, u', \tau) \quad (2.34)$$

and $\mathcal{K}_0(u, u', \tau)$ is the diffusion (heat) kernel

$$\begin{aligned} \mathcal{K}_0(u, u', \tau) &= e^{\tau \partial_u^2} \delta(u - u') = \int_{-\infty}^{\infty} \frac{d\nu}{2\pi} e^{i\nu(u-u')} e^{-\nu^2 \tau} \\ &= \frac{1}{2\sqrt{\pi\tau}} e^{-(u-u')^2/4\tau}, \end{aligned} \quad (2.35)$$

where again τ is defined in (2.29). This result is of the form (1.8), and, as discussed in the introduction, is similar in form to that of [17, 18]. Note that it is consistent with the ultraviolet conformal symmetry of the field theory: scale invariance (translation of the u coordinate) and inversion symmetry (reflection of the u coordinate) require dependence only on $(u - u')^2$.

Let us now consider the kernel at nonzero $t < 0$, working in the regime u, u' large and positive ($r \gg r_0$), and with $|t| \gg \Lambda^2$. In this regime the kernel is determined only by the conformally-invariant region of the gauge theory, and is independent of confinement effects, which we will treat later. This problem was first solved in the BFKL context in position space [28]. The result we obtain here bears some resemblance to the form anticipated in [31] and recently reconsidered in [41]. We obtain it directly in momentum space.

From (2.24) and (2.29), the exponential operator appearing in the kernel at $t \leq 0$ is (at leading order in $\ln s$) of the form $e^{-H\tau}$, where H is the Hamiltonian for Liouville quantum mechanics

$$-\sqrt{\lambda}\alpha'\Delta_2 \equiv H = -\partial_u^2 + V(u) \quad (2.36)$$

$$V(u) = 4 - z_0^2 t e^{-2u}. \quad (2.37)$$

Since $t < 0$ here, this is an exponentially growing potential as u decreases. If $z_0^2|t| = |t|/\Lambda^2 \gg 1$ the particle is repelled from the small- u region, so confinement effects are highly suppressed and the calculation becomes identical to the computation in a conformally invariant theory. The eigenvalue spectrum for H determines the location of the singularities in the j -plane, where $j = 2 - E/2\sqrt{\lambda}$. There is a continuum beginning at $E = 4$, with eigenvalues $E = 4 + \nu^2$, and corresponding eigenfunctions,

$$\psi(\nu, u) = \sqrt{2/\pi} K_{i\nu}(z_0\sqrt{|t|}e^{-u})/\Gamma(i\nu), \quad \nu > 0. \quad (2.38)$$

(For $t = 0$, this spectrum reduces to the free particle momentum states $e^{i\nu u}$.) Thus, independent of t , there is a cut in the j plane beginning at $E = 4$, that is, $j = j_0 = 2 - 2/\sqrt{\lambda}$. The kernel itself, however, has nontrivial t -dependence, since the exponential potential suppresses the eigenfunctions in regions where $u \ll u_t \equiv \ln(z_0\sqrt{|t|})$. The kernel can be written [42]

$$\mathcal{K}_0(u, u', \tau, t) = \frac{2}{\pi^2} \int_0^\infty d\nu \nu \sinh \pi\nu K_{i\nu}(z_0|t|^{1/2}e^{-u})K_{-i\nu}(z_0|t|^{1/2}e^{-u'})e^{-\nu^2\tau}. \quad (2.39)$$

This kernel is exponentially suppressed if either u or u' is much less than u_t .

For $u, u' \gg u_t$, the behavior of the kernel at small τ resembles the $t = 0$ kernel, while for $\tau \gg uu'$ the kernel falls¹² to zero as $\tau^{-3/2}$. This is due to the reflection of the diffusion off the exponentially rising potential. Indeed, the kernel is moderately well-approximated by the $t = 0$ kernel combined with reflection off a wall at $u = u_t$ with a Dirichlet boundary condition. To see this, it is useful to write $K_{i\nu}(x) = (i\pi/2)[I_{i\nu}(x) - I_{-i\nu}(x)]/\sinh \pi\nu$, so that incoming (“L”, for left-moving) and reflected waves (“R”-moving) are more explicit. The kernel now is a sum of LL , LR , RL and RR subkernels. Interference between the LL , RR terms and the LR , RL terms removes the $1/\nu$ pole as $\nu \rightarrow 0$, so the integrand goes as ν^2 near $\nu = 0$ and gives $\tau^{-3/2}$

¹²More precisely, at fixed τ and large $u, u' \gg u_t$, perturbation theory around the $t = 0$ case yields

$$\mathcal{K}_0(u, u', \tau, t) = \frac{1}{2\sqrt{\pi\tau}} e^{-\frac{(u-u')^2}{4\tau}} e^{\tau(z_0^2 t) \frac{(e^{-2u} - e^{-2u'})}{2(u-u')}}.$$

At large τ (for fixed $u, u' \gg u_t$) the kernel is dominated by the lowest mode, so for $\sqrt{\tau} \gg u, u' \gg u_t$

$$\mathcal{K}_0(u, u', \tau, t) \simeq \frac{1}{2\sqrt{\pi\tau^3}} K_0(z_0\sqrt{-t}e^{-u})K_0(z_0\sqrt{-t}e^{-u'}).$$

behavior. Meanwhile, the $t = 0$ kernel is obtained by going to large positive u , so that the barrier at $u = 0$ is infinitely distant and the $I_{i\nu}$ become plane waves; the LR and RL interference terms are exponentially suppressed after the ν integration, while the LL and RR terms can be seen as the $\nu > 0$ and $\nu < 0$ parts of the integral in (2.35). The $1/\nu$ pole multiplying the $I_{i\nu}(x)$ is no longer cancelled, and the standard $\tau^{-1/2}$ behavior of a diffusion kernel is obtained.

This $\tau^{-3/2}$ feature is very general and survives even when conformal symmetry breaking is introduced in the infrared, as we will see later. It corresponds to having a softened branch point in the j plane compared to the $t = 0$ conformal kernel. More precisely, the “partial-wave” amplitude, obtained by a Mellin transform of $\mathcal{K}(s)$, has a vanishing square-root type singularity,

$$\tilde{\mathcal{K}}(j, t, u, u') \sim \sqrt{j - j_0} + \text{regular}. \quad (2.40)$$

By contrast, at $t = 0$, where as we just saw the ν^2 factor is cancelled giving a non-vanishing contribution at $\nu = 0$, there is a divergent singularity in j ,

$$\tilde{\mathcal{K}}(j, t, u, u') \sim \frac{1}{\sqrt{j - j_0}} + \text{regular}. \quad (2.41)$$

Correspondingly, the large τ behavior is $s^{j_0}/\tau^{1/2}$ at $t = 0$. Thus, the branch cut in the j -plane begins at a t -independent point j_0 , but the nature of the cut differs at negative t from its form at $t = 0$.

The same physics — the reflection of the diffusion off an effective barrier at $e^{2u} \sim k_{\perp}^2 \sim |t|$ — leads to identical powers of τ at weak coupling. The barrier is absent at $t = 0$, so the eigenmodes are just plane waves in $\ln k_{\perp}$, giving the $\tau^{-1/2}$ behavior of Eq. (1.6). For $t < 0$, however, the eigenmodes are a combination of incoming and reflected modes, with the leading $\tau^{-1/2}$ behavior removed by destructive interference between them.

To see this, consider the standard weak-coupling BFKL calculation at finite t [28, 29]. The amplitude is expressed in terms of a $t < 0$ kernel and impact factors Ψ_A, Ψ_B ,

$$\frac{\text{Im } A(s, t)}{s} = \frac{\mathcal{G}}{(2\pi)^4} \int d^2 p_{\perp} d^2 p'_{\perp} \Psi_A(p_{\perp}, k_{\perp}) \mathcal{K}(s, k_{\perp}, p_{\perp}, p'_{\perp}) \Psi_B(p'_{\perp}, k_{\perp}) \quad (2.42)$$

where

$$\mathcal{K}(s, k_{\perp}, p_{\perp}, p'_{\perp}) = \frac{1}{(2\pi)^6} \int d\nu \left[\frac{\nu}{\nu^2 + 1/4} \right]^2 e^{\alpha_s \chi(\nu)\tau} \psi_{\nu}(p_{\perp}, k_{\perp}) \psi_{\nu}^*(p'_{\perp}, k_{\perp}). \quad (2.43)$$

Here ψ_{ν} is a conformal wave function, an eigenfunction of the homogeneous BFKL equation.¹³

¹³Our notation corresponds to a BFKL kernel that, as a four-point function, carries external

Care must be taken in comparing the weak- and strong-coupling representations since the effective degrees of freedom used are different. However, since conformal invariance plays an essential role here, it is not surprising that they share many qualitative and some quantitative similarities. In particular, the Bessel function in $\psi_\nu(p_\perp, k_\perp)$, while not identical in form to the one appearing in (2.39), shares the feature that it can be written as an incoming and an outgoing wave, and that the $t = 0$ kernel is obtained by effectively dropping the interference between them, resulting in a change in the ν -dependence at small ν . Thus the analytic structure in the j -plane, and the τ dependence, of the weak- and strong-coupling kernels agree.

We have not attempted to obtain more precise connections with weak coupling calculations — as is clear from the above formulas, the weak-coupling kernel at finite t is structurally more complicated than the $t = 0$ case — but we believe it should be possible to do so.

3. A systematic derivation

The result in the previous section is simple and intuitive, but it is useful to present a more systematic derivation. For one thing we have begun with an expression (2.9) in which the scattering is local in the bulk, and then (when s is taken large with λ) we have found a diffusive effect that makes the scattering arbitrarily nonlocal in the bulk. As a result we have had to guess about such things as operator ordering. For another, we are retaining all orders in $\ln s/\sqrt{\lambda}$. From the point of view of the world-sheet theory this is a resummation of perturbation theory, and we would like to determine its exact nature. We will see that it is something familiar: that the large s amplitudes will involve world-sheet distances of order $1/s$, so this is simply a renormalization group improvement in the world-sheet field theory.

3.1 Regge behavior in flat spacetime

We first analyze Regge scattering in flat spacetime in a rather general way which may have other applications. For any process in which the external particles (which

transverse momenta $p_\perp \pm k_\perp/2$ and $p'_\perp \pm k_\perp/2$, with $t = -k_\perp^2$; it has a dimension of $[length]^6$. We have retained only the leading order term, i.e., the so-called $n = 0$ term, for the BFKL kernel, with χ in Eq. (2.43) related to \hat{j} of (1.3) by $\hat{j} = 1 + \alpha_s \chi$. To match the formulas in the BFKL literature, e.g., [19], we have normalized the dummy variable ν in a way *which differs from that used in the rest of the paper* by a factor of 2, as noted earlier. We find that the conformal wave function can be expressed, defining the functions $a_1^2 \equiv x(1-x)(k_\perp^2/p_\perp^2)$, and $a_2^2 \equiv |p_\perp + (x - \frac{1}{2})k_\perp|^2/p_\perp^2$, as

$$\begin{aligned} \psi_\nu(p_\perp, k_\perp) &= \frac{(2\pi)(|k_\perp|/2)^{2i\nu}}{\Gamma^2(\frac{1}{2} + i\nu)} \int_0^1 \frac{dx}{\sqrt{x(1-x)}} \int_0^\infty dr r^2 J_0(a_2|p_\perp|r) K_{-2i\nu}(a_1|p_\perp|r) \\ &= \frac{(2\pi)^2(\nu^2 + 1/4)(k_\perp/2)^{2i\nu}}{\cosh \pi\nu \Gamma^2(\frac{1}{2} + i\nu)} \int_0^1 \frac{dx}{p_\perp^3 [x(1-x)]^2} F(-i\nu + 3/2, i\nu + 3/2; 1; -a_2^2/a_1^2). \end{aligned}$$

may include D-branes as well as strings) can be divided into two sets that are at large relative boost, we derive the leading behavior of the amplitude.

3.1.1 Example: Bosonic string tachyons

Consider the Virasoro-Shapiro amplitude, for bosonic string tachyon scattering:¹⁴

$$\mathcal{A} = \int d^2w |w|^{-4-\alpha't/2} |1-w|^{-4-\alpha's/2} . \quad (3.1)$$

When s and t are both large, the integrand has a saddle point at $w = t/(s+t)$. When the integral is appropriately defined by analytic continuation, this point indeed dominates [43]. If this were to continue to apply for large s at fixed t , then w of order s^{-1} would dominate in the Regge regime. This is true but the integral can no longer be evaluated by the saddle point method, rather we must integrate it explicitly in the small- w region:

$$\begin{aligned} \mathcal{A} &\sim \int d^2w |w|^{-4-\alpha't/2} e^{\alpha's(w+\bar{w})/4} \\ &= 2\pi \frac{\Gamma(-1-\alpha't/4)}{\Gamma(2+\alpha't/4)} (e^{-i\pi/2} \alpha's/4)^{2+\alpha't/2} . \end{aligned} \quad (3.2)$$

The integral is defined by continuation from $-4 > \alpha't > -8$ and positive imaginary s .

Since w is small we should be able to reproduce the above Regge behavior via the OPE,

$$e^{ip_1 \cdot X(w, \bar{w})} e^{ip_2 \cdot X(0)} \sim |w|^{-4-\alpha't/2} e^{ik \cdot X(0)} , \quad k = p_1 + p_2 . \quad (3.3)$$

However, this reproduces only the first term in the integrand (3.1): it gives the tachyon pole but not the Regge behavior. The point is that because sw is of order one we must retain additional terms in the OPE, which are normally subleading. The result is still quite simple:

$$e^{ip_1 \cdot X(w, \bar{w})} e^{ip_2 \cdot X(0)} \stackrel{\text{Regge}}{\sim} |w|^{-4-\alpha't/2} e^{ik \cdot X(0) + ip_1 \cdot (w\partial + \bar{w}\bar{\partial})X(0)} . \quad (3.4)$$

Contractions involving $p_1 \cdot (w\partial + \bar{w}\bar{\partial})X(0)$ will generate a factor of s for each factor of w . We insert the OPE into the vertex operator amplitude,

$$\begin{aligned} &\langle e^{ip_1 \cdot X(w, \bar{w})} e^{ip_2 \cdot X(0)} e^{ip_3 \cdot X(1)} e^{ip_4 \cdot X(\infty)} \rangle \\ &\sim |w|^{-4-\alpha't/2} \left\langle e^{ik \cdot X(0) + ip_1 \cdot (w\partial + \bar{w}\bar{\partial})X(0)} e^{ip_3 \cdot X(1)} e^{ip_4 \cdot X(\infty)} \right\rangle . \end{aligned} \quad (3.5)$$

¹⁴In order to keep equations uncluttered, we adopt simple overall normalizations in Eqs. (3.1), (3.6), but keep all later equations normalized with respect to these. For the same reason we omit the momentum delta functions in the translationally invariant directions.

Evaluating the contractions reproduces the integrand in eq. (3.2). It is also interesting to instead carry out the w integral first, at the operator level:

$$\int d^2w e^{ip_1 \cdot X(w, \bar{w})} e^{ip_2 \cdot X(0)} \overset{\text{Regge}}{\approx} \Pi(\alpha't) e^{ik \cdot X(0)} [p_1 \cdot \partial X p_1 \cdot \bar{\partial} X(0)]^{1+\alpha't/4}, \quad (3.6)$$

where we have defined

$$\Pi(\alpha't) = 2\pi \frac{\Gamma(-1 - \alpha't/4)}{\Gamma(2 + \alpha't/4)} e^{-i\pi - i\pi\alpha't/4}, \quad (3.7)$$

with $t = -k^2$. Inserting this matrix element into the expectation value (3.5) immediately gives the Regge amplitude (3.2).

The result (3.6) displays the essential idea that we will need for analyzing Regge behavior in curved spacetime as well. We can think of the operator on the right as a Pomeron vertex operator. For $t = -4/\alpha'$ it is the tachyon, for $t = 0$ it is the graviton, and so on. Note that it is always on shell in the sense of satisfying the physical state conditions,¹⁵ even when t is not the mass-squared of a physical particle, but it is outside the normal Hilbert space because of the fractional power. In spite of the importance of Regge physics in the history of string theory, we are unaware of any previous introduction of such a vertex operator.

3.1.2 Generalizations

The result (3.6), derived for four tachyons, can be broadly generalized. First, let us note that the OPE (3.4) is essentially the same for any pair of vertex operators,

$$\mathcal{V}_1(w, \bar{w}) \mathcal{V}_2(0) \sim C_{12} |w|^{-4-\alpha't/2} e^{ik \cdot X(0) + ip_1 \cdot (w\partial + \bar{w}\bar{\partial})X(0)}. \quad (3.8)$$

The tensor terms in the vertex operators contract to give a constant C_{12} times a power of $|w|$, and then the rest is as for the tachyons; the final power of $|w|$ depends only on the momentum transfer. We can again integrate this directly in operator form,

$$\int d^2w \mathcal{V}_1(w, \bar{w}) \mathcal{V}_2(0) \sim C_{12} \Pi(\alpha't) e^{ik \cdot X(0)} [p_1 \cdot \partial X p_1 \cdot \bar{\partial} X(0)]^{1+\alpha't/4}. \quad (3.9)$$

The constant C_{12} can be interpreted as the coupling of the Pomeron to states 1 and 2; we will express this coupling in another form in eq. (3.19) below.

Having the relation (3.9) in operator form immediately allows a broad generalization: we can replace the tachyon vertex operators $\mathcal{V}_3, \mathcal{V}_4$ with any number $l \geq 2$ of vertex operators, for any collection of string states. The Möbius group fixes \mathcal{V}_2 plus two of the l additional vertex operators. Let \mathcal{W} denote the product of the l vertex

¹⁵To be precise, we should replace $2p_1$ with $p_1 - p_2 = p_{12}$; these are equivalent in the Regge limit but p_{12} is exactly orthogonal to k .

operators and their $l - 2$ position integrations. Then the standard string amplitude is

$$\mathcal{A}_{12\mathcal{W}} \sim C_{12} \Pi(\alpha't) \left\langle e^{ik \cdot X(0)} [p_1 \cdot \partial X p_1 \cdot \bar{\partial} X(0)]^{1+\alpha't/4} \mathcal{W} \right\rangle . \quad (3.10)$$

This captures the asymptotic behavior as the vertex operators in \mathcal{W} are boosted to some large rapidity y , relative to \mathcal{V}_1 and \mathcal{V}_2 . Then

$$e^y = s/s_0 , \quad y = 2\sqrt{\lambda}\tau + \text{const} , \quad (3.11)$$

where s_0 is the center of mass energy-squared when the relative boost is zero and τ is the diffusion time introduced earlier. Contractions of $\partial X(0)$ or $\bar{\partial} X(0)$ in the Pomeron vertex operator with fields in \mathcal{W} are of order e^y , producing a factor of $e^{(2+\alpha't/2)y}$. We will refer to $\mathcal{V}_{1,2}$ as right-moving and \mathcal{W} as left-moving along the direction of the boost.

The results so far are still special, in that we have an arbitrary left-moving process but on the right-moving side there is just 1-to-1 scattering. To derive the Regge amplitude in full generality, let \mathcal{W}_R and \mathcal{W}_L denote arbitrary sets of l_R and l_L vertex operators together with their associated $l_R - 2$ and $l_L - 2$ world-sheet integrations. This leaves a single integration over world-sheet coordinates, corresponding to an overall scaling of the coordinates in \mathcal{W}_L . The string amplitude is then

$$A_{\mathcal{W}_L \mathcal{W}_R} = \int d^2w \left\langle \mathcal{W}_R w^{L_0-2} \bar{w}^{\tilde{L}_0-2} \mathcal{W}_L \right\rangle , \quad (3.12)$$

where L_0 and \tilde{L}_0 are the right- and left-moving Virasoro operators which generate the world-sheet scale transformations,

$$L_0 = \frac{\alpha'}{4} k^2 + N , \quad \tilde{L}_0 = \frac{\alpha'}{4} k^2 + \tilde{N} , \quad (3.13)$$

and N and \tilde{N} are the right- and left-moving excitation levels. This is a standard way of organizing string amplitudes for purposes of discussing unitarity: the integral over the region $|w| < 1$ produces the closed string propagator in the t -channel,

$$\frac{\delta_{L_0 - \tilde{L}_0}}{L_0 + \tilde{L}_0 - 2} . \quad (3.14)$$

Note also that the OPE (3.4) can similarly be written

$$\begin{aligned} e^{ip_1 \cdot X(w, \bar{w})} e^{ip_2 \cdot X(0)} &\stackrel{\text{Regge}}{\sim} |w|^{-4-\alpha't/2} e^{ik \cdot X(0) + ip_1 \cdot (w\partial + \bar{w}\bar{\partial})X(0)} \\ &= w^{L_0-2} \bar{w}^{\tilde{L}_0-2} e^{ik \cdot X(0) + ip_1 \cdot (\partial + \bar{\partial})X(0)} ; \end{aligned} \quad (3.15)$$

for the bosonic string N and \tilde{N} just count the number of ∂ and $\bar{\partial}$ in the vertex operator.

We wish to study the amplitude in the limit that the two sets differ by a large boost in the \pm plane, so that the momenta in \mathcal{W}_R have large $+$ components and the

momenta in \mathcal{W}_L have large $-$ components; the exchanged momentum k is orthogonal to the \pm plane. The generalization of the OPE is to insert a complete set of string states in the matrix element (3.12) but again to retain only those that survive in the Regge limit $sw \sim 1$:

$$A_{\mathcal{W}_L \mathcal{W}_R} \sim \sum_{m,n=0}^{\infty} \int d^2 w \frac{2^{m+n} w^{m-2-\alpha't/4} \bar{w}^{n-2-\alpha't/4}}{\alpha'^{m+n} m! n!} \langle \mathcal{W}_R e^{ik \cdot X} (\partial X^-)^m (\bar{\partial} X^-)^n \rangle \langle e^{-ik \cdot X} (\partial X^+)^m (\bar{\partial} X^+)^n \mathcal{W}_L \rangle . \quad (3.16)$$

Note that $\partial X, \bar{\partial} X$ are the vertex operator factors for the string excitations $\alpha_{-1}, \tilde{\alpha}_{-1}$. After inserting the states, we have explicitly evaluated $w^{L_0-2} \bar{w}^{\tilde{L}_0-2}$ acting on the intermediate vertex operator. The next step is typographically tricky. We note that all the m -dependent terms combine to form an exponential, and similarly all the n -dependent terms:

$$\exp(2w \partial X_R^- \partial X_L^+ / \alpha' + 2\bar{w} \bar{\partial} X_R^- \bar{\partial} X_L^+ / \alpha') , \quad (3.17)$$

where the subscripts indicate whether the operator appears in the expectation value with \mathcal{W}_R or the one with \mathcal{W}_L . Acting now with $\int d^2 w |w|^{-4-\alpha't/2}$ (where the integral is defined by continuation as before), the exponential (3.17) becomes

$$\Pi(\alpha't) (2\partial X_R^- \bar{\partial} X_R^- / \alpha')^{1+\alpha't/4} (2\partial X_L^+ \bar{\partial} X_L^+ / \alpha')^{1+\alpha't/4} \quad (3.18)$$

Inserting this back in the amplitude gives

$$A_{\mathcal{W}_L \mathcal{W}_R} \sim \Pi(\alpha't) \times \langle \mathcal{W}_R e^{ik \cdot X} (2\partial X^- \bar{\partial} X^- / \alpha')^{1+\alpha't/4} \rangle \langle e^{-ik \cdot X} (2\partial X^+ \bar{\partial} X^+ / \alpha')^{1+\alpha't/4} \mathcal{W}_L \rangle . \quad (3.19)$$

We could have guessed this by symmetrizing the earlier result (3.10). We can also make the Regge behavior more explicit by boosting the states \mathcal{W}_L and \mathcal{W}_R back to their approximate rest frames (denoted by a subscript 0), so that the large boost $e^y = s/s_0$ enters explicitly:

$$A_{\mathcal{W}_L \mathcal{W}_R} \sim \Pi(\alpha't) (s/s_0)^{2+\alpha't/2} \langle \mathcal{W}_{R0} \mathcal{V}_P^- \rangle \langle \mathcal{V}_P^+ \mathcal{W}_{L0} \rangle . \quad (3.20)$$

The result (3.20) has a simple interpretation as a Pomeron propagator, of the form $\Pi(\alpha't) (s/s_0)^{2+\alpha't/2}$, times the couplings of the Pomeron to the two sets of vertex operators, with Pomeron vertex operator

$$\mathcal{V}_P^\pm = (2\partial X^\pm \bar{\partial} X^\pm / \alpha')^{1+\alpha't/4} e^{\mp ik \cdot X} . \quad (3.21)$$

Note that this formalism works equally well for Regge scattering of strings and D-branes or of D-branes and D-branes. For coupling to a D-brane one simply replaces the vertex operators in \mathcal{W} with a world-sheet hole with appropriate boundary

conditions, and the factorization analysis goes through unchanged. Thus, scattering processes involving ultrarelativistic D-branes will also display Regge behavior [44].

This analysis extends readily to the superstring. Let us start for simplicity with the OPE of two type II tachyons; these have the wrong GSO projection but their product is then GSO-allowed. We work in the 0 picture because this is most closely analogous to the bosonic string and to other formulations of the superstring. Then

$$\begin{aligned}
& \int d^2w d^2\theta d^2\theta' e^{ip_1 \cdot \mathbf{X}(w,\theta)} e^{ip_2 \cdot \mathbf{X}(0,\theta')} \\
& \sim \int d^2w d^2\theta d^2\theta' |w - \theta\theta'|^{-2-\alpha't/2} e^{ik \cdot \mathbf{X}(0,\theta') + ip_1 \cdot (w\partial_w + [\theta - \theta']\partial_{\theta'}) \mathbf{X}(0,\theta')} \\
& = \hat{\Pi}(\alpha't) \int d^2\theta' e^{ik \cdot \mathbf{X}} p_1 \cdot D_{\theta'} \mathbf{X} p_1 \cdot D_{\bar{\theta}'} \mathbf{X} (p_1 \cdot \partial \mathbf{X} p_1 \cdot \partial \mathbf{X})^{\alpha't/4} |_{0,\theta'} \\
& \equiv \hat{\Pi}(\alpha't) \hat{\mathcal{V}}_P .
\end{aligned} \tag{3.22}$$

The Pomeron vertex operator has the same bosonic part as in the bosonic string, together with fermionic terms as required by world-sheet supersymmetry. The Pomeron propagator no longer has a tachyon pole:

$$\hat{\Pi}(\alpha't) = 2\pi \frac{\Gamma(-\alpha't/4)}{\Gamma(1 + \alpha't/4)} e^{-i\pi\alpha't/4} . \tag{3.23}$$

This result, derived for the simplest vertex operators, can then be generalized broadly as in the bosonic case:

$$\mathcal{A}_{\mathcal{W}_L \mathcal{W}_R} \sim \hat{\Pi}(\alpha't) (s/s_0)^{2+\alpha't/2} \left\langle \mathcal{W}_{R0} \hat{\mathcal{V}}_P^- \right\rangle \left\langle \hat{\mathcal{V}}_P^+ \mathcal{W}_{L0} \right\rangle . \tag{3.24}$$

3.2 Regge behavior in warped spacetime

Now let us try to repeat these steps in a warped metric

$$ds^2 = e^{2A(y)} \eta_{\mu\nu} dX^\mu dX^\nu + ds_\perp^2 . \tag{3.25}$$

We again start with the bosonic string to avoid tensor complications.¹⁶ In the Gaussian limit the string wavefunctions (2.4) translate directly into vertex operators $e^{ip \cdot X} \psi(Y)$, where the capital letters denote world-sheet fields. We start with the OPE

$$\begin{aligned}
& e^{ip_1 \cdot X(w,\bar{w})} \psi_1(Y(w,\bar{w})) e^{ip_2 \cdot X(0)} \psi_2(Y(0)) \\
& \stackrel{\text{Regge}}{\sim} w^{L_0-2} \bar{w}^{\bar{L}_0-2} e^{ik \cdot X(0) + ip_1 \cdot (\partial + \bar{\partial}) X(0)} \psi_1(Y(0)) \psi_2(Y(0)) .
\end{aligned} \tag{3.26}$$

¹⁶We do not know of any AdS_5 solutions for the bosonic string, so this is slightly formal. However, there is an $AdS_3 \times S^3 \times T^{20}$ solution, to which the analysis at $t = 0$ applies. This solution might be interesting to explore further because the world-sheet CFT is exact.

This is identical in form to the flat spacetime OPE (3.15): we naively multiply the vertex operators, keeping only those terms that survive in the Regge limit, and the w -dependence arises from the Virasoro generators. Now, however, we need to go beyond the Gaussian approximation to include terms of order $(\ln s)/\sqrt{\lambda} \sim |\ln w|/\sqrt{\lambda}$. In the form (3.26) it is clear how this is done: we must keep terms of order $1/\sqrt{\lambda}$ in the world-sheet dimension L_0 . This is precisely the renormalization group improvement referred to at the beginning of the section.

In order to diagonalize L_0 we must go to a basis of definite spin,

$$\mathcal{V}(j) = (\partial X^+ \bar{\partial} X^+)^{j/2} e^{ik \cdot X} \phi_{+j}(Y) , \quad (3.27)$$

working again in the frame where the large momentum is p_+ . The operator on the right of the OPE (3.26) can be expanded in such a basis. The one-loop world-sheet dimension of $\mathcal{V}(j)$ (which includes all terms up to second derivatives in space-time) must be of the form

$$L_0 \mathcal{V}(j) = \tilde{L}_0 \mathcal{V}(j) = (\partial X^+ \bar{\partial} X^+)^{j/2} \left[\frac{j}{2} - \frac{\alpha'}{4} (\Delta_j + \delta_j) \right] e^{ik \cdot X} \phi_{+j}(Y) , \quad (3.28)$$

where Δ_j is the covariant Laplacian defined before and δ_j is an unknown shift of order R^{-2} . The calculation of δ_j is an interesting exercise in string theory, which perhaps already exists in some form in the literature, but for our present purposes we can argue as in the previous section. That is, for $j = 2$ we know from the low energy field equations that $\delta_2 = 0$, and the relevant j are close to 2, and so

$$L_0 \mathcal{V}(j) = \tilde{L}_0 \mathcal{V}(j) = (\partial X^+ \bar{\partial} X^+)^{j/2} \left[\frac{j}{2} - \frac{\alpha'}{4} \Delta_j \right] e^{ik \cdot X} \phi_{+j}(Y) + O(1/\lambda) . \quad (3.29)$$

Note that we are keeping $\Delta_j = e^{(j-2)A} \Delta_2 e^{-(j-2)A}$ rather than the simpler Δ_2 for good form, because it has the correct covariance properties.

Applying this to the OPE, Eq. (3.26), the j -dependent factors, $e^{\pm jA}$ in Δ_j can be combined as $(e^{2[A(Y_L) - A(Y_R)]} \partial X^+ \bar{\partial} X^+)^{j/2}$, where we have again introduced an ordering notation, such that $A(Y_L)$ and $A(Y_R)$ are understood to act to the left or right of the Laplacian, respectively. Then

$$\begin{aligned} & e^{ip_1 \cdot X(w, \bar{w})} \psi_1(Y(w, \bar{w})) e^{ip_2 \cdot X} \psi_2(Y) \\ &= e^{\{ik \cdot X + ie^{[A(Y_L) - A(Y_R)]} p_1 \cdot (w\partial + \bar{w}\bar{\partial})X\}} e^{-2A(Y)} |w\bar{w}|^{-2 - \alpha' \Delta_2/4} e^{2A(Y)} \psi_1(Y) \psi_2(Y) \\ &= e^{\{ik \cdot X + ie^{[A(Y_L) - A(Y_R)]} p_1 \cdot (w\partial + \bar{w}\bar{\partial})X\}} F(Y) , \end{aligned} \quad (3.30)$$

where

$$F(y) = e^{-2A(y)} |w\bar{w}|^{-2 - \alpha' \Delta_2/4} e^{2A(y)} \psi_1(y) \psi_2(y) .$$

Fields without arguments are understood to be at the origin, for compactness.

Now consider the matrix element

$$\begin{aligned} & \langle \mathcal{V}_1(w, \bar{w}) \mathcal{V}_2(0) \mathcal{V}_3(1) \mathcal{V}_4(\infty) \rangle \\ &= \left\langle e^{ik \cdot X + ie^{A(Y_L) - A(Y_R)} p_1 \cdot (w\partial + \bar{w}\bar{\partial})X} F(Y) e^{ip_3 \cdot X(1)} \psi_3(Y(1)) e^{ip_4 \cdot X(\infty)} \psi_4(Y(\infty)) \right\rangle. \end{aligned} \quad (3.31)$$

We next evaluate this in the semiclassical approximation. At the saddle point, $X^M(\sigma^1, \sigma^2) = x^M$ is constant on the world-sheet: to first approximation we just replace the fields with the zero modes. The leading contribution of the $p_1 \cdot \partial_a X$ in the exponent comes from their contraction with $p_3 \cdot X(1)$, where the propagator is evaluated at fixed values of the zero modes. The action for the X^μ is multiplied by $e^{2A(y)}/\alpha'$, so this gives

$$-\frac{\alpha'}{2} e^{-A(Y_L) - A(Y_R)} p_1 \cdot p_3 = [\alpha'_{\text{eff}}(Y_L) \alpha'_{\text{eff}}(Y_R)]^{1/2} \frac{S}{4} \equiv \bar{\alpha}' \frac{S}{4} \quad (3.32)$$

for each contraction. Integrating the zero mode with weight $\sqrt{-G} = e^{4A} \sqrt{G_\perp}$, the matrix element becomes

$$\text{const.} \times \int d^6 y \sqrt{G_\perp} e^{2A(y)} \psi_3(y) \psi_4(y) e^{-\bar{\alpha}' s (w + \bar{w})/4} |w\bar{w}|^{-2 - \alpha' \Delta_2/4} e^{2A(y)} \psi_1(y) \psi_2(y). \quad (3.33)$$

Finally, taking $\int d^2 w$ gives

$$\mathcal{T}_4 = \text{const.} \times \int d^6 y \sqrt{G_\perp} e^{2A(y)} \psi_3(y) \psi_4(y) \Pi(\alpha' \Delta_2) (\bar{\alpha}' s)^{2 + \alpha' \Delta_2/2} e^{2A(y)} \psi_1(y) \psi_2(y). \quad (3.34)$$

Noting that $\alpha' \Delta_2 \approx \alpha'(r)t$, this reproduces the earlier result (2.24). The operator ordering issue raised there has been resolved, and in particular the kernel is symmetric (note that $\Delta_2 = e^{2A} (\sqrt{G_\perp}^{-1}) \partial_M e^{-4A} \sqrt{G_\perp} G^{MN} \partial_N e^{2A}$). Also, the appearance of $\bar{\alpha}'$ confirms the assertions about the diffusion time that were made in footnote 11.

The logic of the world-sheet calculation is exactly as in any weakly coupled field theory for a correlation function with a large hierarchy of separations: we evaluate the OPE in lowest order, renormalize the resulting operators with the one loop anomalous dimension, and evaluate the final matrix element to lowest order. The result (3.34) is extended readily to the superstring and to any external scalars.

3.3 BFKL and anomalous dimensions

Our result on $j_0 - 2$ is situated in a wider context. The study of the relationship between Regge singularities and anomalous dimensions of certain operators has a long history [45]. In $\mathcal{N} = 4$ supersymmetric Yang-Mills theory, it has been argued that properties of BFKL and DGLAP operators are related by analyticity [46, 47, 48, 49]. We can understand this connection also from the string theory side of the duality. In

this subsection we do so in the large- λ approximation that we have used throughout; in the next we argue that it extends to all values of λ .

This discussion takes place in the conformal limit, where the spacetime is $AdS_5 \times W$. The AdS/CFT dictionary relates string states to local operators in the gauge theory [36, 37]. Consider the vertex operator

$$(\partial X^+ \bar{\partial} X^+)^{j/2} e^{ik \cdot X} \phi_{+j}(Y), \quad \phi_{+j}(Y) = e^{\zeta U}. \quad (3.35)$$

That is, the transverse part of the vertex operator depends only on the radial coordinate U . Under scale transformations $\delta U = \epsilon$, $\delta X^\mu = -\epsilon X^\mu$, this has weight $\zeta - j$. It corresponds to a perturbation

$$\int d^4x \mathcal{O}, \quad (3.36)$$

where \mathcal{O} is an operator of spin j and dimension Δ ; the scale transformation determines that

$$\Delta - 4 = \zeta - j. \quad (3.37)$$

The physical state conditions $L_0 = \tilde{L}_0 = 1$ determine ζ and hence Δ as a function of j . This is the ‘nonnormalizable mode’ [36, 37]; the space-time inversion symmetry implies a second solution $\Delta \rightarrow 4 - \Delta$. The vertex operators (3.35) for integer $j \geq 2$ (in the IIB theory) correspond to the lightest string states of given spin, and so are dual to the lowest dimension operators of those spins. These would be the leading twist operators, whose gauge part is $\text{tr}(F_{+\mu} D_+^{j-2} F_+^\mu)$. Thus the physical state conditions determine the dimensions of the leading twist operators.

On the other hand, the vertex operators (3.35) are of the same form as the Pomeron vertex operator that controls the Regge behavior. As in Eqs. (2.30)–(2.35), we take plane wave normalizable states. In the invariant inner product

$$\int d^4x du \sqrt{-G} (G_{+-})^{-j} \phi_{+j} \phi_{-j} = \int d^4x du e^{(4-2j)u} \phi_{+j} \phi_{-j}, \quad (3.38)$$

the plane wave states would be $e^{(j-2)u} e^{i\nu u}$, that is, $\zeta = j - 2 + i\nu$. The dimension (3.37) is then

$$\Delta = 2 + i\nu. \quad (3.39)$$

We have seen that the Pomeron vertex operator gets extended to general j in the analysis of the Regge limit. Similarly the gauge theory operators can be extended to general j [50] (they are no longer local). Thus it is natural to think of Δ as a function of complex j , or more precisely that the physical state conditions define a curve in the Δ - j plane. The operator dimensions (which enter into DGLAP evolution) are given by $\Delta(j)$ at $j = 2, 3, 4, \dots$. The BFKL exponents are given by the inverse function $j(\Delta)$ at $\Delta = 2 + i\nu$, and in particular $j_0 = j(2)$.

Let us now repeat the large- λ calculation of j_0 in light of the above discussion. We have the physical state condition

$$1 = L_0 = \frac{j}{2} - \frac{1}{4\sqrt{\lambda}}(\Delta - 2)^2 + \frac{1}{\sqrt{\lambda}}. \quad (3.40)$$

The first term on the right is the oscillator level. The form of the second term is determined by inversion symmetry; its coefficient follows by lifting the Virasoro generators (3.13) to curved space and matching the term $-(\alpha'/4R^2)\partial_u^2$. The value of the final constant follows from the solution $j = 2, \Delta = 4$, corresponding to the energy-momentum tensor. Finally, $j_0 = 2 - 2/\sqrt{\lambda}$ is obtained by setting $\Delta = 2$. This is similar to the discussion in ref. [40].

3.4 Extension to general λ

Thus far we have leaned heavily on semiclassical calculations on the world-sheet. In this section we would like to set up the framework as much as possible without this assumption. We might hope in the future to extend our results to higher order in $1/\sqrt{\lambda}$, and also to attempt to make some contact with the strongly coupled world-sheet theories that would be dual to perturbative gauge theories. In order to have some constraint on the structure we will focus on the high energy conformal regime.

The calculations thus far indicate the general strategy, factorizing in the t -channel in terms of a sum over Pomeron vertex operators. We keep only the leading Regge trajectory, meaning vertex operators constructed from the undifferentiated $X^{3,4}$ and U fields, and from $\partial_{w,\bar{w}}X^\pm$. That is, we are assuming that as λ is varied the dominant Pomeron states are in one-to-one correspondence with those at large λ ; this appears to be consistent with what is known at small λ , as we note below. At $t = 0$, a complete set of vertex operators is of the form

$$\mathcal{V}_{\pm j, \nu, 0} = e^{(j-2+i\nu)U} (\partial X^\pm \bar{\partial} X^\pm)^{j/2}. \quad (3.41)$$

In the previous section we used a semiclassical argument to justify this, but we believe that it is simply a consequence of symmetry: these are the principal continuous representations of the conformal group [51]. Similarly for negative $t = -k^2$,

$$\mathcal{V}_{\pm j, \nu, k} \propto e^{ik \cdot X} e^{(j-2)U} K_{i\nu}(z_0|t|^{1/2} e^{-U}) (\partial X^\pm \bar{\partial} X^\pm)^{j/2}; \quad (3.42)$$

for positive t the Bessel function becomes $J_{i\nu}$. Again these forms should be completely determined by conformal symmetry.

The quantum numbers (j, ν, k) commute with L_0, \tilde{L}_0 , so

$$L_0 \mathcal{V}_{j, \nu, k} = \tilde{L}_0 \mathcal{V}_{j, \nu, k} = h_{j, \nu} \mathcal{V}_{j, \nu, k}, \quad (3.43)$$

where the weight h is a function of the spin and the $SO(2, 2)$ Casimir; for example, at strong coupling eq. (3.40) gives $h_{j, \nu} = \frac{1}{2}j + \frac{1}{4}(\nu^2 + 4)/\sqrt{\lambda}$. The coefficient of the

unit operator in the OPE of two such operators is then

$$\mathcal{V}_{j,\nu,k}(w, \bar{w})\mathcal{V}_{j',\nu',k'}(0, 0) \sim \frac{c_{j,\nu}}{(w\bar{w})^{h_{j,\nu}}}(2\pi)^4\delta(j+j')\delta(\nu+\nu')\delta^2(k+k') . \quad (3.44)$$

General principles of CFT (see Chapter 6.7 of [52]) then give the factorization

$$\langle \mathcal{W}_R w^{L_0-2} \bar{w}^{\bar{L}_0-2} \mathcal{W}_L \rangle = \int \frac{dj d\nu}{(2\pi)^2} \frac{(w\bar{w})^{h_{j,\nu}-2}}{c_{j,\nu}} \langle \mathcal{W}_R \mathcal{V}_{j,\nu,k} \rangle \langle \mathcal{V}_{-j,-\nu,-k} \mathcal{W}_L \rangle . \quad (3.45)$$

We are using a non-standard Hilbert space for the \pm oscillators, so we must determine the path of the j -integral. We can think of j as being introduced through a Mellin transformation with respect to s , and so the j integral is an inverse Mellin transformation. Thus the j integral runs parallel to the imaginary axis, $\text{Re}(j) = j_*$, and to the right of all singularities.

Now take the integral d^2w in a neighborhood of the origin; in order for this to converge at 0 we first deform the contour to large j_* . Integrating and also boosting back to the approximate rest frames, we have

$$\mathcal{T} \sim \int \frac{dj d\nu}{(2\pi)^2} \frac{(s/s_0)^j}{c_{j,\nu}(h_{j,\nu}-1)} \langle \mathcal{W}_{R0} \mathcal{V}_{j,\nu,k} \rangle \langle \mathcal{V}_{-j,-\nu,-k} \mathcal{W}_{L0} \rangle . \quad (3.46)$$

In order to obtain the large- s asymptotics we now deform the contour back toward negative j_* , picking up the pole in $h_{j,\nu}-1$ having the largest j ; call this $j(\nu)$. Then

$$\mathcal{T} \sim \int \frac{d\nu}{(2\pi)} \frac{(s/s_0)^{j(\nu)} \text{Res}(\nu)}{c_{j(\nu),\nu}} \langle \mathcal{W}_{R0} \mathcal{V}_{j(\nu),\nu,k} \rangle \langle \mathcal{V}_{-j(\nu),-\nu,-k} \mathcal{W}_{L0} \rangle . \quad (3.47)$$

From this formal argument we can anticipate that much of the qualitative physics at large λ will persist to smaller values of λ . The inversion symmetry of the conformal group, which takes $u \rightarrow u_0 - u$ for any u_0 , implies that $j(\nu)$ can depend only on ν^2 . Therefore $\nu = 0$ is an extremum, presumably a maximum,¹⁷ of $j(\nu)$. This ensures there is a cut extending from some value $j = j_0$ at $\nu = 0$ down to smaller values of j . The leading behavior at large s will always be given by expanding

$$j(\nu) \approx j_0 - \mathcal{D}\nu^2 + \text{order}(\nu^4) . \quad (3.48)$$

Evaluating the ν integral (3.47) by saddle point again gives, at $t = 0$, a diffusion kernel in U . For negative t , the vertex operators (3.42) are damped at small U , generalizing the result found in the effective quantum mechanics at large λ ; there is effectively a repulsive potential in this region. Meanwhile, the end of the cut, j_0 , is t -independent for all λ , because the eigenvalue $h_{j,\nu}$ can be obtained at large U , where the vertex operator is asymptotically independent of t . See our discussion surrounding Eq. (2.39).

¹⁷At weak coupling, Ref. [49] gives $j(\nu)$ in $\mathcal{N} = 4$ Yang-Mills through three loops.

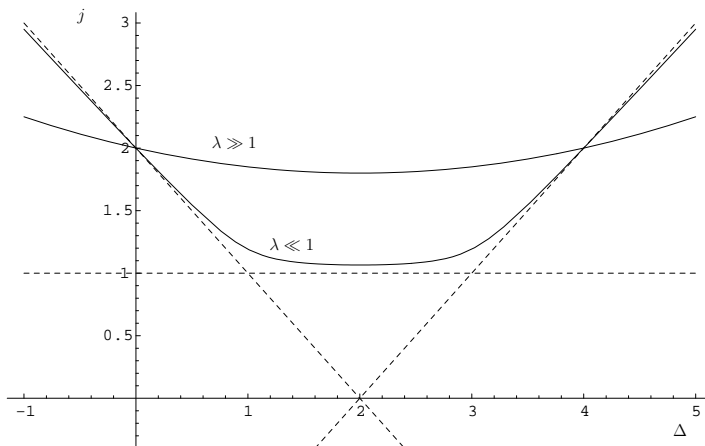


Figure 2: Schematic form of the $\Delta - j$ relation for $\lambda \ll 1$ and $\lambda \gg 1$. The dashed lines show the $\lambda = 0$ DGLAP branch (slope 1), BFKL branch (slope 0), and inverted DGLAP branch (slope -1). Note that the curves pass through the points $(4, 2)$ and $(0, 2)$ where the anomalous dimension must vanish. This curve is often plotted in terms of $\Delta - j$ instead of Δ , but this obscures the inversion symmetry $\Delta \rightarrow 4 - \Delta$.

The DGLAP dimensions and BFKL exponent are still determined by the same vertex operator, so the relation discussed in the previous section should hold for all λ , consistent with the weak coupling result. That is, j_0 is determined by $\Delta(j_0) = 2$. In the large- λ limit we have studied the Δ - j relation only near $j = 2$, where it takes the form (3.40).

In the weakly coupled limit the (Δ, j) locus has a complicated structure [45]. In the normal operator analysis one has $\Delta = 2 + j + O(g^2)$, i.e. twist two in the free limit. BFKL identify another branch to the solution, where $j = 1 + O(g^2)$. The inversion symmetry $\Delta \rightarrow 4 - \Delta$ implies a third branch $\Delta = 2 - j + O(g^2)$. It follows that at zero coupling the Pomeron physical state condition must be

$$(\Delta - 2 - j)(\Delta - 2 + j)(j - 1) = 0 \quad (3.49)$$

in order to capture all three branches of the solution. At one loop we would expect a correction

$$(\Delta - 2 - j)(\Delta - 2 + j)(j - 1) = a(\Delta, j)g^2. \quad (3.50)$$

Let us analyze the solution near the point $(\Delta, j) = (3, 1)$ where the BFKL and DGLAP lines meet. We assume that $a(\Delta, j)$ is nonsingular there and approximate it by a constant $a \equiv a(3, 1)$; we can also approximate $\Delta - 2 + j = 2$. The intersection of the BFKL and DGLAP lines is then resolved into a smooth hyperbola, one branch of which is shown in Fig. 2.

If we approach this point along the BFKL branch, the physical state condi-

tion (3.50) becomes

$$j = 1 + \frac{ag^2}{2(\Delta - j - 2)} = 1 + \frac{ag^2}{2(\Delta - 3)} + O(g^4) . \quad (3.51)$$

If we approach it along the DGLAP branch, then

$$\Delta = 2 + j + \frac{ag^2}{2(j - 1)} . \quad (3.52)$$

Thus the physical state condition (3.50) reproduces the known perturbative poles in the BFKL exponent and anomalous dimensions; the common value $a = -N/\pi^2$ gives the correct coefficient in both (3.51) and (3.52). We emphasize that this result, that the BFKL calculation determines the $j = 1$ singularity in the anomalous dimensions, is well-known [45, 46, 47, 48, 49]; we are simply giving a different perspective on it.¹⁸

For the ρ trajectory [53, 54, 55, 56, 57] the BFKL exponent goes to 0 at weak coupling, so the BFKL and DGLAP curves all meet at the point (2, 0) that determines the BFKL exponent. That the weak-coupling BFKL exponent in this case is of order $\sqrt{\lambda}$, rather than the perturbative λ , is presumably connected with this fact.

4. Derivation in light-cone gauge

The light-cone has proven to be a natural formalism for studying the high energy limits of quantum field theories, leading to a vivid physical picture in Feynman's parton language. It is interesting to re-interpret our results for the BFKL singularity in this framework.

The light-cone gauge for a superstring [58] in $AdS_5 \times W$ eliminates all spurious degrees of freedom by fixing the bosonic co-ordinates $X^+(\sigma, \tau) = (X^0 + X^1)/\sqrt{2} = \tau$, $P^+(\sigma, \tau) = \text{const}$, and the first derivatives of $X^-(\sigma, \tau) = (X^0 - X^1)/\sqrt{2}$ as quadratic functions of the transverse fields via the Virasoro constraints.¹⁹ (See Refs. [52, 59] for details.) The remaining physical bosonic degrees of freedom are two transverse co-ordinates $X_\perp(\sigma, \tau) = (X_2, X_3)$, the radial field $Z(\sigma, \tau)$ in AdS^5 , (its zero-mode being $z = R^2/r$), and five fields $\Theta(\sigma, \tau)$ in W , plus the center of mass coordinates $x^- = (x^0 - x^1)/\sqrt{2}$ and conjugate momentum $p^+ = (p^0 + p^1)/\sqrt{2}$. The fermionic sector is treated analogously, but we can safely ignore it in our present discussion.

¹⁸The full structure is even richer than we have indicated, because the poles that we have found are just the first of infinite sets, arising from Ψ functions. Thus there are evidently an infinite number of additional branches to the solution of the physical state condition at $\Delta = 2 + j + m$, $\Delta = 2 - j - m$, and $j = 1 - m$ for positive integer m ; these do not intersect with the branch we are focussing on. There are also additional contributions from states with nonzero spin in the 2-3 plane. Presumably all these additional contributions correspond to the exchange of string states with higher oscillators excited.

¹⁹It is convenient in this section to use τ to denote worldsheet time. In other sections τ denotes the Regge diffusion ‘‘time’’.

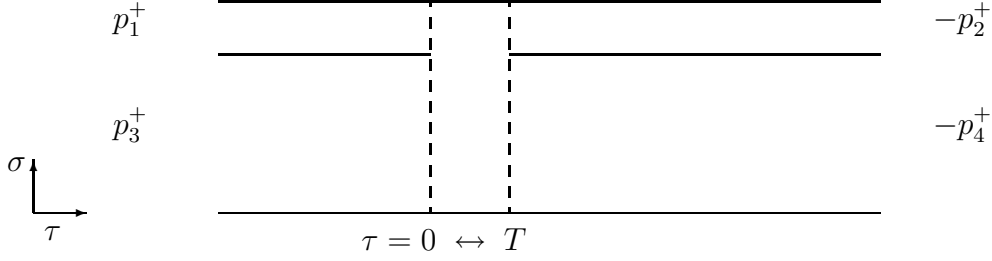


Figure 3: The light-cone worldsheet domain, $X^+ = \tau \in [-\infty, \infty]$, $\sigma \in [0, p^+]$, with $p^+ = p_1^+ + p_3^+$ for elastic scattering in the brickwall frame.

We will first discuss how to extract the Regge limit for an elastic open-string scattering amplitude ($p_1, p_3 \rightarrow -p_2, -p_4$) in a light-cone setting, before generalizing the analysis to closed-string scattering. After treating scattering in flat space, we will deal with the case of warped spacetime.

The elastic scattering amplitude for external states with momentum vectors $p_i^M = (p_i^+, p_i^-, p_i^\perp)$, and corresponding vertex operators V_i , can be expressed as a Euclidean Polyakov path integral in light-cone gauge,

$$\mathcal{A}(s, t) \delta^2 \left(\sum p_i^\perp \right) = \int dT \int \mathcal{D}X_\perp \mathcal{D}Z \ e^{-\int d\tau \int_0^{p^+} d\sigma \mathcal{L}[X_\perp, Z]} \prod_1^4 V_i \ , \quad (4.1)$$

where we ignore the bosonic modes in W as well as all fermionic modes, since they don't contribute to the leading j -plane singularity. Scattering can be shown to take place on a worldsheet of fixed width given by the total $p^+ = p_1^+ + p_3^+$ in the s -channel, as illustrated in Fig. 3. Open strings obey Neumann boundary condition on the boundaries of the worldsheet (the horizontal solid line segments in Fig. 3). The worldsheet has a single modulus T specifying the duration of the interaction in worldsheet time τ . (Closed strings obey periodic boundary conditions and have an additional modulus to enforce level matching.)

4.1 Open string scattering in flat spacetime

The open string tachyon elastic scattering amplitude in flat space has the well-known Veneziano form,

$$\mathcal{A}(s, t) = \int_0^1 dw (1-w)^{-2-\alpha's} w^{-2-\alpha't} \simeq \Gamma(-1-\alpha't) (e^{-i\pi} \alpha's)^{1+\alpha't} \ , \quad (4.2)$$

where the integral in the Regge limit is dominated by $w = O(1/s)$. In Sec. 3 this observation for the closed string led naturally to the use of the OPE for the p_1 - p_2 vertex operators. The methods of Sec. 3 analogously give

$$\mathcal{V}_R^\pm(k, w) = (\partial_w X^\pm(w))^{1+\alpha't} e^{\mp i k X(w)} \quad \text{and} \quad \Pi_R(\alpha't) = \Gamma(-1-\alpha't) e^{-i\pi - i\pi\alpha't} \ . \quad (4.3)$$

for the open string Reggeon vertex operator and propagator in flat space.²⁰

We shall explain in this subsection how we can arrive at these results starting from the flat-space light-cone path integral, given by (4.1) without the Z coordinate. In conformal gauge, we integrate over the position w of one of the vertex operators. In a light-cone approach, all external vertices are fixed, while the modulus T is integrated over. The conformal Christoffel transformation [59] which maps the upper half complex w -plane into the light-cone worldstrip in Fig. 3, takes the region $w = O(1/s)$ that dominates the integral in the Regge limit into the regime $T = O(1/p^+)$. This difference notwithstanding, we will see that we can still identify factors in the light-cone derivation closely related to $\mathcal{V}_R^\pm(k, w)$ and $\Pi_R(\alpha't)$ above.

4.1.1 Brief discussion for light-cone gauge at high energies

Since the density of $P^+(\sigma)$ is conserved in the light-cone gauge, it is traditional, for scattering processes, to label each string segment (or string bit) $\Delta\sigma$ by equal quanta Δp^+ , and to choose the string length²¹ to be $l_s = p^+$. Since this gauge is not manifestly Lorentz invariant, it is helpful to pick a convenient frame. We have chosen the *brickwall frame* in the center of momentum, where the transverse momenta are reflected by the collision: $p_\tau^\perp = \pm k^\perp/2$. In this frame²² the two strings joining at $(\sigma, \tau) = (\sigma_{int}, 0)$, split at (σ_{int}, T) with exactly the same value of σ or string bit, as illustrated in Fig. 4.

A major simplification of this frame is the fact that the t -channel worldsheet diagram ($T < 0$) vanishes identically, leaving only the s -channel contribution ($T \geq 0$). In this case the path integral can be evaluated by first cutting the worldsheet along the horizontal dashed line in Fig. 4 at fixed $\sigma = \sigma_{int}$, so that it forms two independent strips of fixed width $p_1^+ = -p_2^+$ and $p_3^+ = -p_4^+$ respectively. The two independent strings must then be rejoined along the dashed line by imposing there a Dirichlet boundary condition, with a delta-functional constraint,

$$\int \mathcal{D}k^\perp(\tau) \exp\left[i \int_0^T d\tau k^\perp(\tau) (X_\perp^{3-4}(\sigma_{int}, \tau) - X_\perp^{1-2}(\sigma_{int}, \tau))\right]. \quad (4.4)$$

Effectively what we have done is insert a non-local vertex operator

$$\exp\left[-i \int_0^T d\tau k^\perp(\tau) X_\perp^{1-2}(\sigma_{int}, \tau)\right] \quad (4.5)$$

²⁰We also note in passing that using the vertex operator (4.3) considerably reduces the labor of earlier methods used in extracting the asymptotic multi-Regge behavior for general n -point functions [60, 61, 62].

²¹We have set the world sheet speed of propagation to be $c = 1/(2\pi\alpha')$. More generally, $c = l_s/(2\pi\alpha'p^+)$ [52].

²²To be precise, we define the brickwall frame with transverse momenta $p_1^\perp = p_2^\perp = k^\perp/2$, and rapidities $\exp[\pm y_i] = \sqrt{2}p_i^\pm/\sqrt{(M_i^2 + k_\perp^2/4)}$, so that the invariants are $t = -k_\perp^2$ and $s = M_1^2 + M_3^2 + \sqrt{M_1^2 + k_\perp^2/4} \sqrt{M_3^2 + k_\perp^2/4} \cosh(y_1 - y_3)$. Boosting to the center of longitudinal momentum frame sets $y_1 = -y_3$.

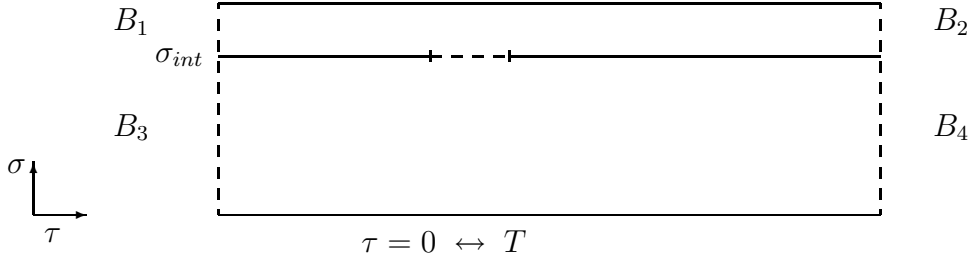


Figure 4: The light-cone worldsheet domain splits into two parallel sheets which join only at the dashed line at $\tau \in [0, T]$ and $\sigma = \sigma_{int}$. Solid (dashed) lines have Neumann (Dirichlet) boundary conditions respectively.

on the $\sigma = \sigma_{int}$ boundary of the 1-2 string, and a corresponding vertex on the boundary of the 3-4 string. The path integrals over the worldsheets of the 1-2 and 3-4 strings can now be performed separately, followed by the integral over $\int dT \int \mathcal{D}k^\perp(\tau)$.

The Regge limit represents a collinear boost into what is sometimes referred to as an *infinite momentum* frame, in which the boosted 3-4 string grows in length ($p_3^+ = -p_4^+ \sim O(\sqrt{s})$) and the 1-2 string decreases in length ($p_1^+ = -p_2^+ = O(1/\sqrt{s})$). Therefore, in the Regge limit, it is convenient to refer to these as the “long” and “short” strings respectively. They propagate in τ independently, except in the interaction region. As a consequence, the non-trivial physics involves a very small area of the worldsheet, $\Delta\tau = T \sim 1/p_3^+ \sim 1/\sqrt{s}$ and $\Delta\sigma \sim p_1^+ \sim 1/\sqrt{s}$, so one should be able to associate the Regge mechanism with a “local” conformal worldsheet transformation near the interaction region. The sole impact of this brief interaction is to constrain the ends of the long and short strings to coincide. As we shall show below, the Regge behavior comes entirely from the growth of the long string with the total center-of-mass energy \sqrt{s} .

Before proceeding to this analysis, it is useful to first fix the normalization for the amplitude. We do this by considering the Regge limit of the scattering amplitude at $t = 0$, *i.e.*, for $p_r^\perp \equiv 0$. In this limit, the path integral in (4.1) can be carried out (recall we are not including a warped coordinate Z at this point), and the forward amplitude reduces to a single integral over T [63]

$$\mathcal{A}(s, 0) \simeq \int \frac{dT}{T^2} 2\alpha' p^+ e^{p^- T} = -\alpha' s \int_\epsilon^\infty \frac{d\zeta}{\zeta^2} e^{-\zeta} \simeq -\frac{\alpha' s}{\epsilon}, \quad (4.6)$$

with $\zeta = -p^- T$. The divergence at $T = 0$ corresponds to the pole in the propagator, $\Pi_R(\alpha' t)$, in Eq. (4.3) from “photon” exchange at $t = -k_\perp^2 = 0$. The divergence at $T = \infty$ is due to s -channel poles; we evaluate the integral by analytic continuation to $\mathcal{R}e p^- < 0$. This is consistent with our expectation that the leading Regge singularity is dominated by contributions from the small T region. For later reference we define the measure $d\mu(T) = [2\alpha' p^+ \exp(p^- T)/T^2]dT$.

4.1.2 Regge behavior

In flat space, the light-cone Lagrangian density is

$$\mathcal{L} = \frac{1}{2}(\partial_\tau X_\perp)^2 + \frac{1}{2} \frac{1}{(2\pi\alpha')^2} (\partial_\sigma X_\perp)^2. \quad (4.7)$$

The light-cone Hamiltonian $H = p^-$ is the generator of translations in x^+ . The Virasoro constraints set $-\partial_\tau X^-$ equal to the Lagrangian: $\mathcal{L} = -\partial_\tau X^-$. (In what follows, we shall use the notation $\dot{X}_\perp \equiv \partial_\tau X_\perp$ and $X'_\perp \equiv \partial_\sigma X_\perp$.) Next we introduce the vertex functions for ground state tachyons on the vertical boundaries B_r in Fig. 4,

$$V_r[p_r, X] = \exp \left[(1/p_r^+) \int_{B_r} d\sigma [ip_r^\perp X_\perp(\sigma, \tau_r) + p_r^- X^+(\sigma, \tau_r)] \right], \quad (4.8)$$

with center of mass coordinates: $\tau_r = (1/p_r^+) \int_{B_r} d\sigma X^+$ and $x_\perp^{(r)} = (1/p_r^+) \int_{B_r} d\sigma X_\perp$. The limits $\tau_r \rightarrow \mp\infty$ for in/out states put the scattering amplitude on shell.

We will compute the worldsheet path integral by first evaluating it in six rectangular blocks, holding the worldsheet fields on the boundaries of the blocks fixed, and then finally integrating over the boundary data of the blocks. The six rectangular regions, shown in Fig. 5, are formed by cutting the worldsheet at $\sigma = \sigma_{int}$ into the 1-2 and 3-4 strips described above, and then dividing each strip into three regions: incoming ($\tau < 0$), interacting ($\tau \in [0, T]$), and outgoing ($\tau > T$) segments. In Fig. 5, these six regions are labeled by the contributions $\Phi^{(r)}$ to the path integral from the four external states, and the Green's functions $G^{(1,2)}$ and $G^{(3,4)}$ for the interactions regions. On the vertical boundary of each region marked $\Phi^{(r)}$, $r = 1, 2, 3, 4$, we hold the transverse fields fixed to $X_\perp^{(r)}(\sigma)$:

$$\begin{aligned} X_\perp(\sigma, 0) &= X_\perp^{(1)}(\sigma - \sigma_{int})\theta(\sigma - \sigma_{int}) + X_\perp^{(3)}(\sigma)\theta(\sigma_{int} - \sigma) \\ X_\perp(\sigma, T) &= X_\perp^{(2)}(\sigma - \sigma_{int})\theta(\sigma - \sigma_{int}) + X_\perp^{(4)}(\sigma)\theta(\sigma_{int} - \sigma) \end{aligned} \quad (4.9)$$

Note that $\sigma_{int} = p_3^+$. This leads to an exactly factorized representation for the amplitude,

$$\mathcal{A}(s, t) \delta^2(p_1^\perp + p_2^\perp + p_3^\perp + p_4^\perp) \simeq \int d\mu(T) \int \mathcal{D}k^\perp(\tau) \mathcal{V}_{12}[k^\perp(\tau)] \mathcal{V}_{34}[-k^\perp(\tau)]. \quad (4.10)$$

Each \mathcal{V}_{rs} is given by a *one-dimensional* path integral over the boundary fields $X_\perp^{(r)}(\sigma)$,

$$\mathcal{V}_{rs}[k^\perp(\tau)] = \int \mathcal{D}X_\perp^{(r)} \int \mathcal{D}X_\perp^{(s)} \Phi^{(r)}[X_\perp^{(r)}] G^{(r,s)}[X_\perp^{(r)}, X_\perp^{(s)}, k^\perp(\tau)] \Phi^{(s)}[X_\perp^{(s)}], \quad (4.11)$$

where Φ^r and $G^{(r,s)}$ are the results of the *two-dimensional* path integrals over the corresponding regions, with fixed boundary values given by $X_\perp^{(r)}(\sigma)$, with $0 \leq \sigma \leq |p_r^+|$. Both the incoming and the outgoing regions involve free string propagation, so

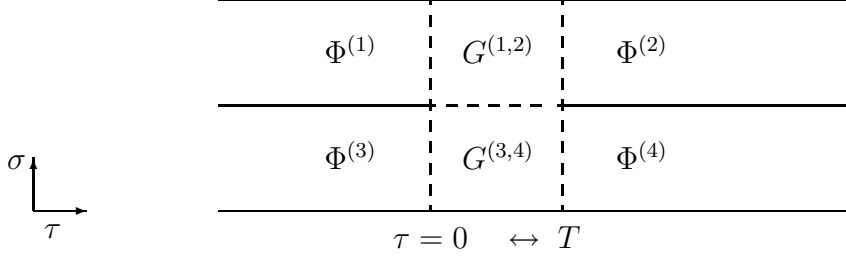


Figure 5: The six rectangular regions for evaluating the elastic scattering path integral in the brickwall frame.

the $\Phi^{(r)}$ are just the usual Gaussian wave functions for propagating tachyon boundary states,

$$\Phi_r[X_\perp^{(r)}] = \exp[ip_r^\perp x_\perp^{(r)} - \frac{1}{2} \sum_{n=1}^{\infty} \omega_n^{(r)} X_n^{(r)} X_n^{(r)}]. \quad (4.12)$$

We have used a standard normal mode expansion for each boundary field,

$$X_\perp^{(r)}(\sigma) = x_\perp^{(r)} + \sqrt{\frac{2}{p_r^+}} \sum_{n=1}^{\infty} X_n^{(r)} \cos(\omega_n^{(r)} \sigma / c). \quad (4.13)$$

With our choice of Euclidean worldsheet parameters, the frequencies of the modes, $\omega_n^{(r)} = n/(2\alpha'|p_r^+|)$, are scaled by $1/|p_r^+|$ on each string.

$G^{(1,2)}$ and $G^{(3,4)}$ can be obtained explicitly by a variety of methods [64]. They obey mixed boundary conditions: Dirichlet boundary conditions on the vertical (dashed lines at fixed τ), Neumann boundary condition at the free end (solid line at fixed σ) and a fixed Fourier distribution in $k^\perp(\tau)$ for the interaction between the strings (dashed line at σ_{int} as described above). At this point our treatment is still general. However we now choose to evaluate them approximately in the Regge limit, by making a semi-classical approximation which is more easily generalizable to our subsequent warped background.

In the Regge limit, one string is much shorter than the other, and the interaction time T goes to zero. In analogy with the OPE expansion, we consider an expansion in T . At $T = 0$, we can identify the boundary values of the worldsheet fields at $\tau = 0$ and $\tau = T$. It is therefore useful to distinguish between the differences, $[X_\perp^{(1)}(\sigma) - X_\perp^{(2)}(\sigma)]$ and $[X_\perp^{(3)}(\sigma) - X_\perp^{(4)}(\sigma)]$, that are being set to zero and the averages, $\overline{X}_\perp^{(12)}(\sigma) = [X_\perp^{(1)}(\sigma) + X_\perp^{(2)}(\sigma)]/2$ and $\overline{X}_\perp^{(34)}(\sigma) = [X_\perp^{(3)}(\sigma) + X_\perp^{(4)}(\sigma)]/2$. Now the delta-functionals in Eq. (4.4) become ordinary delta-functions

$$(2\pi)^2 \delta^2(\overline{X}_\perp^{(12)}(0) - \overline{X}_\perp^{(34)}(p_3^+)) = \int d^2 k^\perp e^{-ik^\perp \overline{X}_\perp^{(12)}(0)} e^{ik^\perp \overline{X}_\perp^{(34)}(p_3^+)}, \quad (4.14)$$

for the average coordinates: The only quantity we need to evaluate to first order in T is the action, $\Delta S = \Delta S_{12} + \Delta S_{34}$, in the $\tau \in [0, T]$ region,

$$\Delta S_{12}[\overline{X}_\perp^{(12)}] \simeq T \int_0^{p_1^\dagger} d\sigma \mathcal{L} \quad \text{and} \quad \Delta S_{34}[\overline{X}_\perp^{(34)}] \simeq T \int_0^{p_3^\dagger} d\sigma \mathcal{L} . \quad (4.15)$$

Consequently $G^{(1,2)}$ can be approximated by

$$G^{(1,2)}[X_\perp^{(1)}, X_\perp^{(2)}, k^\perp] \sim \delta[X_\perp^{(1)}(\sigma) - X_\perp^{(2)}(\sigma)] \exp \left[-ik^\perp \overline{X}_\perp^{(12)}(0) - \Delta S_{12}[\overline{X}_\perp^{(12)}] \right] , \quad (4.16)$$

and similarly for $G^{(3,4)}$. The remaining path integral over $\overline{X}_\perp^{(12)}$ and $\overline{X}_\perp^{(34)}$ can be carried out in terms of sums over their respective normal modes.

Let us first examine the interaction region for the short string. Since the excitation frequencies in the wave functions $\Phi^{(1)}$ and $\Phi^{(2)}$ grow with s , ($\omega_n = n/2\alpha'p_1^\dagger \sim n\sqrt{s}$), the short string interacts like a rigid point-like object, and its center of mass effectively coincides with the interaction point, $x_\perp^{(1)} = x_\perp^{(2)} \simeq X_\perp^{(1)}(0) = X_\perp^{(2)}(0)$. The action for the short string during the interaction time, ΔS_{12} , provides a UV cutoff in the mode sum, leading to an approximate local point-like short string vertex,

$$\mathcal{V}_{12}(k^\perp) \sim \int \frac{d^2 x_\perp^{(1)}}{(2\pi)^2} e^{ix_\perp^{(1)}(p_1^\dagger + p_2^\dagger - k^\perp)} = \delta^2(p_1^\perp + p_2^\perp - k^\perp) . \quad (4.17)$$

On the other hand, in the interaction region for the long string, the situation is reversed, with frequencies in the wave functions $\Phi^{(3)}$ and $\Phi^{(4)}$ becoming smaller at high energy ($\omega_n = n/2\alpha'p_3^\dagger \sim n/\sqrt{s}$). When s is increased, higher modes become increasingly important, and the long string also becomes extended in the transverse space, x_\perp . As we shall see, without an effective cutoff in the mode sum, the transverse size of the string would be logarithmic divergent. The interaction to first order in T can be written explicitly as

$$\Delta S_{34} = \frac{T}{2} \int_0^{p_3^\dagger} d\sigma [\dot{X}_\perp^2 + \frac{1}{(2\pi\alpha')^2} X_\perp'^2] = -T \int_0^{p_3^\dagger} d\sigma \dot{X}^-(\sigma, 0) , \quad (4.18)$$

using the Virasoro constraints to express in terms of $\dot{X}^-(\sigma, 0)$. Inclusion of this interaction term will be shown next to render \mathcal{V}_{34} a finite function of k_\perp , T and p_3^\perp , and will also directly lead us to the desired Regge behavior.

Assembling all the factors, one is led to a long string form factor,

$$\begin{aligned} F_{34}(-k^\perp, s) &\equiv F_{34} \equiv \int d\mu(T) \mathcal{V}_{34}(-k^\perp) \\ &\simeq \int d\mu(T) \int DX_\perp \Phi_3(X_\perp) \Phi_4(X_\perp) e^{T \int_0^{p_3^\dagger} d\sigma \dot{X}^-(\sigma, 0)} e^{ik^\perp X_\perp(p_3^\dagger, 0)} . \end{aligned} \quad (4.19)$$

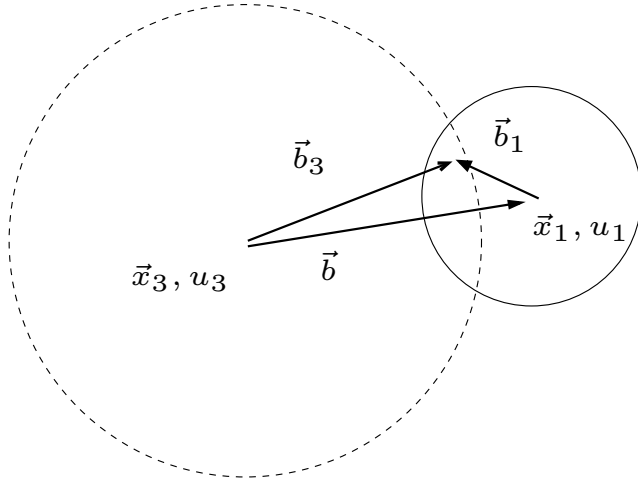


Figure 6: At the interaction the impact parameter is given by $\vec{b} = \vec{b}_3 - \vec{b}_1$ where \vec{b}_i is the vector from the center of mass of each string to its end point. In AdS space the strings are separated by an additional transverse co-ordinate $u = u_1 - u_3 = \ln(z_3/z_1)$ in the radial direction.

This can be evaluated directly by expanding in normal modes, so that

$$F_{34} \simeq \delta^2(p_3^\perp + p_4^\perp + k^\perp) (2\alpha' p^+) \int dT T^{-2} e^{p^- T} \exp \left[- \sum_n \frac{\alpha' k_\perp^2}{n + n^2 T / 2\alpha' p_3^+} \right]. \quad (4.20)$$

The sum in the exponent, at large $p_3^+ \simeq p^+ \simeq s/2p^-$, leads to a logarithmic growth,

$$\begin{aligned} F_{34} &\simeq \delta^2(p_3^\perp + p_4^\perp + k^\perp) (-\alpha' s) \int d\zeta \zeta^{-2} e^{-\zeta} \exp[-\alpha' k_\perp^2 \log(-\alpha' s/\zeta) + O(1/s)] \\ &\simeq \delta^2(p_3^\perp + p_4^\perp + k^\perp) (-\alpha' s) \Gamma(-1 + \alpha' k_\perp^2) \exp[-\alpha' k_\perp^2 \log(-\alpha' s)]. \end{aligned} \quad (4.21)$$

Finally combining the vertices for both short and long strings and performing the k^\perp integral gives the final result,

$$\mathcal{A}(s, t) \simeq \Gamma(-1 - \alpha' t) (e^{-i\pi} \alpha' s)^{1 + \alpha' t}. \quad (4.22)$$

4.1.3 Diffusion in transverse space

Looking back at this derivation, we can see that Regge behavior is caused, in the infinite-longitudinal-momentum transverse-brickwall frame, by the logarithmic growth in s of the average fluctuation of the end of the “long” string, $X_\perp^{(3)}(p_3^+)$, relative to its center of mass, $x_\perp^{(3)}$.

It is instructive to examine further the physics of the interaction region ($\tau \simeq 0$) from the perspective of the transverse space. The size of an incoming string can be characterized by the separation between its center of mass and its end point where

it interacts with the other strings: $\vec{b}_1 = X_\perp^{(1)}(0) - x_\perp^{(1)}$ and $\vec{b}_3 = X_\perp^{(3)}(p_3^+) - x_\perp^{(3)}$. With the constraint $X_\perp^{(1)}(0) = X_\perp^{(3)}(p_3^+)$ at the interaction, the conventional impact parameter is given by

$$\vec{b} \equiv x_\perp^{(1)} - x_\perp^{(3)} = \vec{b}_3 - \vec{b}_1, \quad (4.23)$$

as illustrated in Fig. 6. We could have chosen, in our light-cone analysis, to represent the scattering amplitude (4.10) in impact-parameter space, Fourier transforming from k^\perp to x_\perp . After integrating the fluctuations, we would find the “kernel”, $\mathcal{K}(y; x_\perp^{(1)}, x_\perp^{(3)})$, as the Fourier transform of the s -dependent factor in Eq. (4.22). The kernel satisfies a diffusion equation,

$$[\partial_y - 1 - \alpha' \partial_{x_\perp^{(1)}}^2] \mathcal{K}(y; x_\perp^{(1)}, x_\perp^{(3)}) = \delta(x_\perp^{(1)} - x_\perp^{(3)}) \delta(y), \quad (4.24)$$

where the evolution parameter is the rapidity, $y \sim \log(\alpha' s)$. Since one works only with physical degrees of freedom, the light-cone path integral has the advantage that we can follow the evolution of the physical transverse motion of the string “bits”, directly leading to a diffusion picture at high energies.

In flat space, the diffusive growth in impact parameter is equivalent to the “Regge shrinkage” for the Regge “form factor”, $\exp[\alpha' t \log(\alpha' s)]$. The amplitude decreases more rapidly in $|t|$ at large values of the energy. Historically, Regge behavior was first exhibited in a relativistic setting by summing “ladder graphs”, or more generally, “multiperipheral ladders” [65]. A crossing symmetric generalization led to the consideration of “fishnet diagrams” [66, 67], which played an influential role in the construction of early string theories. Here, we have reversed the argument, and have shown how a string-string interaction in the Regge limit reproduces the underlying diffusion phenomenon. This picture will be generalized in the next subsection to treat the case of warped spacetime.

Our computation is related in an interesting way to that of Ref. [68]. Suppose we introduce a local conserved vector current coupled to charges at the end of a single open string. As emphasized in Ref. [68], in light-cone gauge such a form factor would (naively) be obtained by introducing a local vertex $\dot{X}_\mu(\sigma, \tau) \exp[ik^\perp X_\perp(\sigma, \tau)]$ at $(\sigma, \tau) = (p^+, 0)$ onto a straight worldsheet of width p^+ and infinite length. The calculation is very similar to our Regge computation for the long string, but with T strictly taken to zero, which results in a logarithmic divergence, $\langle \Delta X_\perp^2 \rangle \sim \sum_n 1/n$, in the transverse size $\Delta X_\perp = X_\perp - x_\perp$. This is the well-known disease for local currents in flat space [68]. In contrast, the Regge “form factor” F_{34} of the long string, Eqs. (4.20)–(4.20), has its divergence cut off by the interaction operator, $\exp[T \int d\sigma \dot{X}^-]$, that we obtained working to first order in T .

If we compare our light-cone Regge form factor F_{34} in Eq. (4.20), with the product of the conformal Regge vertex and its propagator in Eq. (4.3),

$$\Pi_R(\alpha' t) \mathcal{V}_R^\pm(k, w) = \int_0^\infty d\zeta \zeta^{-2-\alpha' t} e^{\zeta \partial_w X^\pm(w)} e^{\mp i k X(w)}, \quad (4.25)$$

we note that they are clearly not the same. However we have checked by direct calculation that the light-cone-gauge-fixed version of the conformal Reggeon vertex,

$$\mathcal{V}_R^{\pm(lc)}(k, w) = [\partial_w X^\pm(w)]^{1+\alpha't} e^{\mp i k^\perp X_\perp(w)}, \quad (4.26)$$

also reproduces the scattering amplitude in the Regge limit using the Virasoro constraints. A derivation of this form of the Regge vertex from the light-cone path integral would be nice.

4.2 Regge behavior in warped spacetime

Now we consider the effect of adding a warped transverse direction, the AdS radial direction, Z . The light-cone action in an AdS space of curvature radius R is [58]

$$\begin{aligned} \int_0^{p^+} d\sigma \mathcal{L} &= \frac{1}{2} \int_0^{p^+} d\sigma \left[\dot{X}_\perp^2 + \dot{Z}^2 + \frac{1}{(2\pi\alpha'R^{-2}Z^2)^2} (X_\perp'^2 + Z'^2) \right], \\ &= \frac{1}{2} \int_0^{p^+} d\sigma \left[\dot{X}_\perp^2 + R^2 e^{-2U} \dot{U}^2 + \frac{1}{(2\pi\alpha')^2} (e^{4U} X_\perp'^2 + R^2 e^{2U} U'^2) \right], \end{aligned} \quad (4.27)$$

where we have introduced $U(\sigma, \tau) = -\log(Z(\sigma, \tau)/R)$. In the light-cone frame the conformal group $O(4, 2)$ is restricted to the subgroup $SL(2, C)$: $Z \rightarrow \lambda Z, X_\perp \rightarrow \lambda X_\perp, \tau \rightarrow \lambda \tau, \sigma \rightarrow \sigma/\lambda$, which is the isometry of Euclidean AdS_3 for the three transverse coordinates, (x_\perp, z) . To exploit this invariance, we work with the U variable and make a semi-classical expansion around the zero modes, $U = u$ and $X_\perp = x_\perp$. The essential new feature is an effective string slope, $\alpha'_{\text{eff}}(u) = \alpha' e^{-2u}$, which leads to local dependence on u . The dressed wavefunctions to Gaussian order become

$$\Phi_r[X, U] = \exp \left[i p_r^\perp x_\perp^{(r)} - \frac{1}{2} \sum_n \omega_n^{(r)} [e^{2u} X_n^{(r)} X_n^{(r)} + R^2 U_n^{(r)} U_n^{(r)}] \right] \psi_r(u_r), \quad (4.28)$$

to be compared with Eq. (4.12).

The calculation proceeds along the same line as that for the flat background, with the addition of the one extra transverse coordinate u (see Fig. 6). Factorization of the Dirichlet constraint on U in the interaction region requires that Eq. (4.14) be supplemented with an additional delta-function,

$$\delta \left(U_\perp^{(1)}(0) - U_\perp^{(3)}(p_3^+) \right) = \int \frac{d\nu}{2\pi} \exp \{ -i\nu [U^{(1)}(0) - U^{(3)}(p_3^+)] \}. \quad (4.29)$$

Again diffusion takes place only for the “long” boosted string, and we must keep the interaction ΔS_{34} to first order in T . The details are similar to the flat space derivation, except that $\alpha' k_\perp^2$ is replaced by $\alpha'_{\text{eff}}(u) k_\perp^2 + \nu^2$, in the new version of Eq. (4.20). For $k_\perp^2 = 0$, due to conformal invariance, the ν^2 term corresponds to flat

space diffusion in the u -direction. For non-zero $k_{\perp}^2 \neq 0$, we must replace ν by an operator $i\partial_u$ conjugate to u and take care with operator ordering.

In fact to deal rigorously with the operator ordering problem, one must go beyond the Gaussian approximation to one loop order [69] for the worldsheet sigma model. The result of this calculation would be to introduce a shift $\nu^2 \rightarrow \nu^2 + 2i\nu$, identical to that in the computation of the anomalous dimension of the on-shell photon vertex operator [36]. We choose an alternative approach, fixing this ambiguity by matching the Regge spectrum with the on-mass-shell wave equation ($L_0 = 1$ at $j = 1$) for the vector field in AdS space. Either way this results in the following Hermitian differential equation,

$$[\partial_y - 1 - \alpha'_0 e^{-2u} \partial_{x_{\perp}}^2 - \frac{1}{\sqrt{\lambda}}(\partial_u^2 - 1)] \mathcal{K}_V(y; x_{\perp}, u, x'_{\perp}, u') = \delta(x_{\perp} - x'_{\perp})\delta(u - u')\delta(y), \quad (4.30)$$

which determines the leading j -plane singularity to leading order in α'_0 . In momentum space, this is equivalent to a Euclidean Schrödinger equation for the open string Reggeon kernel,

$$[\partial_y - 1 - \alpha'_0 t e^{-2u} - \frac{1}{\sqrt{\lambda}}(\partial_u^2 - 1)] \mathcal{K}_V(y; t, u, u') = \delta(u - u')\delta(y). \quad (4.31)$$

Since large u suppresses the corresponding diffusion in x_{\perp} , diffusion in u gives rise to the BFKL cut. This will be made more precise in the next section where we explore this quantum mechanical analogy. This effect could have been anticipated qualitatively in terms of the boosted incoming wave function (4.28). The U_n modes enter like ordinary transverse modes in flat space. The hadrons are peaked at small u , but as p^+ increases, diffusion in u pushes the incoming hadron wave function into the large u (UV) region. This then acts to increase the effective energies ($\omega_n e^{2u}$) of the X_n^{\perp} modes, suppressing diffusion in x_{\perp} . It is interesting to compare this with the physics in flat space, where increasing p^+ reduces effective energies ($\omega_n \sim n/p^+$) for the modes of all transverse directions; this effect is responsible for the Regge shrinkage of the small-angle scattering peak. Eq. (4.31) leads to a BFKL-like cut for the open string Regge exchange [53, 54, 55, 56, 57] starting at $j = 1 - 1/\sqrt{\lambda}$.

To generalize this to the closed string, one must introduce periodic boundary condition on the strings and an additional modulus θ that rotates the Riemann surface around a cut on the s -channel intermediate closed string. The integral over θ forces level matching between holomorphic and anti-holomorphic modes. This has the effect of replacing $\alpha'_0 \rightarrow \frac{1}{2}\alpha'_0$. Again, to get the full contribution to leading order in strong coupling, we should do a one loop correction to the Gaussian approximation, this time resulting in the anomalous shift $\nu^2 \rightarrow \nu^2 + 4i\nu$, for the graviton vertex, consistent with the on-shell linearized graviton equation and general covariance in the AdS^5 background. The final result, when transformed back to a momentum

representation, is

$$[\partial_y - 2 - \frac{\alpha'_0}{2} t e^{-2u} - \frac{1}{2\sqrt{\lambda}}(\partial_u^2 - 4)] \mathcal{K}(y; t, u, u') = \delta(u - u')\delta(y). \quad (4.32)$$

As noted before, the spectral decomposition for this Schrödinger operator, Eq. (2.36), gives the leading BFKL singularity at $j = 2 - 2/\sqrt{\lambda}$ in strong coupling. It is also interesting to note that the same anomalous shift $\nu^2 \rightarrow \nu^2 + 4i\nu$ for the graviton vertex was found in Ref. [68] to be essential in giving a finite form factor at non-zero k_\perp^2 . The BFKL singularity, power behavior at wide angles [25, 26] and finite power-behaved form factors all have a common origin, at least in strongly coupled ultraviolet-conformal theories.

5. Regge Trajectories in UV-conformal Theories

Our previous computations of the kernel were done in conformally-invariant theories, or in kinematic regimes where confinement played no role. We now consider the effects of confinement, while keeping the ultraviolet strictly conformal. A simple example of such a theory is the $\mathcal{N} = 1^*$ model studied in [70]. This discussion is by necessity less precise than the previous ones, simply because there is model-dependence in the confining region. Our goal in this section is to make as many model-independent remarks as possible, and examine where model-dependence is to be found.

If confinement sets in at a scale Λ in the gauge theory, this leads to a change in the metric away from $AdS_5 \times W$ in the region near $z = R^2/r \sim 1/\Lambda \equiv z_0$. Typically [12, 70, 71] the space is cut off, or rounded off, in some natural way at $z = z_0$, or equivalently $u = u_0$. This leads to a theory with a discrete hadron spectrum, with mass splittings of order Λ among hadrons of spin ≤ 2 . The theory will also have confining flux tubes (assuming these are stable) with tension $1/\alpha'_0 = 2\sqrt{\lambda}\Lambda^2$; the same scale sets the slope of the Regge trajectories for the high-spin hadrons of the theory. Note the separation of the two energy scales, by a factor of $\lambda^{1/4}$; this is an important feature of the large- λ regime.

Since the metric is changed near u_0 , the form of the differential operator $\Delta_j \approx \Delta_2$, defined in (2.21), is likewise changed in this region. The effective potential $V(u)$ for the Schrödinger problem associated to the kernel approaches Eq. (2.37) only for $u \gg u_0$. However, for $-t \gg \Lambda^2$, the exponentially rising potential for $u \ll \ln(\sqrt{|t|}\Lambda)$ implies the kernel is insensitive to the region near u_0 . This is consistent with the expectation in the QCD literature that the BFKL calculation is infrared-safe for large negative t , while the effects of confinement become important as $t \rightarrow 0^-$, and for any $t > 0$. The regime where confinement-independent results are obtained will be discussed further below.

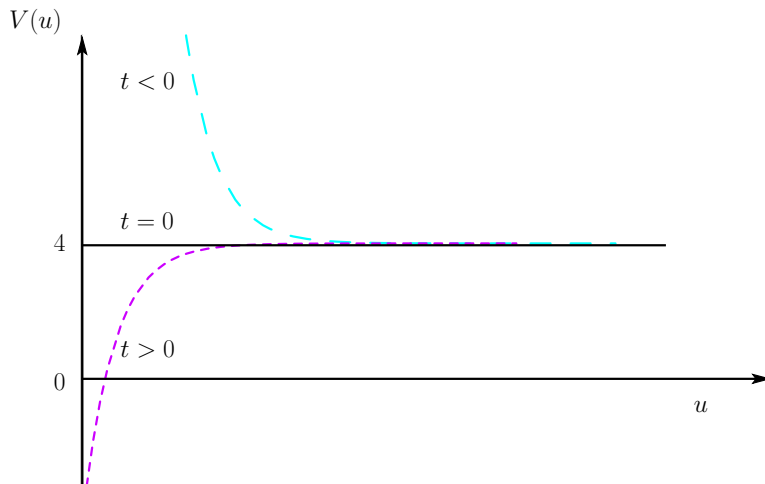


Figure 7: The potential for the effective Schrödinger problem in the hard-wall model, for $t = 0$ (solid), $t > 0$ (short dash), and $t < 0$ (long dash).

5.1 The hard-wall model

To begin this discussion, it is instructive to work our way through the “hard-wall” toy model. While this model is not a fully consistent theory, it does capture key features of confining theories with string theoretic dual descriptions.

In the simplest form of the hard-wall model, the metric takes an $AdS_5 \times W$ form (2.1) for $u > u_0$ and has a sharp boundary at $u = u_0$; without loss of generality we take $u = -\ln z/z_0$ and thus $u_0 = 0$. This metric does not satisfy the supergravity equations, but experience has shown [25, 30, 72] that it captures much of the phenomenology encoded in the metrics of consistent four-dimensional theories with confining dynamics [70, 71]. In particular, phenomena for which the details of the metric in the confining region are not important — potentially universal features of gauge theory — are often visible in this model. One can identify infrared-insensitive quantities and general features of the hadronic spectrum, hadronic couplings, etc, including, as we will see, aspects of Regge trajectories and of the Pomeron. Meanwhile, model-dependent aspects of these and other phenomena also can be recognized, through their sensitivity to small changes in the model.

The main advantage of the hard-wall model is that it can be treated analytically, and the kernel can be written explicitly. Since the metric is still $AdS_5 \times W$, we have the same quantum mechanics problem to solve as in the conformal case, with potential $V(u)$ given in Eq. (2.37), except for a cutoff on the space at $u = 0$. The boundary condition at the wall on the five-dimensional graviton (and its trajectory for general j) is constrained by energy-momentum conservation in the gauge theory. We must impose the boundary condition $\partial_r(r^{-2}\phi_{+j}) = 0$ at $r = r_0$ for the analogue quantum mechanics system. The logic is the same as in deriving the wave equation (2.22): the pure gauge solution $h_{++} = r^2/R^2$ must be retained, else conservation of the energy-

momentum tensor will be violated. This condition extends to the Pomeron for small $|j - 2|$, which will be the regime we will mainly consider below.

5.1.1 Scattering of hadrons for $t < 0$.

For $t \leq 0$, the potential (2.37) has an exponential growth at small u and goes to a constant at large u . Consequently, the spectrum of Δ_j is continuous. The kernel can readily be expressed in terms of a set of delta-function-normalized eigenfunctions,

$$\mathcal{K}_0(u, u', \tau, t) = \int_0^\infty d\nu |c(\nu, t)|^2 \{I_{i\nu}(\xi) + R(\nu, t)I_{-i\nu}(\xi)\}^* \{I_{i\nu}(\xi') + R(\nu, t)I_{-i\nu}(\xi')\} e^{-\tau\nu^2} \quad (5.1)$$

where $I_\nu(\xi)$ is the modified Bessel function, $\tau \sim \ln s/2\sqrt{\lambda}$ is defined in Eq. (2.29), $\xi = z\sqrt{-t} = (\sqrt{-t}/\Lambda)e^{-u}$, and $R(\nu, t)$ is fixed by the boundary condition at $u = 0$:

$$R(\nu, t) = -\frac{\partial_\xi[\xi^2 I_{i\nu}(\xi)]}{\partial_\xi[\xi^2 I_{-i\nu}(\xi)]} \Big|_{\xi=(\sqrt{-t}/\Lambda)}. \quad (5.2)$$

The parameter ν is related to the energy eigenvalue by $E = 4 + \nu^2$. The coefficients

$$|c(\nu, t)|^2 = \frac{\nu}{2 \sinh \pi\nu} \quad (5.3)$$

are normalization constants chosen so that $\mathcal{K}_0(u, u', 0, t) = \delta(u - u')$; because of conformal invariance at large u, u' , the coefficients are actually t -independent.

Since each Bessel function approaches a plane wave at $\xi \simeq 0$, $R(\nu, t)$ is proportional to the reflection coefficient for a plane-wave incident from $u = +\infty$. It will later be useful to introduce a one-dimensional unitary S-matrix,

$$S(\nu, t) \equiv e^{2i\delta(\nu, t)} = \left[\frac{\Gamma(1 + i\nu)}{\Gamma(1 - i\nu)} \left(\frac{-t}{4\Lambda^2} \right)^{-i\nu} \right] R(\nu, t). \quad (5.4)$$

Let us first validate our expectations regarding scattering of hadronic states. At large $-t \gg \Lambda^2$, the scattering should be model-independent, since the large momentum transfer shields the scattering from the confinement region, as shown in Fig. 7. Thus for large $-t$ and large u, u' , the kernel should be almost identical to the kernel (2.39) of a conformal theory. This can straightforwardly be verified by comparing (2.39) to (5.1), with the use of (5.2) and (5.3).

As $t \rightarrow 0^-$, however, the effects of confinement become important. This can most easily be seen in the $t = 0$ kernel. At $t = 0$, the Bessel function $I_{i\nu}$ in (5.1) reduces to a plane-wave and the kernel becomes

$$\mathcal{K}_0(u, u', \tau, t) = \int_{-\infty}^\infty \frac{d\nu}{4\pi} \{e^{-i\nu u} + S(\nu, 0)e^{i\nu u}\}^* \{e^{-i\nu u'} + S(\nu, 0)e^{i\nu u'}\} e^{-\tau\nu^2} \quad (5.5)$$

with

$$S(\nu, 0) = \frac{\nu - 2i}{\nu + 2i} \quad (5.6)$$

The integral can be performed, giving

$$\mathcal{K}_0(u, u', \tau, t = 0) = \frac{e^{-(u-u')^2/4\tau}}{2\sqrt{\pi\tau}} + F(u, u', \tau) \frac{e^{-(u+u')^2/4\tau}}{2\sqrt{\pi\tau}}, \quad (5.7)$$

where

$$F(u, u', \tau) = 1 - 4\sqrt{\pi\tau}e^{\eta^2}\text{erfc}(\eta), \quad \eta = (u + u' + 4\tau)/\sqrt{4\tau}. \quad (5.8)$$

Note $F = 1$ for $\tau \rightarrow 0$ and $F = -1$ as $\tau \rightarrow \infty$, with cross-over at $\tau \sim u + u'$ (for sufficiently large u, u').

The formula (5.7) is easy to interpret. The first term is the model-independent kernel (2.35) which describes diffusion from u' to u ; the second term, which involves diffusion of the image charge at $-u'$, is sensitive to the reflection off the wall at $u = 0$ and is thus model-dependent. Whether a given physical process is model-dependent is determined by the relative importance of these two terms. For instance, the scattering of two delta-function disturbances localized at $u_1 \gg u_2 \gg 0$ will be model-independent until $\ln s$ is large enough to permit diffusion from $-u_2$ to u_1 , and even then the second term will be small compared to the first until still larger values of $\ln s$.

However, while hadrons of size ρ typically peak at $u \sim -\ln \rho\Lambda$, they also have power law tails extending out to large u , of the form $r^{-\Delta} \sim e^{-\Delta u}$, where Δ (for a scalar hadron) is the dimension of the lowest dimension interpolating operator for the hadron. (More generally it is the lowest-twist operator which determines the power.) Consequently, the scattering at $t = 0$ of a small hadron, or off-shell photon, of size $\rho_1 \ll \Lambda^{-1}$ (with a wave function extending down to $u_1 \sim -\ln \rho_1\Lambda$) off of an ordinary hadron of size $\rho_2 \sim \Lambda^{-1}$ (with a wave function peaking near the wall but sporting an $e^{-\Delta u}$ tail) has several regimes. Diffusion is unimportant for small $\ln s$, model-independent but Δ -dependent for moderate $\ln s$, and model-dependent for $\ln s$ large compared to $\sqrt{\lambda}u_1^2$. These issues are addressed in the final calculations of [30] and will be revisited elsewhere.

5.1.2 Regge trajectories at $t > 0$

The hard-wall model has a spectrum of hadrons typical of a confining theory, including spin-two glueballs and their associated Regge trajectories. The spin-two glueballs are simply the discrete spectrum of “cavity modes” of the Laplacian for a five-dimensional spin-two field. This Laplacian is the operator Δ_2 , slightly reinterpreted, as we now discuss.

We have already explained that we may view the operator Δ_j as an effective Schrödinger operator $-\partial_u^2 + V(u)$, with $V(u)$ given in (2.37) (and shown in Fig. 7) and with energy eigenvalues E that are related to the corresponding spin j by

$$E = -2\sqrt{\lambda}(j - 2), \quad (5.9)$$

as we explained preceding Eq. (2.32). For sufficiently positive t this operator has a discrete set of normalizable “bound-state” modes with eigenvalues $E = E_n < 4$. The bound state eigenvalues $E_n(t)$, $n = 1, 2, \dots$, determine the Regge trajectories, where each trajectory has $j_n(t) = 2 - E_n(t)/2\sqrt{\lambda}$. The theory has a physical spin-two glueball state of mass m for each $t = m^2$ such that $E_n(t) = 0$ for some n [9, 10, 11, 73, 74]. (Note $V(u)$ goes to a positive constant as $u \rightarrow \infty$, so $E_n(t) = 0$ can only occur for $t > 0$.) Higher spin hadrons on the trajectories lie outside the supergravity regime.²³ Meanwhile, since $V(u)$ goes asymptotically to 4 at large u , the spectrum of Δ_j also has a continuum that extends over $E \geq 4$ ($j \leq j_0$); this is the same continuum as was present for $t < 0$.

The bound states of the hard-wall model’s auxiliary quantum mechanics have wave functions, in terms of $\chi = z\sqrt{t} = \sqrt{t}e^{-u}/\Lambda = i\xi$, proportional to

$$J_{\sqrt{4-E}}(\chi) \tag{5.10}$$

for those discrete values of E where $\partial_\chi[\chi^2 J_{\sqrt{4-E}}(\chi)]$ vanishes at the wall ($\chi = \sqrt{t}/\Lambda$). These values of E correspond precisely to poles of the one-dimensional S-matrix, Eq. (5.4), continued to $t > 0$:

$$S(\nu, t) \equiv e^{2i\delta(\nu, t)} \rightarrow - \left[\frac{\Gamma(1+i\nu)}{\Gamma(1-i\nu)} \left(\frac{t}{4\Lambda^2} \right)^{-i\nu} \right] \frac{(\chi^2 J_{i\nu}(\chi))'}{(\chi^2 J_{-i\nu}(\chi))'} \Big|_{\chi=(\sqrt{t}/\Lambda)} \tag{5.11}$$

when ν lies on the positive imaginary axis. The glueball states, found when $E_n(t) = 0$, have masses m_n proportional to the zeroes of $4J_2(x) - xJ_3(x)$; for $n \gg 1$ they are approximately equally spaced, and by an amount $\Delta m \sim \pi\Lambda$. The equal spacing in mass for large n is required by the WKB approximation applied to the potential Eq. (2.37).

The continuum states for $E > 4$ can be read off from (5.1), with $I_{i\nu}(\xi)$ replaced by $J_{i\nu}(\chi)$, $\chi = (\sqrt{t}/\Lambda)e^{-u}$. They take the form

$$J_{i\sqrt{E-4}}(\chi) + R\left(\sqrt{E-4}, t\right) J_{-i\sqrt{E-4}}(\chi) \tag{5.12}$$

where the function R is given in Eq. (5.2).

We have plotted the spectrum as a function of $j - 2$ [linearly related to $-E$ by Eq. (5.9)] in Fig. 8. The massive tensor glueball states, marked with dots, are at $j - 2 = 0$. The familiar graph of approximately linear Regge trajectories is supplemented by the continuum of states (the BFKL-like cut) that begins at $j = j_0 = 2 - 2/\sqrt{\lambda}$. The unequal and nonconstant slopes of the trajectories near $j = 2$, like the equally-spaced hadron masses m_n , are a model-independent feature of the supergravity limit $\lambda \gg 1$ for $j \approx 2$. As j increases the slopes gradually become parallel and equal to $\alpha'_0 = (2\sqrt{\lambda}\Lambda^2)^{-1}$, which is the reciprocal of 2π times the confining string tension. The transition to linear trajectories can be understood as follows. As t increases, the

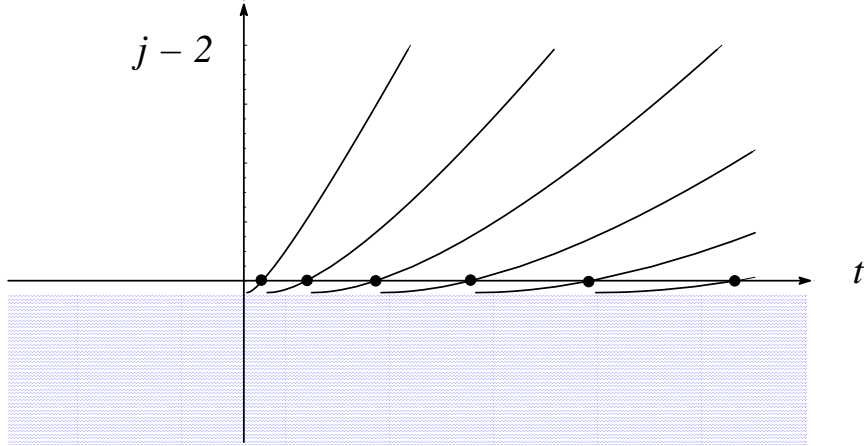


Figure 8: The analytic behavior of Regge trajectories in the hard-wall model, showing the location of the bound-state poles at $j = 2$ and the t -independent continuum cut (shaded) at $j = j_0 = 2 - 2/\sqrt{\lambda}$ into which the Regge trajectories disappear. The lowest Regge trajectory intersects the cut at a small positive value of t . At sufficiently large t each trajectory attains a fixed slope, corresponding to the tension of the model's confining flux tubes.

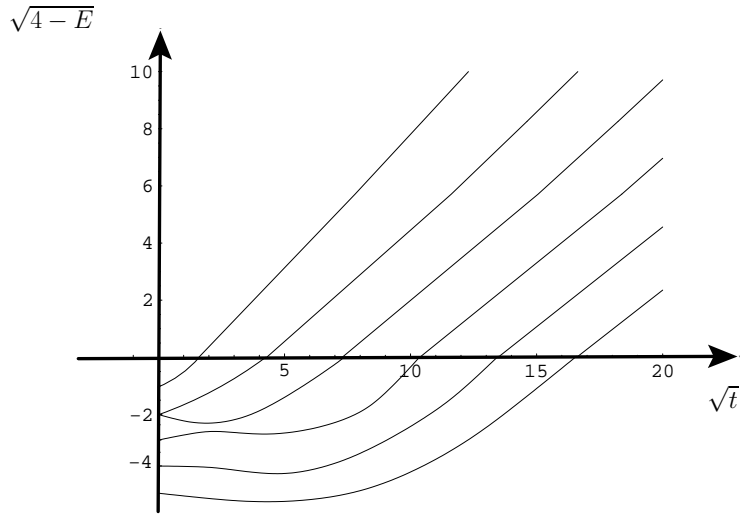


Figure 9: The analytic behavior of Regge trajectories in the hard-wall model plotting real $\sqrt{4 - E}$ against \sqrt{t} . As t decreases, each bound state pole moves from positive to negative $\sqrt{4 - E}$, passing under the continuum cut in the j plane and moving on the the second sheet.

effective potential $4 - \Lambda^{-2}te^{-2u}$ becomes deeper, and the states become more localized near the minimum at $u = 0$. The energy is then approximately $E \approx -\Lambda^{-2}t$, that is, $j \approx t/2\Lambda^2\sqrt{\lambda}$, giving the linear slope. For a given trajectory $j_n(t)$, the WKB approximation shows that it reaches its asymptotic slope for $(j - 2) \gg n^2/\sqrt{\lambda}$.

²³For a review, see [75].

The condition that the state be localized near the minimum, $\delta u \ll 1$, is consistent with the supergravity approximation, which requires that $R\delta u \gg \sqrt{\alpha'}$ or $\delta u \gg \lambda^{-1/4}$. Thus the transition to linear trajectories occurs within the range of validity of supergravity. However, to reach the excited states on the linear trajectory, where $j - 2 = O(1)$, requires $\alpha'_0 t$ to be of order one. This is outside the range of validity of supergravity: the momenta are of order the string scale. The supergravity regime thus describes the Pomeron trajectory for all negative t , and for positive $t \ll \alpha'_0^{-1}$.

In fact, our effective quantum mechanical description, obtained from the physical state condition $L_0 = 1$, extends to larger t . Once $\alpha'_0 t$ is of order one, higher derivative terms in L_0 are potentially unsuppressed. However, because we know that the flat spacetime L_0 is exactly quadratic in derivatives, these higher derivative terms are suppressed by at least one power of the curvature, a factor of $\lambda^{-1/2}$. Hence to this accuracy we can continue to use

$$L_0 = \frac{j}{2} - \frac{\alpha'_0 t e^{-2u}}{4} - \frac{1}{4\sqrt{\lambda}} \frac{\partial^2}{\partial u^2} + O(\lambda^{-1/2}) . \quad (5.13)$$

The hard-wall cutoff gives rise to an unwanted artifact, because the states become localized right at the wall. A better model would have a smooth minimum. For example, consider the variant

$$L_0 = \frac{j}{2} - \frac{\alpha'_0 t}{4(e^{2u} + e^{-2u} - 1)} - \frac{1}{4\sqrt{\lambda}} \frac{\partial^2}{\partial u^2} + O(\lambda^{-1/2}) , \quad (5.14)$$

combined with an orbifolding $u \rightarrow -u$. The potential has been designed to have the same large- u behavior and the same minimum as before. Also, the boundary condition required for energy-momentum conservation in this model is consistent with the orbifold. This model gives a simple correction to the linearity of the trajectories. For states near the quadratic minimum we can use the harmonic oscillator spectrum (even states only),

$$1 = L_0 = \frac{j}{2} - \frac{\alpha'_0 t}{4} + (2n + \frac{1}{2})(\alpha'_0 t)^{1/2} \lambda^{-1/4} + O(\lambda^{-1/2}) , \quad (5.15)$$

and so we obtain a $(\alpha'_0 t)^{1/2}$ correction to the slope, as in ref. [76]. (The hard-wall model, where the potential is linear near the wall, gives an $(\alpha'_0 t)^{2/3}$ correction.)

We should note that the form (5.15) holds only for $\alpha'_0 t = O(1)$, and breaks down at a yet higher energy $\alpha'_0 t = O(\lambda^{1/2})$. At this point the Pomeron becomes a rotating string with a length of order the AdS radius, and we must carry out a full string quantization [76]. The radial fluctuations (which are responsible for the $(\alpha'_0 t)^{1/2}$ term above) are ultimately exponentially suppressed, because the radial fluctuations are massive on the world-sheet. The leading correction to the linearity of the trajectories is then the Lüscher term from the massless fluctuations [77], which gives a negative constant shift.

5.2 The analytic structure at all t (constant coupling)

Although it is a crude toy model, the hard-wall model may be interpreted as capturing key universal features that will be true in any quantum field theory with ultraviolet conformal invariance, infrared confinement, large λ and large N . Some of these features, especially those that have to do with the analytic structure of amplitudes, may be valid in any large- N gauge theory at any λ , and may in some cases survive to small N as well.

Certain phenomena visible in Fig. 8 will hold universally in any similar theory. Ultraviolet conformal invariance assures that the auxiliary quantum mechanics problem in Eq. (2.36) will have a potential which goes to the constant 4 for large u . Conformal invariance and analyticity assure that its t dependence at large u will be qualitatively similar; the deviations of $V(u)$ from 4 will have a sign opposite to that of t and a size that shrinks exponentially at large u . From this several consequences follow: the spectrum will have

- At all values of t , a continuum of states for $E \geq 4$ (the BFKL-type cut at $j \leq 2 - \frac{2}{\sqrt{\lambda}}$), independent of the confinement physics at small u .
- For sufficiently large positive t , bound states with energies $E_n(t)$, $n = 1, 2, \dots$ (*i.e.* Regge trajectories, with spins $j_n(t)$ and positive slopes); the WKB approximation assures that for fixed j the trajectories at large t are equally spaced in \sqrt{t} , while for sufficiently large j the slopes of the trajectories at low t become parallel, with slope of order $(\lambda\Lambda^2)^{-1}$. The trajectories remain linear, with a $(\alpha'_0 t)^{1/2} \lambda^{-1/4}$ correction, in the resonance regime $\alpha'_0 t = O(1)$.
- For sufficiently negative t , no bound states; as t decreases the bound states move into the continuum, potentially becoming resonances, and thus the Regge trajectories disappear under the cut and move onto the second sheet of the j plane.
- Since $j_0 < 2$, a spin-two glueball with mass $m_n = \sqrt{t}$ at each t for which $j_n(t) = 2$ (equivalently, $E_n(t) = 0$); the WKB approximation ensures that $m_n \propto n$ for large n , not \sqrt{n} as in flat-space string theory.

These quasi-universal phenomena are in contrast to certain important model-dependent features. The low-lying bound states of the quantum mechanics problem, and the behavior of the trajectories $j_n(t)$, $n \sim 1$, near $j = j_0$ — the value of t at which they touch the end of the cut, and their behavior once they move onto the second sheet of the j plane — are sensitive to the details of the potential. These aspects of the physics will be model-dependent even at large λ and large N . The strongest model-dependence is to be found where the leading trajectory disappears into the cut, which unfortunately is a region of great physical importance. Specifically, the

value $t = t_1$ satisfying $E_1(t_1) = 4$, where the leading trajectory intersects the cut at $j = j_0$, is not strongly constrained by general arguments. It appears that one may vary the potential $V(u)$ to obtain either sign for t_1 , suggesting that different confining models may lead to either sign. Thus, *whether the BFKL-type cut at $j \leq j_0$ or the leading Regge pole $j_1(t)$ dominates the large- s , $t = 0$ behavior of the kernel appears to be model-dependent.* This is relevant for a number of processes whose amplitudes are dominated by (or related through the optical theorem to) forward scattering.

At smaller λ (but still with large N and a conformal ultraviolet) certain aspects of Fig. 8 will be modified. From QCD data and BFKL calculations, we expect that the Regge trajectories become steeper as λ becomes smaller, and that j_0 decreases from 2 toward 1. Our results are consistent with these expectations: the trajectories have slope $\sim 1/\sqrt{\lambda}\Lambda^2$, and $j_0 = 2 - 2/\sqrt{\lambda}$. The supergravity states and higher-spin string states begin to overlap as $\lambda \rightarrow 1$, and the simple picture from the supergravity regime must be supplemented; our auxiliary quantum mechanics problem becomes non-local. The analytic structure that we have found, however, may remain intact. This is because of the overall stability of the cut, whose presence at all t is required by conformal invariance, and of the trajectories, which are required by confinement and the existence of glueballs at positive t .

Conversely, however, our results support weak-coupling arguments against applying BFKL to physics at $t = 0$. Single-Pomeron exchange for $|t| \sim \Lambda^2$ is sensitive to the details of confinement, and the dominant contribution from this regime need not be determined by the physics of the model-independent cut — the hard Pomeron — obtained at large negative t . Different models with the same value of j_0 can have different $t \rightarrow 0$ soft-Pomeron physics. While we have argued this in the regime $1 \ll \lambda \ll N$, we see no reason for it to change when $\lambda \ll 1 \ll N$, or for smaller N .

In sum, the analytic structure realized in Fig. 8 follows at large λ on very general grounds, with few assumptions, from the constraints of ultraviolet conformal invariance and the physics of confinement. Its generality suggests that its rough form survives to smaller λ .

6. Effect of Running Coupling

Up to this point, we have considered only theories for which the beta function vanishes at high energies. A logarithmically-running coupling λ makes a substantial qualitative change to the kernel.

The effect on the differential operator appearing in the heat kernel is simple enough: as long as the running is slow, one may view λ as changing adiabatically, and replace $\sqrt{\lambda}$ with $\sqrt{\lambda(u)}$, or equivalently R with $R(u)$, in Δ_2 . This reasoning is valid both in QCD and in large- λ theories such as the duality cascade. Corrections to this approximation are proportional to derivatives of $\sqrt{\lambda}$, which, as we will show, are parametrically small in the region relevant to our computation.

However, as is well-known from weak-coupling analyses, this small change in the operator has a dramatic effect on the analytic structure of the kernel [28]. For a negative beta function, the continuous spectrum of the operator is replaced with a discrete spectrum of bound states, even for $t < 0$; the BFKL cut is replaced with a dense set of poles, the first of which is often called the “hard Pomeron” (in a shift of the terminology formerly used to describe the cut.) For a positive beta function, the coupling in the ultraviolet is unbounded and the cut simply begins at $j = 2$, the infinite- λ expectation.

6.1 Effect in UV

For a negative beta function (as in QCD) results are most easily obtained at large negative t , where the details of the ultra-strongly-coupled infrared physics are unimportant. The calculations are dominated by the region where $1 \ll \lambda(u) \ll N$, that is, where the running coupling satisfies $g^2 \ll 1 \ll g^2 N$.

Examples of gauge theories with negative beta functions and string-theoretic dual descriptions are known. One such theory [78] has IIB strings on a space with an orientifold 7-plane, 4 D7 branes displaced far from the orientifold, and N D3 branes on the orientifold; this $\mathcal{N} = 2$ $Sp(2N)$ gauge theory has a negative beta function

$$\beta_\lambda = -\frac{4}{N} \frac{\lambda^2}{4\pi^2} . \quad (6.1)$$

It is important to note that $\beta_\lambda \sim 1/N$ in this model, which is also true of the duality cascade (for which $\beta_\lambda > 0$.) In such models the dual strings propagate on a space which is approximately $AdS_5 \times W$, with a slowly varying metric and/or dilaton.²⁴

For the general $\beta_\lambda < 0$ case, we define

$$0 < B \equiv -\beta_\lambda/\lambda^2 \sim \frac{1}{N} .$$

The coupling varies slowly, as

$$\frac{1}{\lambda(\mu)} = \frac{1}{\lambda(\mu_0)} + B \ln(\mu/\mu_0) \quad (6.2)$$

Viewed from the ten-dimensional point of view, the coupling depends on z , or equivalently u , as

$$\frac{1}{\lambda(u)} = \frac{1}{\lambda(u_0)} + B(u - u_0) \quad (6.3)$$

since $u \propto -\ln z \propto \ln r$ and $r \sim \mu$ in the AdS/CFT correspondence. In this section it will be convenient to take $\lambda(u_0) = \infty$ and $u_0 = 0$, so that $\lambda(u) = (Bu)^{-1}$; note

²⁴This statement need not be strictly correct; in fact it is violated by the metric of the orientifold model, at any u , in the region near the orientifold plane. However, the space-time region in which it is false decreases without limit as u becomes large. This issue plays no role here and we will proceed without examining it further.

that in the previous section we set $u = 0$ to be at the confinement scale Λ , but we will not assume so here.

What is the effect of this running coupling? The details are model-dependent, but only in regions at small u . At large u the effect can only be an adiabatic alteration of the $AdS_5 \times W$ metric (except possibly, as noted in the previous footnote, at isolated regions of small measure on the internal space W , which will have no effect on the calculation.) Working in string frame, the metric will take the form, to leading order at large u ,

$$ds^2 = e^{2A(u)} dx^2 + R^2(u) [du^2 + ds_W^2(u)] \quad (6.4)$$

where, to leading order, $A \approx u$ and

$$R^4(u) = 4\pi\lambda(u)\alpha'^2 = \frac{4\pi\alpha'^2}{Bu} . \quad (6.5)$$

It will prove inconvenient to have a running g^{uu} , so for later use we may put the metric in the form

$$ds^2 = e^{2A(w)} dx^2 + \alpha' dw^2 + R^2(w) ds_W^2(w) . \quad (6.6)$$

using a variable w satisfying

$$dw = \frac{R(u)}{\sqrt{\alpha'}} du \Rightarrow u = Cw^{4/3} \quad (6.7)$$

where $C \propto B^{1/3}$.

We now turn to the differential operator whose spectrum determines the kernel. This is $\Delta_j \approx \Delta_2$, as defined in (2.21), with the replacement of the factor r/R by e^A :

$$\Delta_2 = e^{2A} \nabla_0^2 [e^{-2A} \phi_{++}] . \quad (6.8)$$

(In the hard-wall model below, the boundary condition at the wall will now be $\partial_w(e^{-2A} \phi_{++}) = 0$.) In the adiabatic regime, all terms in the metric vary slowly at large u except for the warp factor $e^{2A(u)}$. We need therefore only keep derivatives acting on $A(u)$, while dropping all derivatives acting on $R(u)$ and on the slowly-varying metric on W . Similarly, if the theory has other varying fields, their slow variations need not be retained at large u .

In the w coordinate, the differential operator is of Schrödinger form. Diagonalizing the operator is equivalent to solving a Schrödinger problem

$$\mathcal{H}\Psi_{\mathcal{E}}(w) = [-\partial_w^2 + V(w)]\Psi_{\mathcal{E}}(w) = \mathcal{E}\Psi_{\mathcal{E}}(w) \quad (6.9)$$

with potential

$$V(w) = \left(\frac{8}{3}C\right)^2 w^{2/3} - h(w)t e^{-2Cw^{4/3}} \quad (6.10)$$

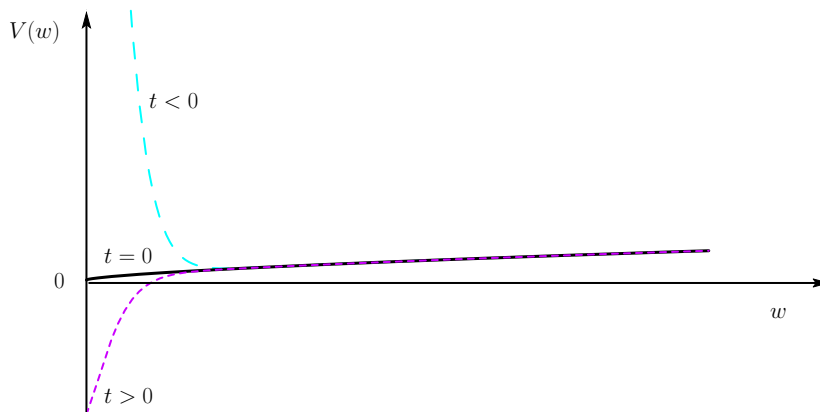


Figure 10: The form of the potential $V(w)$ in a model with a running coupling, where confinement is implemented with a hard wall. Curves are shown for positive, zero, and negative values of t . Compare to Fig. 7.

where $h(w)$ is a positive-definite function (of mass dimension -2) whose form depends on details beyond the adiabatic approximation; its effect is subleading, because it varies slowly compared to the exponential that it multiplies. (To the same level of approximation, the boundary condition in the hard wall is $\partial_w[e^{-2Cw^{4/3}}\Psi_{\mathcal{E}}(w)] = 0$.) Here the operator \mathcal{H} and the eigenvalue \mathcal{E} differ from our earlier conventions; in the limit of a vanishing beta function, $\mathcal{H} = \sqrt{\lambda}H$ and $\mathcal{E} = \sqrt{\lambda}E$. With a running coupling, our earlier H and E are not defined, since they were expressed in terms of what is now a running R ; but $\mathcal{E} = 2(2 - j)$ is well-defined. Normal-ordering issues involving \mathcal{H} and the running λ are subleading within the adiabatic approximation.

The nonadiabatic corrections to these expressions are of order $1/u \sim (R/\sqrt{\alpha'})/w \sim B\lambda(u)$; since $B \sim 1/N$ this implies corrections are of order $\lambda(u)/N$, which is small in the region of interest. Said another way, if t is large and negative, but not exponentially large, the repulsive exponential potential forces the calculation to the region of large u , where $1 \ll \lambda(u) \ll N$ and our adiabatic approximations and supergravity are both valid. Thus the large negative t region is, as in the conformal case, model-independent. This is consistent with earlier weak-coupling results [28, 29] and is illustrated in Fig. 10.

The potential, for $t < 0$, grows to infinity at both small and large w , which implies that the spectrum of Δ_2 consists of discrete bound states. More precisely, this is true only within the supergravity approximation, where $|E| \ll \sqrt{\lambda}$, and $|j - 2| \sim 1/\sqrt{\lambda}$. At large w , where the coupling constant becomes small, the supergravity approximation breaks down and perturbative field theory becomes valid. In this regime one can match on to existing results for BFKL with a running coupling [20, 21, 79, 80, 81, 82, 83]. It is well-known [28] that in this case the discrete poles²⁵ end at $j = 1$, where a cut begins and extends to $j \rightarrow -\infty$.

²⁵For the non-vacuum $q\bar{q}$ system, the corresponding poles end at $j = 0$ [55].

For the bound states lying within the supergravity approximation, the slowly-growing potential at large w ensures that the spacing of their energy eigenvalues decreases at higher eigenvalues. The lowest eigenvalue, not surprisingly, lies near

$$j_1(t) \sim 2 - \frac{2}{\sqrt{\lambda(\mu)|_{\mu=\sqrt{|t|}}} - \mathcal{O}(\sqrt{B}) = 2 - \sqrt{2B \ln [z_0^2 |t|]} - \mathcal{O}(\sqrt{B}) . \quad (6.11)$$

This is simply the conformal result for the beginning of the cut but with λ replaced with the running coupling $\lambda(\mu)$, evaluated at $\mu \sim \sqrt{|t|}$, with corrections from zero-point fluctuations around the minimum of the effective potential.²⁶

Strictly speaking, none of these calculations can be done entirely within the large λ regime, since $\lambda(\mu) \rightarrow 0$ in the ultraviolet. However, because $B \sim 1/N$, this occurs at very large u , in particular $u \gg N$. The leading BFKL poles, associated with eigenstates of Δ_2 , have exponentially damped eigenfunctions at large u , and are not sensitive to this region.

For sufficiently large $-t$, the region of small u makes an exponentially suppressed contribution, but the above calculations will have to be modified at small u as $|t|$ decreases. There are two possible effects that should be accounted for: at small u our adiabatic approximation may break down, and also ultra-strong-coupling effects and confinement become important. In fact these two conditions are related, and both occur around $u \sim 1$, or more precisely at $u \sim 1/BN$. Therefore either $-t$ is large enough that both effects can be neglected, or $-t$ is small enough that infrared effects such as confinement must be accounted for. In short we expect the results just obtained for large negative t will be reliable for $-t \gg \Lambda^2$, requiring modification only at the scale where confinement effects set in.²⁷

It is straightforward to repeat this exercise for the case of a positive beta function. The result is quite different, because the effective potential is bounded as $u \rightarrow \infty$. The spectrum again consists of a cut, which begins at $j_0 = 2 - 2/\sqrt{\lambda_{max}}$ where λ_{max} is the largest value obtained by the coupling. In the case of the duality cascade [71], the 't Hooft coupling formally runs to infinity and $j_0 = 2$.

6.2 The analytic structure at all t (running coupling)

Now let us turn to the properties of the kernel at values of t where confinement is

²⁶To see this it is sufficient to do a variational calculation or harmonic-oscillator-approximation for the ground state in the potential (6.10). One must use the fact that $C \sim B^{1/3}$ is small, that $h(w)$ is slowly varying, that $Cw^{2/3} \sim \sqrt{Bu} \sim 2/\sqrt{\lambda(u)}$, and that the answer must be consistent with our previous result for the conformal regime, $j_0 = 2 - 2/\sqrt{\lambda}$, in the limit $B \rightarrow 0$, $t \rightarrow \infty$ with $\lambda(\sqrt{|t|})$ fixed. Higher states are better described using the WKB approximation, in a form which is quite similar to the weak coupling calculations of [29].

²⁷This can be seen in particular examples. For example, in the orientifold model, the subleading terms become important where the dilaton reaches the value of order 1; this is also where large deviations in the metric are expected. In a confining version of the orientifold model, along the lines of the $\mathcal{N} = 1^*$ model [70], the confinement regime must set in at or above this scale.

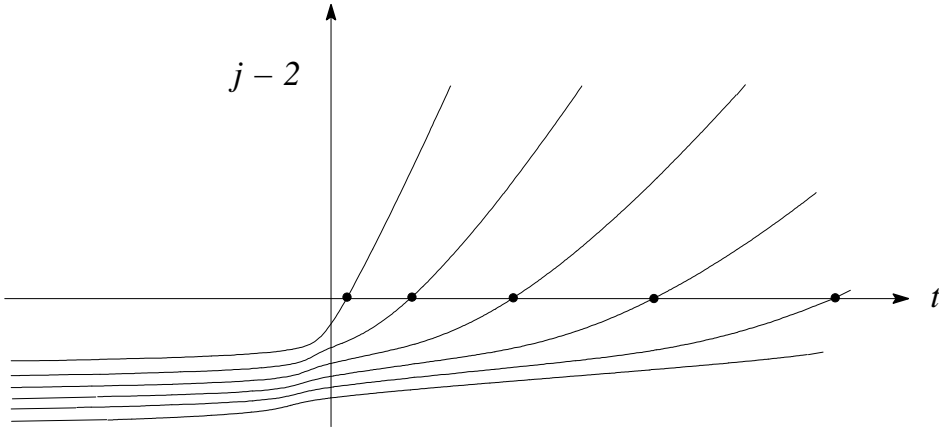


Figure 11: The analytic behavior of Regge trajectories with a running coupling. The figure represents the spectrum of a hard-wall model with potential (6.10); for definiteness we have set $h(w) = 1$ and put the wall at a point where the exponential term is of order one. For $t > 0$ the bound-state poles are only logarithmically changed from Fig. 8, but for $t < 0$ the cut in Fig. 8 disintegrates into poles which are the continuation of the Regge poles at positive t . As t decreases, the poles slowly descend; weak coupling considerations indicate they move toward $j = j_{min} \geq 1$, where a cut begins.

important. As before, we focus on the general properties of confining theories, whose essential feature is the ending of the dual spacetime at some $u \sim 1$, or equivalently, some $w \sim N^{1/4}$. In Sec. 5 we considered the hard-wall model with a conformal ultraviolet, and inferred general lessons from it. Rather than pursue a similar strategy here, we will now modify the lessons of Sec. 5.2 as required for the case of a running coupling.

Many features of ultraviolet-conformal infrared-confining theories continue to apply here. Again the quantum mechanics problem in the large positive t region is characterized by a set of bound states with negative energy eigenvalues (that is, with positive values of $j - 2$) which are well-separated and form the Regge trajectories of the supergravity regime. Again the $|t| \sim \Lambda^2$ regime is model-dependent in its details. The major new feature is that the continuum of states with positive eigenvalues (the cut at $j \leq j_0$) is no longer present, for any t , because of the growing potential at large w . The operator has a discrete spectrum at any t , consisting of an infinite number of closely spaced states with a positive eigenvalue ($j < 2$), and for $t > 0$ a finite number of well-spaced negative-eigenvalue ($j > 2$) states. As t is increased, the eigenvalue $E_n(t)$ of any given state will move continuously from positive to negative; correspondingly its spin $j_n(t)$ will move smoothly from below 2 to above 2. This is shown in Fig. 11. Thus, in contrast to the conformal case, where the spin j of each Regge trajectory, as t is decreased, moves down to $j = j_0$ and disappears below the BFKL-type cut, here each trajectory moves down to become one of the BFKL-type poles. In particular, the leading Regge trajectory (often called the soft Pomeron)

smoothly becomes the leading pole (the hard Pomeron) as t moves from positive to negative. This is consistent with the suggestion of [31]. It is interesting to compare the figure with the results in [84]; see also [19].

As in the UV-conformal case, this basic form of Fig. 11 is model-independent, while some details, such as the precise nature of the transition near $|t| \sim \Lambda^2$, are not. Specifically, the value $j_1(t)$ of the leading pole at and near $t = 0$ is sensitive to the details of confinement, as was also true in the ultraviolet conformal case.

It seems likely that the analytic structure shown in Fig. 11 is preserved into theories with a parametrically larger beta function, including large- N QCD, for which the small- λ regime is much closer to the confinement regime and the large- λ regime is very small. QCD data [15] and lattice results on the hadron spectrum [7, 8, 85], and BFKL calculations at $-t \gg \Lambda^2$ [28, 29, 84], suggest that our results match the analytic structure of QCD at $|t| \gg \Lambda^2$, for both signs of t . The logarithmically-violated conformal invariance of the theory continues to put constraints on the form of the kernel at large negative t , while the Regge trajectories at positive t are not expected to be much affected by the beta function. A smooth transition between the two behaviors, as in Fig. 11, is not required theoretically, but seems plausible.

An interesting feature is that the leading Regge trajectory in Fig. 11 has $dj/dt > 0$ everywhere, and so the $t = 0$ behavior of the amplitude must have faster growth with s than the $t < 0$ behavior. The data are ambiguous as to whether this applies in real-world QCD, as we now discuss.

7. Outlook

We have obtained the j -plane singularity structure of the Pomeron, as a function of t , at large 't Hooft coupling. One may ask if our strong-coupling results are consistent with those which have already been obtained at weak coupling. In particular, since the location j_0 of the leading singularity has been obtained to second- or third-order in certain weakly-coupled theories, using BFKL computational methods, one may ask if the weak- and strong-coupling results can be suitably compared. A theory in which this comparison is well-posed is $\mathcal{N} = 4$ Yang-Mills theory. This theory has a constant and fully adjustable coupling α , and the quantity $\lambda = R^4/(\alpha')^2 = 4\pi\alpha N$, where α is the constant Yang-Mills coupling. Can our result $j_0 = 2 - 2/\sqrt{\lambda}$ be interpolated with the weak-coupling result? The answer is shown in Fig. 12. The leading-order BFKL computation of j_0 , Eq. (1.3), grows from 1 toward 2 as αN increases, but dramatically overshoots our result well before one would trust the strong-coupling calculation. However, the next-to-leading-order correction to the coefficient j_0 is substantial and negative [48] — though much smaller than the correction in QCD itself (on which we will have more to say below.) The two-loop formula for the BFKL

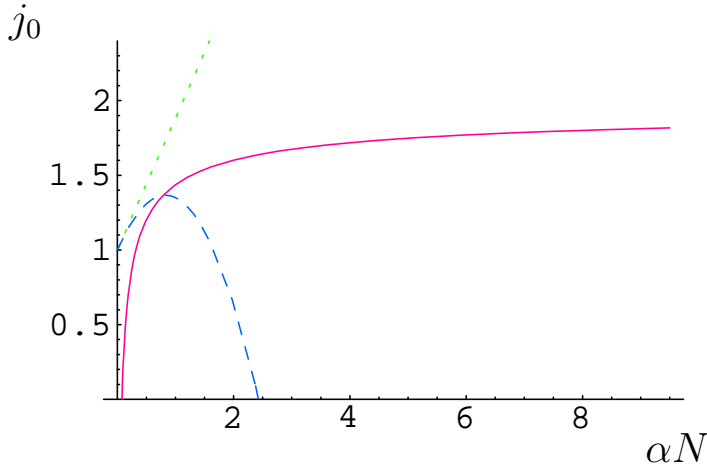


Figure 12: In $\mathcal{N} = 4$ Yang-Mills theory, the weak- and strong-coupling calculations of the position j_0 of the leading singularity for $t \leq 0$, as a function of αN . Shown are the leading-order BFKL calculation (dotted), the next-to-leading-order calculation (dashed), and the strong-coupling calculation of this paper (solid). Note the latter two can be reasonably interpolated.

exponent j_0

$$j_0 = 1 + 4 \ln 2 \frac{\alpha N}{\pi} \left(1 - 7.58 \frac{\alpha N}{4\pi} \right) \quad (7.1)$$

does not overshoot the strong-coupling result, and indeed matches on to it quite reasonably at $\alpha N \sim 1$. Thus, at least in $\mathcal{N} = 4$ Yang-Mills, the results appear compatible.

Let us now try to relate our dual string picture to the Pomeron physics of QCD itself. The latter is still a subject of great confusion; we cannot fully resolve this here, but the simple and unified picture that we have found gives a useful framework for organizing the discussion.

One of the most striking aspects of high-energy hadronic scattering is the rise in the total cross section, $\sigma_T(s)$, at the highest available energies to date. In Regge language, this requires a leading j -plane singularity with vacuum quantum numbers, i.e. the Pomeron, and an intercept above $j = 1$. For instance, in the well-known work of Donnachie-Landshoff [6], hadron cross-sections are fitted to a single-Pomeron exchange model that gives $j_0 = 1.08$ for the Pomeron at $t = 0$. On the other hand, there is also evidence, for example from the small- x behavior of parton distribution functions, for a much larger intercept, perhaps as large as 1.5 [86].

It is common to ascribe these behaviors to two distinct components of the Pomeron. The exchanged object relevant for processes dominated by infrared physics is called the “soft” Pomeron, while in processes in which scales above the confinement scale are dominant, it is the “hard” Pomeron which is relevant. This distinction has a simple meaning in our picture, where the Pomeron depends on the fifth coordinate

r : this degree of freedom corresponds to the overall size of the hadron wavefunction, $\delta x \propto R^2/r$, so the soft Pomeron has a size set by the confinement scale while the hard Pomeron is much smaller.

The two-component Pomeron still presents a significant puzzle, however. Consider the large- N limit of QCD, where we can isolate the contribution from single Pomeron exchange. The leading Pomeron is a pole, due to the running coupling, and we have the sharp question: what is its intercept — is it near 1.08, or much larger? The present theoretical understanding is not sufficient to answer this. If we start at large negative t , where the potential barrier forces the Pomeron to be small, then the perturbative BFKL analysis applies and gives an exponent

$$j_0 = 1 + \frac{4 \ln 2}{\pi} \alpha(t) N \left(1 + \mathcal{O} \left[\frac{\alpha(t) N}{\pi} \right] \right) . \quad (7.2)$$

As we reduce $|t|$, the effective coupling increases and so does the exponent, until at some point infrared effects take over and the growth stops, leading to a finite intercept at $t = 0$.²⁸ If we make even the seemingly conservative assumption that the BFKL result holds down to $\alpha = 0.25$ (for $N = 3$ QCD), we obtain the large exponent $j_0 \sim 1.6$. However, it is known that the two-loop correction to the exponent is very large and negative,

$$j_0 = 1 + 4 \ln 2 \frac{\alpha N}{\pi} \left(1 - \left[25.8 + 0.2 \frac{N_f}{N} \right] \frac{\alpha N}{4\pi} \right) , \quad (7.3)$$

and within the regime in which the calculation is reliable — at most $\alpha < 0.1$, or more usefully $\alpha N < 0.3$ — the value of j_0 does not exceed 1.10 [20]. The leading- and next-to-leading expressions for j_0 as a function of αN are shown in Fig. 13, along with a horizontal line at 1.08. Thus there is no reliable indication that the true intercept as $t \rightarrow 0$ must exceed 1.10, and perhaps the all-orders BFKL calculation would predict nothing larger than 1.08. We cannot resolve this issue, but let us discuss how the various possibilities could be consistent with the two-component Pomeron picture.

If the true exponent for the hard Pomeron is large compared to 1.08, how could we see a much smaller exponent in the total cross section? There are two possibilities here: that the total cross section is still in a regime dominated by single Pomeron exchange, or that we are seeing the effects of multiple Pomeron exchange. If we are seeing single-Pomeron exchange, then the soft Pomeron must be some sort of resonance. Recall that the energy in the potential model appears with a negative sign in the exponent, so a lower exponent is a higher energy. In the potential model, there could be a barrier between the small- r and large- r region, with the true Pomeron ground state (the hard Pomeron) concentrated at large r , and the soft Pomeron being

²⁸In our strong-coupling potential model with running coupling, the exponent is monotonically increasing with t . This is likely to be true at all λ , since even if $|t|$ is small we can take a small Pomeron wavefunction as a variational approximation, giving a lower bound on the exponent.

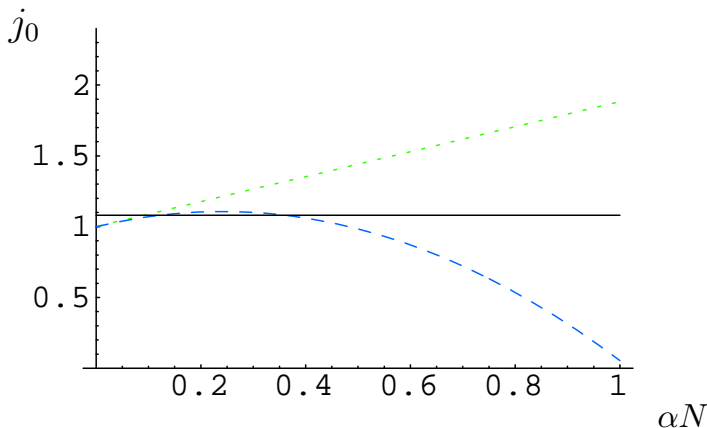


Figure 13: In QCD, the leading-order and next-to-leading-order calculations of the position j_0 of the leading singularity as a function of αN . Shown are the leading-order BFKL calculation (dotted), the next-to-leading-order calculation (dashed), with $N_f = 3$, and the value 1.08 of the phenomenological soft-Pomeron intercept as extracted from data [6] (solid). There is no convincing evidence that j_0 ever exceeds 1.08.

an excited state at small r . Despite the fact that $dj_0/dt > 0$ for the leading pole, the effect of the resonance would be to make it appear that $dj_0/dt < 0$ in a region where the resonance begins to dominate but before the asymptotic Regge behavior is reached. We should emphasize that at small λ the sharp locality in r no longer holds, and the reduction to the single degree of freedom of the Pomeron size is no longer a precise statement, but we can imagine that there are different regions in the Pomeron wavefunction that mix only weakly [31].

The other possibility is that the single-Pomeron exponent really is large. This leads to rapid growth of the cross section with energy and the apparent value of 1.08 must then be due to unitarization effects, with multi-Pomeron exchange pulling the exponent down toward the Froissart bound of 1-plus-logarithms. We will briefly discuss unitarization in the string picture below. For QCD, if multi-Pomeron exchange dominates, there is the puzzling question of why factorization works so well, in particular that data indicates that $\sigma_{a,b} \simeq \gamma_a \gamma_b$ to the level of 10 – 20%.

If instead the true exponent for the hard Pomeron is no larger, and perhaps even smaller, than that of the soft Pomeron, why do we see a larger exponent in some processes? It is possible that this is a transient effect due to diffusion. If we have a process where some external states are hard and some soft, as in deep inelastic scattering, then the initial overlap of the wavefunctions is small, but as we go to larger s the Pomeron diffusion kernel leads to an increasing overlap, and thereby gives an amplitude that increases faster than the exponent in the kernel. An example of this effect is discussed in [30].

Regardless of the situation in QCD at current energies, it must be true asymp-

totically that multi-Pomeron exchange is important. The BFKL calculation, in the extreme UV where it must be valid, gives a variational lower bound on the Pomeron intercept that is strictly greater than 1. Thus single Pomeron exchange will necessarily violate the Froissart bound. If we consider very large but fixed N , each Pomeron exchange costs a factor of $1/N^2$ but increases without bound at high energy, so at some point multiple Pomeron exchange will dominate.

It is interesting to consider this regime on the dual string side. Giddings studied hadronic total cross sections via gauge-string duality, and argued that the dominant process was black hole production, and moreover that this would saturate the Froissart bound [87] (for some recent followup see refs. [88, 89]). Our work in this paper applies in a different region of parameter space; that is, we take N large compared to all other quantities so that we are strictly limited to one-Pomeron exchange, while black holes are produced as $s \rightarrow \infty$ at fixed N . For completeness we provide here a brief discussion of the latter limit.

Looking first at the scattering process in ten dimensions, the amplitude in the supergravity approximation is

$$\mathcal{T} \sim G\tilde{s}^2/\tilde{t}, \quad G \sim g_{\text{string}}^2\alpha' \sim R^8/N^2;$$

note that we are ignoring dimensionless constants. To get a dimensionless measure of the size of this amplitude we rescale to canonical normalization and go to impact parameter space,

$$\mathcal{T}' \sim R^8\tilde{s}/b^6N^2.$$

where b is the impact parameter of the collision. At any fixed b and N , this is large when $\tilde{s} \gg b^6N^2/R^8$. The minimum effective impact parameter is $\sqrt{\alpha'}$, so perturbation theory first breaks down when $\tilde{s} \sim N^2\alpha'^3/R^8$. This condition is reached first at $r = r_0$, corresponding to $s \sim \Lambda^2N^2\lambda^{-3/2}$.

When perturbation theory breaks down we can go further by the eikonal summation, which in impact-parameter space takes the form

$$\mathcal{T}_{\text{eik}} = -i(e^{i\mathcal{T}'} - 1).$$

There is a simple interpretation: one-graviton exchange breaks down because the center of mass energy is large, and the resummed amplitude represents the interaction of the particles through their coherent gravitational fields.

The eikonal approximation breaks down when the momentum transfer $\partial_b\mathcal{T}'$ is of order \sqrt{s} , or

$$\tilde{s}^{1/2}R^8/b^7N^2 \sim \tilde{s}^{1/2}G/b^7 \gg 1.$$

In ten dimensions this is the same as the condition that the impact parameter is less than the Schwarzschild radius, so the system forms a black hole. Thus at given b there are three parametric regimes with increasing energy: one-graviton exchange, eikonized graviton exchange, and black hole formation. Note also that nonlinearities of

the gravitational field are also small below the black hole scale, so only s -channel ladder plus crossed-ladder graphs are important (the eikonal approximation).

We have neglected Regge shrinkage, which does not qualitatively affect the discussion, as well as the effect of AdS curvature, which slightly reduces the exponent and also gives the graviton a mass; to obtain a Froissart bound we must take the latter into account. Ref. [87] argued that black hole production would saturate the Froissart bound. However, we should note that the eikonal approximation also saturates this bound [90, 91], so the amplitude will take the Froissart form even before black hole production. Note however that the transition from eikonal to black hole behavior is a genuine phase transition, from states with order N^0 degrees of freedom to states with N^2 degrees of freedom (a gluon plasma; see [92] for a recent discussion.)

It is interesting to follow the discussion to smaller λ . For exponent j_0 , the condition for breakdown of the eikonal approximation is $s^{j_0-3/2}f(b)/N^2 \gg 1$. Once j_0 drops below 1.5, the energy dependence cannot overcome the N^2 , and so there should be no analog of the black hole phase; rather the eikonal approximation is valid to all energies. In large- N QCD it seems likely, according to the previous discussion, that the effective exponent is always less than 1.5; then there is no production of a gluon plasma. Ref. [92] came to a similar conclusion by other reasoning.

Let us now comment on a couple of important issues that we have left unresolved. The matching at negative t of the weak-coupling and strong-coupling conformal kernels, discussed at the end of Sec. 2, is subtle, because the two kernels are functions of somewhat different variables. The leading-order weak-coupling kernel is a function of the momenta of two gluons, while the strong coupling kernel is a function of collective coordinates of a string built from an indefinite number of gluons. To make a precise match would require a more complete understanding of how partons emerge from the string description of the theory, which is a question far outside the supergravity approximation. However, it should be possible to clarify the relation of the results without a full understanding of the partonic limit. Note there is a formal similarity between the weak-coupling BFKL amplitude (2.43) and the general string result (3.47); this should be explored further.

Also unaddressed are the formal issues surrounding the adiabatic approximation and the slow running of the coupling. In a conformal theory, both at weak coupling and at strong coupling, one finds a stable t -independent cut, and there is a clear understanding of how this follows from conformal invariance. Meanwhile, a running coupling breaks the cut into a set of running poles, rather than a t -dependent cut. The fact that this occurs must follow from a formal argument involving weakly-broken conformal invariance, but we are not aware of the existence of any direct proof. It should also be possible to study the spacing of the poles and properties of their residues using methods that are valid at any λ .

To conclude, we have in this paper concerned ourselves with a unified treat-

ment of large- N QCD-like theories at high energy, by concentrating on the single Pomeron kernel over the entire range of t . We have limited our discussion to the 2-to-2 scattering of spinless particles, but the formalism can be generalized to treat processes involving particles with low spin, multi-particle production, and others. Our kernel can be directly used to address quarkonium-quarkonium and $\gamma^*\gamma^*$ scattering, with external states involving wave functions which are strongly peaked at large u , to extend earlier discussions of deep inelastic scattering [30], and connect these regimes to the large-angle scattering physics of [25]. Exclusive production processes involving a moderate number of final particles or jets can also be studied [62]. We can also generalize our analysis to apply to inclusive particle production [60, 61]. One particular promising area of study is the inclusive diffractive production of jets, which is expected to have a significant cross section at LHC. Since such events will likely involve a wide range of momentum transfer squared, our unified framework, capable of describing simultaneously both infrared and ultraviolet features, offers a unique vantage point. In particular, the idea of a ‘‘Pomeron structure function’’, which has been a controversial notion from a weak-coupling analysis [93, 94, 95], can be addressed from a fresh perspective. Other specific examples of experimental importance include the study of diffractive production of vector mesons at large t , which has been thoroughly analyzed from a weak coupling approach [96]. We hope to return to these issues in future publications.

Acknowledgements: We are pleased to acknowledge useful conversations with O. Andreev, A. H. Mueller, R. Janik, E. Levin, L. N. Lipatov, and M. Strickman. The work of R.B. was supported by the Department of Energy under Contract. No. DE-FG02-91ER40676, that of C.-I.T. was supported in part by the Department of Energy under Contract No. DE-FG02-91ER40688, Task-A, that of J.P. by NSF grants PHY99-07949 and PHY04-56556, and that of M.J.S. by U.S. Department of Energy grants DE-FG02-96ER40956 and DOE-FG02-95ER40893 and by an Alfred P. Sloan Foundation award. We are grateful to the Kavli Institute for Theoretical Physics for its support of the 2004 QCD and String Theory Program, where this work was initiated.

References

- [1] G. F. Chew and S. Frautschi. *Phys. Rev. Letts.*, **7**, 394 (1961).
- [2] V. N. Gribov. *JETP*, **14**, 478 (1961).
- [3] G. Veneziano, “Origin and Intercept of the Pomeranchuk Singularity,” *Phys. Lett.* **B43** (1973) 413–416.
- [4] A. Capella, J. Tran Thanh Van, U. Sukhatme, and C. I. Tan, “The Pomeron Story.” in *A Passion For Physics*, World Scientific (1984), 79-87.
- [5] A. Capella, U. Sukhatme, C.-I. Tan, and J. Tran Thanh Van, “Dual Parton Model,” *Phys. Rept.* **236** (1994) 225–329.
- [6] A. Donnachie and P. V. Landshoff, “Total Cross-Sections,” *Phys. Lett.* **B296** (1992) 227–232, [hep-ph/9209205](#).
- [7] C. J. Morningstar and M. J. Peardon, “The Glueball Spectrum from an Anisotropic Lattice Study,” *Phys. Rev.* **D60** (1999) 034509, [hep-lat/9901004](#).
- [8] H. B. Meyer and M. J. Teper, “Glueball Regge Trajectories and the Pomeron: A Lattice Study,” *Phys. Lett.* **B605** (2005) 344–354, [hep-ph/0409183](#).
- [9] R. C. Brower, S. D. Mathur, and C.-I. Tan, “Discrete Spectrum of the Graviton in the AdS(5) Black Hole Background,” *Nucl. Phys.* **B574** (2000) 219–244, [hep-th/9908196](#).
- [10] N. R. Constable and R. C. Myers, “Spin-two Glueballs, Positive Energy Theorems and the AdS/CFT Correspondence,” *JHEP* **10** (1999) 037, [hep-th/9908175](#).
- [11] R. C. Brower, S. D. Mathur, and C.-I. Tan, “Glueball Spectrum for QCD from AdS Supergravity Duality,” *Nucl. Phys.* **B587** (2000) 249–276, [hep-th/0003115](#).
- [12] E. Witten, “Anti-de Sitter Space, Thermal Phase Transition, and Confinement in Gauge Theories,” *Adv. Theor. Math. Phys.* **2** (1998) 505–532, [hep-th/9803131](#).
- [13] C. Csaki, H. Ooguri, Y. Oz, and J. Terning, “Glueball Mass Spectrum from Supergravity,” *JHEP* **01** (1999) 017, [hep-th/9806021](#).
- [14] R. de Mello Koch, A. Jevicki, M. Mihailescu, and J. P. Nunes, “Evaluation of Glueball Masses from Supergravity,” *Phys. Rev.* **D58** (1998) 105009, [hep-th/9806125](#).
- [15] A.V. Barnes *et al.*, “Pion Charge Exchange Scattering at High-Energies,” *Phys. Rev. Lett.* **37** (1976) 76.
- [16] L. N. Lipatov, “Reggeization of the Vector Meson and the Vacuum Singularity in Nonabelian Gauge Theories,” *Sov. J. Nucl. Phys.* **23** (1976) 338–345.

- [17] E. A. Kuraev, L. N. Lipatov, and V. S. Fadin, “The Pomeranchuk Singularity in Nonabelian Gauge Theories,” *Sov. Phys. JETP* **45** (1977) 199–204.
- [18] I. I. Balitsky and L. N. Lipatov, “The Pomeranchuk Singularity in Quantum Chromodynamics,” *Sov. J. Nucl. Phys.* **28** (1978) 822–829.
- [19] J. R. Forshaw and D. A. Ross. *Quantum Chromodynamics and the Pomeron*, Cambridge University Press (1997).
- [20] V. S. Fadin and L. N. Lipatov, “BFKL Pomeron in the Next-to-Leading Approximation,” *Phys. Lett.* **B429** (1998) 127–134, [hep-ph/9802290](#).
- [21] G. Camici and M. Ciafaloni, “Irreducible Part of the Next-to-Leading BFKL Kernel,” *Phys. Lett.* **B412** (1997) 396–406, [hep-ph/9707390](#).
- [22] A. H. Mueller, “Unitarity and the BFKL Pomeron,” *Nucl. Phys.* **B437** (1995) 107–126, [hep-ph/9408245](#).
- [23] L. Susskind, “Strings, Black Holes and Lorentz Contraction,” *Phys. Rev.* **D49** (1994) 6606–6611, [hep-th/9308139](#).
- [24] J. M. Maldacena, “The Large N Limit of Superconformal Field Theories and Supergravity,” *Adv. Theor. Math. Phys.* **2** (1998) 231–252, [hep-th/9711200](#).
- [25] J. Polchinski and M. J. Strassler, “Hard Scattering and Gauge/String Duality,” *Phys. Rev. Lett.* **88** (2002) 031601, [hep-th/0109174](#).
- [26] R. C. Brower and C.-I. Tan, “Hard Scattering in the M-Theory Dual for the QCD String,” *Nucl. Phys.* **B662** (2003) 393–405, [hep-th/0207144](#).
- [27] S. J. Brodsky and G. F. de Teramond, “Light-Front Hadron Dynamics and AdS/CFT Correspondence,” *Phys. Lett.* **B582** (2004) 211–221, [hep-th/0310227](#).
- [28] L. N. Lipatov, “The Bare Pomeron in Quantum Chromodynamics,” *Sov. Phys. JETP* **63** (1986) 904–912.
- [29] R. Kirschner and L. N. Lipatov, “Bare Reggeons in Asymptotically Free Theories,” *Z. Phys.* **C45** (1990) 477.
- [30] J. Polchinski and M. J. Strassler, “Deep Inelastic Scattering and Gauge/String Duality,” *JHEP* **05** (2003) 012, [hep-th/0209211](#).
- [31] E. Levin and C.-I. Tan, “Heterotic Pomeron: A Unified Treatment of High-Energy Hadronic Collisions in QCD,” [hep-ph/9302308](#).
- [32] R. Blankenbecler, S. J. Brodsky, J. F. Gunion, and R. Savit, “The Connection between Regge Behavior and Fixed Angle Scattering,” *Phys. Rev.* **D8** (1973) 4117.
- [33] R. A. Janik and R. Peschanski, “High Energy Scattering and the AdS/CFT Correspondence,” *Nucl. Phys.* **B565** (2000) 193–209, [hep-th/9907177](#).

- [34] R. A. Janik, “String Fluctuations, AdS/CFT and the Soft Pomeron Intercept,” *Phys. Lett.* **B500** (2001) 118–124, [hep-th/0010069](#).
- [35] O. Andreev and W. Siegel, “Quantized Tension: Stringy Amplitudes with Regge Poles and Parton Behavior,” *Phys. Rev.* **D71** (2005) 086001, [hep-th/0410131](#).
- [36] S. S. Gubser, I. R. Klebanov, and A. M. Polyakov, “Gauge Theory Correlators from Non-Critical String Theory,” *Phys. Lett.* **B428** (1998) 105–114, [hep-th/9802109](#).
- [37] E. Witten, “Anti-de Sitter Space and Holography,” *Adv. Theor. Math. Phys.* **2** (1998) 253–291, [hep-th/9802150](#).
- [38] V. Balasubramanian, P. Kraus, and A. E. Lawrence, “Bulk vs. Boundary Dynamics in Anti-de Sitter Spacetime,” *Phys. Rev.* **D59** (1999) 046003, [hep-th/9805171](#).
- [39] A. M. Polyakov, “String Theory and Quark Confinement,” *Nucl. Phys. Proc. Suppl.* **68** (1998) 1–8, [hep-th/9711002](#).
- [40] A. V. Kotikov, L. N. Lipatov, A. I. Onishchenko, and V. N. Velizhanin, “Three-Loop Universal Anomalous Dimension of the Wilson Operators in $\mathcal{N} = 4$ SUSY Yang-Mills Model,” [hep-th/0404092v5](#).
- [41] S. Bondarenko, E. Levin, and C. I. Tan, “High Energy Amplitude as an Admixture of Soft and Hard Pomerons,” *Nucl. Phys.* **A732** (2004) 73, [hep-ph/0306231](#).
- [42] E. D’Hoker and R. Jackiw, “Liouville Field Theory,” *Phys. Rev.* **D26** (1982) 3517.
- [43] D. J. Gross and P. F. Mende, “String Theory Beyond the Planck Scale,” *Nucl. Phys.* **B303** (1988) 407.
- [44] C. Bachas, “D-Brane Dynamics,” *Phys. Lett.* **B374** (1996) 37–42, [hep-th/9511043](#).
- [45] T. Jaroszewicz, “Gluonic Regge Singularities and Anomalous Dimensions in QCD,” *Phys. Lett.* **B116** (1982) 291.
- [46] L. N. Lipatov, “Small-x Physics in Perturbative QCD,” *Phys. Rept.* **286** (1997) 131–198, [hep-ph/9610276](#).
- [47] A. V. Kotikov and L. N. Lipatov, “NLO Corrections to the BFKL Equation in QCD and in Supersymmetric Gauge Theories,” *Nucl. Phys.* **B582** (2000) 19–43, [hep-ph/0004008](#).
- [48] A. V. Kotikov and L. N. Lipatov, “DGLAP and BFKL Equations in the $\mathcal{N} = 4$ Supersymmetric Gauge Theory,” *Nucl. Phys.* **B661** (2003) 19–61, [hep-ph/0208220](#).
- [49] A. V. Kotikov, L. N. Lipatov, A. I. Onishchenko, and V. N. Velizhanin, “Three-Loop Universal Anomalous Dimension of the Wilson Operators in $\mathcal{N} = 4$ SUSY Yang-Mills Model,” *Phys. Lett.* **B595** (2004) 521–529, [hep-th/0404092](#).

- [50] I. I. Balitsky and V. M. Braun, “Evolution Equations for QCD String Operators,” *Nucl. Phys.* **B311** (1989) 541–584.
- [51] V. Bargmann, “Irreducible Unitary Representations of the Lorentz Group,” *Annals Math.* **48** (1947) 568–640.
- [52] J. Polchinski, “String Theory. Vol. 1: An Introduction to the Bosonic String,” Cambridge, UK: Univ. Pr. (1998) 402 p.
- [53] J. Kwiecinski, “Leading Q and Anti-Q Regge Singularities in Perturbative QCD,” *Phys. Rev.* **D26** (1982) 3293.
- [54] R. Kirschner and L. N. Lipatov, “Double Logarithmic Asymptotics of Quark Scattering Amplitudes with Flavor Exchange,” *Phys. Rev.* **D26** (1982) 1202–1205.
- [55] M. McGuigan and C. B. Thorn, “Quark - Anti-quark Regge Trajectories in Large $N(c)$ QCD,” *Phys. Rev. Lett.* **69** (1992) 1312–1315, [hep-ph/9205211](#).
- [56] J. Bartels and M. Lublinsky, “Quark Antiquark Exchange in $\Gamma^* \Gamma^*$ Scattering,” *JHEP* **09** (2003) 076, [hep-ph/0308181](#).
- [57] J. Bartels and M. Lublinsky, “ $\Gamma^* \Gamma^*$ Scattering via Secondary Reggeon Exchange in QCD,” *Mod. Phys. Lett.* **A19** (2004) 19691982, [hep-ph/0406273](#).
- [58] R. R. Metsaev, C. B. Thorn, and A. A. Tseytlin, “Light-Cone Superstring in AdS Space-Time,” *Nucl. Phys.* **B596** (2001) 151–184, [hep-th/0009171](#).
- [59] B. Zwiebach, “A First Course in String Theory,” Cambridge, UK: Univ. Pr. (2004) 558 p.
- [60] C.E. DeTar *et al.*, “Helicity Poles, Triple-Regge Behavior, and Single-Particle Spectra in High-Energy Collisions,” *Phys. Rev. Lett.* **26** (1971) 675–676.
- [61] C. E. DeTar, J. H. Weis, K. Kang, and C.-I. Tan, “Duality and Single-Particle Production,” *Phys. Rev.* **D4** (1971) 425–439.
- [62] R. C. Brower, C. E. DeTar, and J. H. Weis, “Regge Theory for Multiparticle Amplitudes,” *Phys. Rept.* **14** (1974) 257.
- [63] S. Mandelstam, “Interacting String Picture of Dual Resonance Models,” *Nucl. Phys.* **B64** (1973) 205–235.
- [64] M. Kaku and K. Kikkawa, “The Field Theory of Relativistic Strings, Part 1: Trees,” *Phys. Rev.* **D10** (1974) 1110.
- [65] D. Amati, A. Stanghellini, and S. Fubini, “Theory of High-Energy Scattering and Multiple Production,” *Nuovo Cim.* **26** (1962) 896–954.
- [66] H. B. Nielsen and P. Olesen, “A Parton View on Dual Amplitudes,” *Phys. Lett.* **B32** (1970) 203.

- [67] B. Sakita and M. A. Virasoro, “Dynamical Model of Dual Amplitudes,” *Phys. Rev. Lett.* **24** (1970) 1146.
- [68] J. Polchinski and L. Susskind, “String Theory and the Size of Hadrons,” [hep-th/0112204](#).
- [69] J. Callan, Curtis G. and Z. Gan, “Vertex Operators in Background Fields,” *Nucl. Phys.* **B272** (1986) 647.
- [70] J. Polchinski and M. J. Strassler, “The String Dual of a Confining Four-Dimensional Gauge Theory,” [hep-th/0003136](#).
- [71] I. R. Klebanov and M. J. Strassler, “Supergravity and a Confining Gauge Theory: Duality Cascades and χ SB-Resolution of Naked Singularities,” *JHEP* **08** (2000) 052, [hep-th/0007191](#).
- [72] S. Hong, S. Yoon, and M. J. Strassler, “On the Couplings of the ρ Meson in AdS/QCD,” [hep-ph/0501197](#).
- [73] H. Boschi-Filho, N. R. F. Braga, and H. L. Carrion, “Glueball Regge Trajectories from Gauge/String Duality and the Pomeron,” [hep-th/0507063](#).
- [74] E. Caceres and C. Nunez, “Glueballs of Super Yang-Mills from Wrapped Branes,” *JHEP* **09** (2005) 027, [hep-th/0506051](#).
- [75] O. Aharony, S. S. Gubser, J. M. Maldacena, H. Ooguri, and Y. Oz, “Large N Field Theories, String Theory and Gravity,” *Phys. Rept.* **323** (2000) 183–386, [hep-th/9905111](#).
- [76] L. A. Pando Zayas, J. Sonnenschein, and D. Vaman, “Regge Trajectories Revisited in the Gauge / String Correspondence,” *Nucl. Phys.* **B682** (2004) 3–44, [hep-th/0311190](#).
- [77] M. Luscher, “Symmetry Breaking Aspects of the Roughing Transition in Gauge Theories,” *Nucl. Phys.* **B180** (1981) 317.
- [78] O. Aharony, A. Fayyazuddin, and J. M. Maldacena, “The Large N Limit of $\mathcal{N} = 2, 1$ Field Theories From Three-Branes in F-Theory,” *JHEP* **07** (1998) 013, [hep-th/9806159](#).
- [79] G. P. Salam, “A Resummation of Large Sub-Leading Corrections at Small x ,” *JHEP* **07** (1998) 019, [hep-ph/9806482](#).
- [80] M. Ciafaloni, D. Colferai, and G. P. Salam, “A Collinear Model for Small- x Physics,” *JHEP* **10** (1999) 017, [hep-ph/9907409](#).
- [81] D. A. Ross, “The Effect of Higher Order Corrections to the BFKL Equation on the Perturbative Pomeron,” *Phys. Lett.* **B431** (1998) 161–165, [hep-ph/9804332](#).

- [82] E. Levin, “The BFKL High Energy Asymptotic in the Next-to-Leading Approximation,” *Nucl. Phys.* **B545** (1999) 481–504.
- [83] S. J. Brodsky, V. S. Fadin, V. T. Kim, L. N. Lipatov, and G. B. Pivovarov, “The QCD Pomeron with Optimal Renormalization,” *JETP Lett.* **70** (1999) 155–160, [hep-ph/9901229](#).
- [84] R. E. Hancock and D. A. Ross, “Solving the Modified Lipatov Equation,” *Nucl. Phys.* **B383** (1992) 575–606.
- [85] H. B. Meyer, “Glueball Regge Trajectories,” [hep-lat/0508002](#).
- [86] **Small x** Collaboration, J.R. Andersen *et al.*, “Small x Phenomenology: Summary and Status 2002,” *Eur. Phys. J.* **C35** (2004) 67–98, [hep-ph/0312333](#).
- [87] S. B. Giddings, “High Energy QCD Scattering, the Shape of Gravity on an IR Brane, and the Froissart Bound,” *Phys. Rev.* **D67** (2003) 126001, [hep-th/0203004](#).
- [88] K. Kang and H. Nastase, “Heisenberg Saturation of the Froissart Bound from AdS-CFT,” *Phys. Lett.* **B624** (2005) 125–134, [hep-th/0501038](#).
- [89] H. Nastase, “The Soft Pomeron from AdS-CFT,” [hep-th/0501039](#).
- [90] S.-J. Chang and T.-M. Yan, “High-Energy Elastic and Inelastic Scattering in ϕ^3 Theory,” *Phys. Rev.* **D4** (1971) 537–558.
- [91] H. M. Fried, “Basics of Functional Methods and Eikonal Models,”. Gif-sur-Yvette, France: Ed. Frontieres (1990) 326 p.
- [92] O. Aharony, S. Minwalla, and T. Wiseman, “Plasma-Balls in Large N Gauge Theories and Localized Black Holes,” [hep-th/0507219](#).
- [93] G. Ingelman and P. E. Schlein, “Jet Structure in High Mass Diffractive Scattering,” *Phys. Lett.* **B152** (1985) 256.
- [94] K. Goulianos, “Renormalization of Hadronic Diffraction and the Structure of the Pomeron,” *Phys. Lett.* **B358** (1995) 379–388.
- [95] C.-I. Tan, “Diffractive Production at Collider Energies and Factorization,” *Phys. Rept.* **315** (1999) 175–198, [hep-ph/9810237](#).
- [96] J. Bartels, J. R. Forshaw, H. Lotter, and M. Wusthoff, “Diffractive Production of Vector Mesons at Large t ,” *Phys. Lett.* **B375** (1996) 301–309, [hep-ph/9601201](#).